UNIVERSITY OF GLASGOW

CHEMISTRY DEPARTMENT

RADIO AND MICROWAVE SPECTROSCOPIC STUDIES OF SOME INORGANIC SOLIDS

being

A thesis submitted in part fulfilment of the requirements for the

DEGREE OF DOCTOR OF PHILOSOPHY

by

WILLIAM HENRY DALGLEISH

October 1975

ProQuest LLC.
789 East Eisenhower Parkway
P.O. Box 1346
Ann Arbor, MI 48106 – 1346

ACKNOWLEDGEMENTS

I would like to express my sincere gratitude to Dr. A.L. Porte for his constant guidance and encouragement in the course of this work.

I thank Professor G.A. Sim in whose laboratories this work was carried out.

I would also like to thank Mr. A. Hislop and the workshop staff for their help in the construction of the high pressure vessels.

My thanks are also extended to the many people in the Chemistry Department of the University of Glasgow whom it would be impossible to mention by name here, whose assistance and advice were of value to me in the course of this work.

Finally I acknowledge with gratitude the award of a Research Studentship by the Science Research Council, during the tenure of which this work was carried out.

William H. Dalgleish, Ph.D. Thesis, 1975

RADIO AND MICROWAVE SPECTROSCOPIC STUDIES OF SOME INORGANIC SOLIDS

Summary

The thesis deals with some chemical applications of nuclear quadrupole resonance spectroscopy and electron paramagnetic resonance spectroscopy, to the study of some inorganic solids. It is divided into two main parts which are summarised separately below.

PART I

The first part of the thesis is devoted to chlorine - 35 nuclear quadrupole resonance investigations of some substituted chloro-cyclotriphosphazenes and some cyclodiphosphazanes. The basic electrostatic interactions of nuclear quadrupole resonance are discussed in Chapter I, with particular reference to the chlorine - 35 nucleus, which has a nuclear spin quantum number I of $\frac{3}{2}$. The way in which quadrupole resonance spectra can be interpreted to obtain information about bonding in chemical compounds is discussed, and the spectrometer used in carrying out this work is briefly described.

In Chapter II the chlorine - 35 nuclear quadrupole resonance spectra of a series of derivatives of hexachlorocyclotriphosphazatriene, $N_3P_3Cl_6$, are investigated in order to assess the usefulness of this technique in obtaining structural information on the cyclophosphazenes. N.q.r. frequencies characteristic of $\equiv PCl_2$, $\equiv PClNR_2$, $\equiv PClPh$ and $\equiv PCl$ $(N = PR_3)$ groups occur in the ranges 26 - 29, 22 - 25, 23 - 25 and 23.5 - 25.5 M.Hz. respectively. The characteristic frequency ranges of the last three groups overlap, and so these functional groups cannot be distinguished by simply measuring the chlorine - 35 nuclear quadrupole resonance frequencies. Cis - and trans - isomers may be distinguished

by their resonance frequencies, by comparing the range of frequencies observed, but only when results for both isomers are available.

Chapter III is concerned with nuclear quadrupole resonance studies of the related species, the cyclodiphosphazanes, $(Cl_3PNR)_2$. It is found that nuclear quadrupole resonance spectroscopy can be used in three ways to distinguish between axial and equatorial chlorine atoms in these compounds; the chlorine - 35 n.q.r. frequencies are different, the temperature coefficients of these frequencies are different, and the pressure coefficients of these frequencies are different. The characteristic frequencies are determined essentially by the differences in the degree of ionic character associated with axial and equatorial bonds in the trigonal bipyramidal environment, while the characteristic effects of temperature and pressure on these frequencies originate essentially in the bending modes of vibration which involve the P - Cl fragments in the chlorocyclodiphosphazanes. It is concluded that the effects of pressure changes and temperature changes on the chlorine - 35 n.q.r. frequencies in other P - Cl systems should be characteristic of these systems, and these ideas are applied to the chlorocyclotriphosphazatrienes in Chapter IV, where the chlorine - 35 n.q.r. spectra of $N_3P_3Cl_6$ and $N_3P_3Cl_5NHPr^i$ have been extensively investigated. A sharp phase change has been found to occur in $N_3P_3Cl_5NHPr^i$ over the temperature range $230 \leq T \leq 235K$. The resonance frequencies in both these compounds are linear functions of pressure within the range $1 \leq P \leq 1000$ Kg.cm^{-2}, so distinguishing these species from the cyclodiphosphazanes studied earlier, for which there is a marked change in the pressure dependence of the n.q.r. frequencies at approximately 650 Kg.cm^{-2}. The effects of pressure and temperature changes on the chlorine - 35 n.q.r. frequencies in $N_3P_3Cl_6$ can again be explained in terms of a localised P - Cl bending mode, but the

vibrational amplitudes for the chlorine atoms in $N_3P_3Cl_5NHPr^i$ appear to be much larger, implying that large amplitude vibrations of the bulky sidechain or of the entire molecule may be more important in this case.

The experimental techniques employed in studying these quadrupole resonance spectra as a function of temperature and pressure, and in weak magnetic fields, are discussed at length in the appendices located at the end of the thesis; particular emphasis is placed on the design of the high pressure vessel.

PART II

The second part of the thesis is concerned with electron paramagnetic resonance spectroscopy. In Chapter V the basic theory of electron paramagnetic resonance spectroscopy is discussed, with particular reference to transition metal complexes containing one unpaired electron. In Chapter VI the available electron paramagnetic resonance data for the pseudotetrahedral vanadium (IV) complex $(\pi\text{-}C_5H_5)_2VCl_2$ is reviewed, and the reasons for the disagreement between the various published studies are discussed. In an attempt to resolve this disagreement, a synthesis of the closely related complex $(CH_2)_3(C_5H_4)_2VCl_2$ has been developed, and the e.p.r. spectra of this compound in both solution and glass phases are reported and analysed.

In the course of this preparative reaction it is found that vanadium tetrachloride is present in tetrahydrofuran solutions as an adduct with tetrahydrofuran, and the e.p.r. spectrum of this adduct, $VCl_4 \cdot 2$ THF, is also reported in Chapter VI. Attempts to purify $(CH_2)_3(C_5H_4)_2VCl_2$ by sublimation result in the formation of a further paramagnetic species, which has not been characterised. This

compound is believed to be produced by a rearrangement reaction of $(CH_2)_3 (C_5H_4)_2 VCl_2$.

PREFACE

This thesis deals with some chemical applications of nuclear quadrupole resonance spectroscopy and electron paramagnetic resonance spectroscopy to the study of some inorganic solids.

The first part of the thesis is devoted to chlorine - 35 nuclear quadrupole resonance investigations of some phosphonitrilic compounds, and the basic theory of nuclear quadrupole resonance underlying these studies is discussed briefly in Chapter I. References are not included in the text of this Chapter.

In Chapter II the chlorine - 35 nuclear quadrupole resonance spectra of a number of substituted chlorocyclotriphosphazatrienes are reported, and the use of the technique as a means of distinguishing positional isomers in these derivatives is discussed; the spectra of some related acyclic compounds are also investigated.

Chapters III and IV are concerned with quadrupole resonance studies of some cyclodiphosphazanes and cyclotriphosphazatrienes whilst these compounds are subjected to varying conditions of temperature and pressure, and the origin of the characteristic effects observed in these circumstances is investigated.

The experimental aspects of these quadrupole resonance studies are discussed at length in the appendices at the end of the thesis.

The second part of the thesis is concerned with electron paramagnetic resonance spectroscopy, the basic theory of which is introduced in Chapter V, and as in Chapter I references are not

included in the text of this chapter. In Chapter VI the available electron paramagnetic resonance data for the pseudo-tetrahedral vanadium (IV) complex $(\pi\text{-}C_5H_5)_2\ VCl_2$ is reviewed, and the synthesis and e.p.r. spectrum of the related derivative $(CH_2)_3(C_5H_4)_2\ VCl_2$ are reported.

The work described in this thesis is original, and was carried out in part fulfilment of the requirements for the degree of Ph.D. in the University of Glasgow.

October 1975. W.H. Dalgleish.

TABLE OF CONTENTS

PART I

CHAPTER I

NUCLEAR QUADRUPOLE RESONANCE SPECTROSCOPY

CHAPTER II

THE USE OF CHLORINE - 35 NUCLEAR QUADRUPOLE RESONANCE SPECTROSCOPY FOR STRUCTURAL ASSIGNMENTS IN CHLOROCYCLOTRIPHOSPHAZATRIENES ; CHLORINE N.Q.R. SPECTRA OF SOME ACYCLIC PHOSPHORYL AND PHOSPHINE COMPLEXES

CHAPTER III

CHLORINE - 35 NUCLEAR QUADRUPOLE RESONANCE SPECTRA OF THE CHLOROCYCLODIPHOSPHAZANES $(Cl_3\ PNR)_2$, AND OF THE CHLOROOXOCYCLODIPHOSPHAZANES $[Cl(O)\ PNR]_2$

CHAPTER IV

THE EFFECTS OF PRESSURE CHANGES AND TEMPERATURE CHANGES ON THE CHLORINE - 35 NUCLEAR QUADRUPOLE RESONANCE SPECTRA OF THE CHLOROCYCLOTRIPHOSPHAZATRIENES $N_3P_3Cl_6$ AND $N_3P_3Cl_5NHPr^i$

PART II

CHAPTER V

ELECTRON PARAMAGNETIC RESONANCE SPECTROSCOPY

CHAPTER VI

ELECTRON PARAMAGNETIC RESONANCE STUDIES OF BIS-(π -CYCLOPENTADIENYL)-BIS - CHLORO VANADIUM (IV); THE SYNTHESIS OF (1.1'- TRIMETHYLENEDI-CYCLOPENTADIENYL) - BIS - CHLORO VANADIUM (IV)

PART I : Nuclear quadrupole resonance spectroscopy.

CHAPTER I

NUCLEAR QUADRUPOLE RESONANCE SPECTROSCOPY

1.1 Introduction

Nuclear quadrupole resonance is a branch of spectroscopy which can be used in certain circumstances to provide information about electronic distributions in molecular solids. The transitions observed in nuclear quadrupole resonance spectroscopy concern levels which originate in the interaction of the nuclear quadrupole moment with the electrostatic field gradient produced by nearby charges. The technique is very sensitive to the electrostatic environment in the vicinity of the nucleus and so with care it provides a potentially extremely sensitive means of studying the electronic distributions in atoms, molecules and solids.

By performing suitable experiments the following three types of information related to the electronic environment of the nucleus may be derived from nuclear quadrupole resonance spectra.

a. The directions of the principal axes of the electric field gradient tensor at the nuclear site.

b. The magnitude of the greatest component of this tensor.

c. The degree of asymmetry of the electric field gradient at the nuclear site.

The chemist's interest in nuclear quadrupole resonance spectroscopy is centred around the interpretation of this information in terms of molecular and electronic structure.

Before discussing the interpretation of quadrupole resonance spectra it is necessary to outline the theory of the interaction of the nuclear quadrupole moment with its neighbouring electric field in order to illustrate the formalism involved, and to introduce the parameters which can be derived from such spectra.

1.2 Quadrupolar energy levels

A nucleus in an atom or molecule or solid experiences a potential, V(r) say, arising from all other charged particles, both electrons and nuclei, in its vicinity. If $\rho(r)$ is the charge density at a point within the nucleus, at vector distance $\underline{r}$ from the nuclear centre of mass, then the interaction energy is

$$E = \int V(r)\,\rho(r)\,d\tau \qquad 1.1$$

where the integral is taken over the nuclear volume. The potential V(r) may be expanded by means of a Taylor series about the origin, the nuclear centre of mass, so that

$$E = V(0)\int \rho(r)d\tau + \sum_{\alpha} V_{\alpha}\int x_{\alpha}\rho(r)d\tau + \tfrac{1}{2}\sum_{\alpha,\beta} V_{\alpha\beta}\int x_{\alpha}x_{\beta}\rho(r)d\tau + \text{higher order terms} \qquad 1.2$$

in which, when $\alpha,\beta = 1,2,3$ then x_{α} and $x_{\beta} = x,y,z$ respectively, and it is understood that

$$V_{\alpha} = \left(\frac{\partial V}{\partial x_{\alpha}}\right)_{r=0} \qquad 1.3$$

$$V_{\alpha\beta} = \left(\frac{\partial^2 V}{\partial x_{\alpha}\,\partial x_{\beta}}\right) r = 0 \qquad 1.4$$

The first term in equation 1.2 is simply the electrostatic energy of the nucleus taken as a point charge, and this can be ignored here since it is independent of nuclear orientation. The second term is the dipole contribution which is zero if the nucleus is in a state of definite parity. The third term in this expression is the electric quadrupole term, which thus gives the orientational energy of the nucleus in the electric field gradient, correct to fourth order. It is convenient to recast the quadrupolar energy in the form

$$E_Q = \tfrac{1}{2} \sum_{\alpha,\beta} V_{\alpha\beta} \int x_\alpha \, x_\beta \, \rho(r) \, d\tau$$
$$= \tfrac{1}{6} \sum_{\alpha,\beta} V_{\alpha\beta} \, Q_{\alpha\beta} + \tfrac{1}{6} \sum_{\alpha,\beta} V_{\alpha\beta} \, \delta_{\alpha\beta} \int r^2 \, \rho(r) \, d\tau \qquad 1.5$$

where the function $Q_{\alpha\beta}$ is defined by the expression

$$Q_{\alpha\beta} = \int_{\substack{\text{nuclear} \\ \text{volume}}} (3x_\alpha \, x_\beta - \delta_{\alpha\beta} r^2) \, \rho(r) \, d\tau \qquad 1.6$$

and

$$\delta_{\alpha\beta} = 1 \quad \text{if} \quad \alpha = \beta$$
$$= 0 \quad \text{if} \quad \alpha \neq \beta \qquad 1.7$$

The second term in equation 1.5 has an equal effect on all states in the manifold of levels belonging to the same I value, where I is the nuclear spin quantum number; this term is ignored here since pure nuclear quadrupole resonance spectroscopy is concerned with transitions between such levels, so that with this understanding the quadrupolar energy simplifies to

$$E_Q = \tfrac{1}{6} \sum_{\alpha,\beta} V_{\alpha\beta} \, Q_{\alpha\beta} \qquad 1.8$$

It is apparent from the definition of $V_{\alpha\beta}$ given earlier that the electric field gradient is a tensor consisting of nine distinct terms. Considerable simplification is possible since a principal axis system can always be chosen for the potential such that all off-diagonal elements are zero, that is

$$V_{\alpha\beta} = 0 \qquad \text{if} \quad \alpha \neq \beta \tag{1.9}$$

while from Laplace's equation, which is valid if the effects of the small electronic charge distribution within the nucleus are neglected,

$$\frac{\partial^2 V}{\partial x^2} + \frac{\partial^2 V}{\partial y^2} + \frac{\partial^2 V}{\partial z^2} = \sum_{\alpha} V_{\alpha\alpha} = 0 \tag{1.10}$$

Thus only two quantities are needed to define the electric field gradient at the nucleus.

To obtain a quantum mechanical expression for the Hamiltonian from the classical energy given in equation 1.8 it is only necessary to replace $\rho(r)$ by its quantum mechanical operator, so that

$$\mathcal{H}_Q = \frac{1}{6} \sum_{\alpha,\beta} V_{\alpha\beta} \, Q^{OP}_{\alpha\beta} \tag{1.11}$$

where $Q^{OP}_{\alpha\beta}$ is of course an operator which acts only on nuclear eigenfunctions.

The transitions of interest in n.q.r. spectroscopy take place between states which differ only in m_I values, corresponding to the ground state value of the nuclear spin quantum number I, so that our nuclear wavefunctions can be written

$$\Psi_{\text{nucl}} = \sum_i c_i \phi_i \tag{1.12}$$

where the basis functions ϕ_i are labelled by the quantum numbers m_I. The variation procedure thus leads to a $(2I + 1) \times (2I + 1)$ secular determinant of the usual form, with diagonal matrix elements $(\mathcal{H}_{m_1 m_1} - E)$ and off diagonal elements $\mathcal{H}_{m_1 m_2}$ where

$$\mathcal{H}_{m_1 m_2} = \int \phi^*_{m_1} \mathcal{H}_Q \phi_{m_2} \, d\tau$$

$$= \frac{1}{6} \sum_{\alpha,\beta} V_{\alpha\beta} \left\langle m_1 \left| Q^{OP}_{\alpha\beta} \right| m_2 \right\rangle \qquad 1.13$$

In this expression m_1 and m_2 refer to basis states whose m_I values are m_1 and m_2 respectively.

These matrix elements are most easily evaluated by making use of the Wigner-Eckart theorem, which in the present context states that the matrix elements of $Q^{OP}_{\alpha\beta}$ are proportional to those of the analogous angular momentum operators, so that

$$\left\langle m_1 \left| Q^{OP}_{\alpha\beta} \right| m_2 \right\rangle = C \left\langle m_1 \left| \frac{3}{2} (I_\alpha I_\beta + I_\beta I_\alpha) - \delta_{\alpha\beta} \underline{I}^2 \right| m_2 \right\rangle \qquad 1.14$$

where C is a constant of proportionality. The constant can be found by considering the diagonal matrix element for which $m_1 = m_2 = I$ and $\alpha = \beta = z$, for which

$$\left\langle I \left| Q^{OP}_{ZZ} \right| I \right\rangle = C \int \phi^*_I (3I_Z^2 - \underline{I}^2) \phi_I \, d\tau$$

$$= CI(2I - 1) \qquad 1.15$$

The left hand side of equation 1.15 is obviously a constant which is characteristic of the nucleus being considered; it

can be replaced by eQ where Q is the nuclear quadrupole moment, defined as the expectation value of the classical and purely geometric quantity

$$\sum_{k \text{ protons}} r_k^2 \, (3 \cos^2\theta_k - 1) \qquad 1.16$$

evaluated for the nucleus in the state $m_I = I$.

The constant C is now given by the expression

$$C = \frac{eQ}{I(2I-1)} \qquad 1.17$$

and the quadrupole Hamiltonian becomes

$$\mathcal{H}_Q = \frac{eQ}{4I(2I-1)} \left\{ V_{zz} \, (3I_z^2 - \underline{I}^2) + (V_{xx} - V_{yy}) \, (I_x^2 + I_y^2) \right\} \qquad 1.18$$

in the principal axis system of the electric field gradient.

The form of the Hamiltonian given here emphasises the point made earlier, that only two parameters are needed to characterize the second derivatives of the potential; the two parameters normally chosen for this purpose are the electric field gradient, $-q$, and the asymmetry parameter, η, defined by

$$-q = V_{zz} \quad ; \quad \eta = \frac{V_{xx} - V_{yy}}{V_{zz}} \qquad 1.19$$

The quantity $-q$ is, by definition, that component of the electric field gradient tensor which has the largest magnitude, and the axes are chosen such that η, which measures the deviation of the e.f.g. tensor from axial symmetry, falls within the range $0 \leqslant \eta \leqslant 1$. In terms of q and η the quadrupole Hamiltonian becomes

$$\begin{aligned} \mathcal{H}_Q &= \frac{eqQ}{4I(2I-1)} \left\{ (3I_z^2 - \underline{I}^2) + \eta (I_x^2 - I_y^2) \right\} \\ &= \frac{eqQ}{4I(2I-1)} \left\{ (3I_z^2 - \underline{I}^2) + \frac{\eta}{2} (I_+^2 - I_-^2) \right\} \end{aligned} \qquad 1.20$$

where the quantity eqQ is known as the quadrupole coupling constant, and I_+ and I_- are the raising and lowering operators

$$I_+ = I_x + iI_y$$
$$I_- = I_x - iI_y \qquad 1.21$$

It should now be a straightforward matter to use equation 1.20 to evaluate the energy levels for each value of the nuclear spin quantum number I for which the nucleus can possess a finite nuclear quadrupole moment, that is for all $I \geq 1$. However the presence of the shift operators in the quadrupolar Hamiltonian leads to mixing of basis states whose m_I value differ by 2, and so in general closed solutions for the energy levels cannot be found for $I \geq \frac{5}{2}$, except in the absence of asymmetry. For this reason we restrict the present discussion to the ^{35}Cl nucleus, for which $I = \frac{3}{2}$; in this case in the presence of an asymmetric field gradient the states $\phi_{+\frac{3}{2}}$ and $\phi_{-\frac{1}{2}}$ are mixed, as are $\phi_{\frac{1}{2}}$ and $\phi_{-\frac{3}{2}}$. The secular determinant can readily be set up and solved, to give the eigenvalues

$$E_{\pm\frac{3}{2}} = \frac{eqQ}{4}\left(1 + \frac{\eta^2}{3}\right)^{\frac{1}{2}}$$
$$E_{\pm\frac{1}{2}} = -\frac{eqQ}{4}\left(1 + \frac{\eta^2}{3}\right)^{\frac{1}{2}} \qquad 1.22$$

There are thus two doubly degenerate energy levels, and only one transition occurs, at a frequency

$$\nu = \frac{eqQ}{2h}\left(1 + \frac{\eta^2}{3}\right)^{\frac{1}{2}} \qquad 1.23$$

Thus for $I = \frac{3}{2}$ the quadrupole coupling constant and asymmetry parameter cannot be determined separately from a pure n.q.r.

experiment. In order to obtain η and hence the quadrupole coupling constant, it is necessary to carry out experiments in the presence of a weak magnetic field. This aspect of the subject is now considered.

1.3 The effect of weak magnetic fields on the quadrupole resonance spectrum of a nucleus with spin quantum number $I = \frac{3}{2}$

The application of a static magnetic field has a marked effect on the n.q.r. spectrum of a nucleus with $I = \frac{3}{2}$. If the sample under investigation is a single crystal then the original single line is split into four components whose separations and intensities depend on the value of η and on the orientation of the magnetic field relative to the directions of the principal axes of the electric field gradient at the nucleus. So long as the magnetic field is weak enough to be regarded as a perturbation, its effect can be expressed mathematically by adding a further term to the quadrupolar Hamiltonian given above. This new Zeeman term is given by

$$\mathcal{H}_m = -\gamma\hbar H_o (I_z \cos\theta + I_x \sin\theta \cos\phi + I_y \sin\theta \sin\phi) \qquad 1.24$$

where γ is the magnetogyric ratio of the nucleus.

The effect of this perturbation on the n.q.r. spectrum is most readily calculated when $\eta = 0$. The I_x and I_y terms in equation 1.24 mix basis functions whose m_I values differ by ± 1, so to first order only the component of H_o which lies along the z axis direction can perturb the basis functions $\psi_{\pm\frac{3}{2}}$, and the Zeeman pattern for these functions is independent of ϕ. The degeneracy of the $m_I = \pm\frac{3}{2}$ levels is removed by the field,

giving a pair of levels whose energies are

$$E_{\pm\frac{3}{2}} = \frac{eqQ}{4I(2I-1)}\left[3m_I^2 - I(I+1)\right] \mp m_I \gamma \hbar H_o \cos\theta \qquad 1.25$$

to first order. However, the situation is more complex for the $m_I = \pm \frac{1}{2}$ states since the Zeeman field causes a zero order mixing of the degenerate $\psi_{+\frac{1}{2}}$ and $\psi_{-\frac{1}{2}}$ basis wavefunctions; the new eigenfunctions are found by degenerate perturbation theory to be

$$\begin{aligned} \psi_+ &= \psi_{+\frac{1}{2}} \sin\alpha + \psi_{-\frac{1}{2}} \cos\alpha \\ \psi_- &= \psi_{-\frac{1}{2}} \sin\alpha - \psi_{+\frac{1}{2}} \cos\alpha \end{aligned} \qquad 1.26$$

where

$$\tan^2\alpha = \frac{f+1}{f-1} \qquad 1.27$$

and

$$f = \left[1 + (I+\tfrac{1}{2})^2 \tan^2\theta\right]^{\frac{1}{2}} \qquad 1.28$$

The energies of these new states are given by

$$E_{\pm} = \frac{eqQ}{4I(2I-1)}\left[\tfrac{3}{4} - I(I+1)\right] \mp \tfrac{1}{2} f \gamma \hbar H_o \cos\theta \qquad 1.29$$

so that the energy level diagram is as shown in Figure 1.1 below. The $\Delta m = \pm 1$ transitions between the new energy levels are illustrated in the figure, the frequencies of these four transitions being

$$\begin{aligned} \nu_\alpha &= \frac{eqQ}{2h} - \frac{3-f}{4\pi} \cdot \gamma H_o \cos\theta \\ \nu_\beta &= \frac{eqQ}{2h} - \frac{3+f}{4\pi} \cdot \gamma H_o \cos\theta \\ \nu_{\alpha'} &= \frac{eqQ}{2h} + \frac{3-f}{4\pi} \cdot \gamma H_o \cos\theta \\ \nu_{\beta'} &= \frac{eqQ}{2h} + \frac{3+f}{4\pi} \cdot \gamma H_o \cos\theta \end{aligned} \qquad 1.30$$

The intensity ratio of the outer, β , pair of resonance lines to the inner, α , pair turns out to be $(f-1)/(f+1)$, and so varies with orientation, as does the separation of the peaks. For $\theta_o = \tan^{-1}\left[2\sqrt{2}/(I+\frac{1}{2})\right]$, i.e. $\theta_o = 54^\circ 44'$ for $I = \frac{3}{2}$, the splittings of the two doublets in the spectrum are given by

$$\Delta\nu_{\alpha\alpha'} = 0 \quad ; \qquad \Delta\nu_{\beta\beta'} = \frac{3\gamma}{\pi h} \cdot H \qquad 1.31$$

The locus of zero splitting for the (α,α') components is defined by H_o lying on a right circular cone with semivertical angle θ_o whose axis coincides with the symmetry axis of the e.f.g. Because a strong line is obtained at the original unperturbed frequency this cone of zero splitting is easy to locate, and the direction of the symmetry axis can thence easily be determined.

In addition to these transitions, a "$\Delta m = 1$" transition is also possible between the states $|+\rangle$ and $|-\rangle$, and this is shown by a dotted line in Figure 1.1 (a); the frequency of this transition is, to first order,

$$\nu = \frac{f\gamma H_o \cos\theta}{2\pi} \qquad 1.32$$

which is too low to be observed in an n.q.r. experiment.

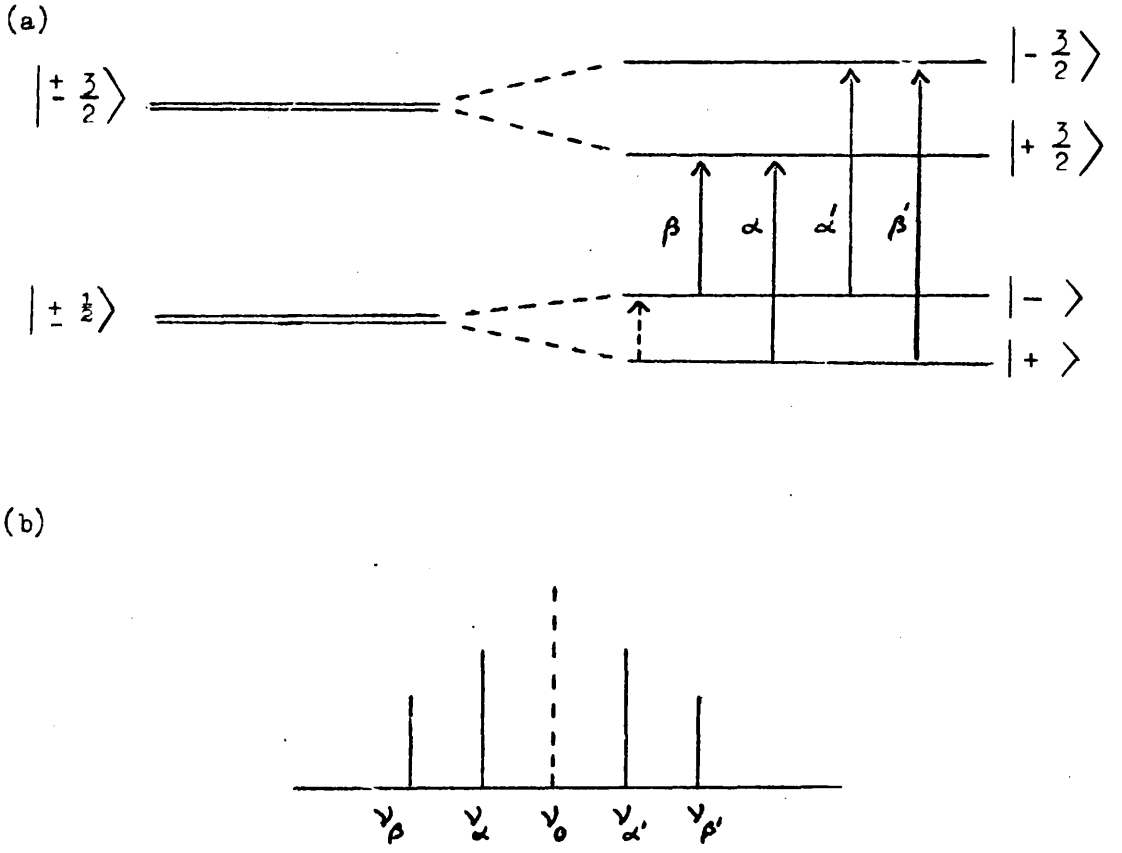

Figure 1.1 (a) The Zeeman splitting of the quadrupolar energy levels for $I = \frac{3}{2}$ when $\eta = 0$.

(b) Observed n.q.r. spectrum for $I = \frac{3}{2}$, $\eta = 0$ in a weak Zeeman field ; ν_o is the n.q.r. frequency in the absence of a magnetic field.

The effect of a magnetic field on a nuclear quadrupole resonance spectrum is much more complex when the electric field gradient is asymmetric. In this case the energy levels can be shown to be given by an expression of the form

$$E_{m\pm} = E_{m(o)} \pm \frac{\gamma\hbar H_o}{2}\left[a_m^2 \cos^2\theta + (b_m^2 + c_m^2 + 2b_m c_m \cos 2\phi)\sin^2\theta\right] \qquad 1.33$$

where $E_{m(o)}$ are the energy levels in the absence of a magnetic field. For $I = \frac{3}{2}$ the coefficients in this expression are given by

$$\begin{aligned} a_{\pm\frac{3}{2}} &= -1 - \frac{2}{\rho} \quad ; \quad a_{\pm\frac{1}{2}} = -1 + \frac{2}{\rho} \\ b_{\pm\frac{3}{2}} &= 1 - \frac{1}{\rho} \quad ; \quad b_{\pm\frac{1}{2}} = 1 + \frac{1}{\rho} \\ c_{\pm\frac{3}{2}} &= -c_{\pm\frac{1}{2}} = \frac{\eta}{\rho} \quad ; \quad \rho = \left(1 + \frac{\eta^2}{3}\right)^{\frac{1}{2}} \end{aligned} \qquad 1.34$$

It can be seen that the presence of the magnetic field once again removes the degeneracy between the states $\pm m_I$. As we found above all four transitions between the two pairs of adjacent levels become possible and once again the spectrum consists of two pairs of lines, each pair equally spaced about the pure n.q.r. frequency. The inner or α pair are again the more intense while the β pair are weak and all lines in the spectrum are dependent on the value of η.

The locus of zero splitting of the α pair can be shown to be given by the expression

$$\sin^2\theta_o = \frac{2}{3 - \eta\cos 2\phi} \qquad 1.35$$

which defines an elliptic cone around the Z-axis. A knowledge of θ_o in two planes, $\theta_o(\phi = 0^\circ)$ and $\theta_o(\phi = 90^\circ)$ now makes it possible to calculate the asymmetry parameter from the expression

$$\eta = \frac{3\left[\sin^2\theta_0(0^\circ) - \sin^2\theta_0(90^\circ)\right]}{\sin^2\theta_0(0^\circ) + \sin^2\theta_0(90^\circ)} \qquad 1.36$$

This, the "zero splitting locus" method of determining η, has been widely used, although greater accuracy can be achieved by an alternative method, the so-called "frequency-field" method developed by Rehn, in which the splitting of the α and β components is measured when the magnetic field is positioned perpendicular to the Z axis. In this orientation the splitting between the α and β components is given by

$$\nu_\alpha - \nu_\beta \cong \frac{\gamma H_0 \eta}{2\pi}\left[1 + \frac{\eta}{6}(\cos 2\phi - \eta)\right] \qquad 1.37$$

Thus a preliminary investigation is needed to determine the principal axis directions, in order to apply this method; a simple frequency measurement with the crystal in the appropriate orientation then yields an accurate measurement of η.

The above discussion can be summarised as follows. For a nucleus which has spin quantum number $I = \frac{3}{2}$, a pure n.q.r. experiment, whether on a polycrystalline or single crystal sample, yields the frequency of the resonance signal, but does not allow an estimate to be made of the quadrupole coupling constant and asymmetry parameter independently. In order to estimate η, and hence eqQ, one of the types of measurement discussed above must be carried out on a single crystal sample in a weak magnetic field. The greatest difficulty with these methods is that a single crystal of about one cubic centimetre in size is needed for such measurements on ^{35}Cl, and this severely restricts the range of substances which can be studied.

An alternative method of determining η is available, which

depends upon the analysis of the lineshape produced when a weak magnetic field is applied to a polycrystalline sample. This technique will be discussed at length in Chapter III, but it is noted at this point that the considerable broadening of the resonance line which occurs in the applied magnetic field restricts the method to those compounds which exhibit very strong quadrupole resonance signals.

If none of these methods is applicable to a particular compound it is often possible to make an approximate estimate of eqQ from the observed pure n.q.r. frequency, by neglecting the term in η in equation 1.23. The quadrupole coupling constant, measured in M.Hz., is then equal to twice the resonance frequency. This is a good approximation if $\eta < 0.1$, which is the case for ^{35}Cl in most species in which chlorine is bonded to only one atom; such an approximation could not be justified however if considerable π - character were expected in the bond to chlorine, or if the latter was present as a bridging ligand.

1.4. Interpretation of nuclear quadrupole resonance data

In the preceding sections we have discussed how the phenomenon of nuclear quadrupole resonance originates in the interaction of a quadrupolar nucleus with its environment, and have illustrated the derivation of the parameters eqQ and η from an n.q.r. experiment involving a nucleus which has spin quantum number $I = \frac{3}{2}$. If Q, the quadrupole moment of the nucleus is known, and it is assumed that changes in the charge distribution external to the nucleus do not alter this nuclear moment, then it follows that the n.q.r. measurements give information about the parameters q and η of

the electric field at the nucleus. Both the electric field gradient and the asymmetry parameter are defined essentially, but not entirely, by the electrons in the neighbourhood of the nucleus, so that in principle if the magnitudes of q and η are known then a great deal of information can be obtained about the wavefunctions describing the distributions of at least some of the electrons.

We can illustrate the relationship between the charge distribution around a nucleus, and the electric field gradient to which the nucleus is subjected as follows. Consider a quadrupolar nucleus situated at the origin of the Cartesian axis system in Figure 1.2 below. An incremental charge Δe at a distance $\underline{r}$ from the nucleus contributes an amount

$$V = \frac{\Delta e}{r} \qquad 1.38$$

to the incremental electrostatic potential at the origin. Hence the contribution of the incremental charge Δe to q, the negative of the field gradient component along the Z axis direction of the co-ordinate system, is

$$\Delta q = \frac{\partial^2 \Delta V}{\partial z^2} = \Delta e \frac{\partial^2}{\partial z^2}\left(\frac{1}{r}\right)$$

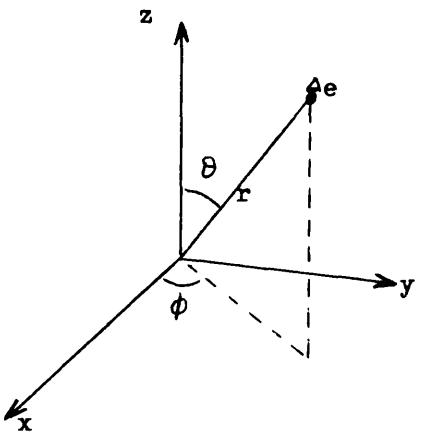

Figure 1.2 Axis system for a molecular electronic charge distribution.

$$= \Delta e \left(3z^2 r^{-5} - r^{-3} \right)$$

$$= \Delta e \left(\frac{3\cos^2\theta - 1}{r^3} \right) \qquad 1.39$$

It can similarly be shown that

$$\frac{\partial^2 \Delta V}{\partial x^2} = \Delta e \left(\frac{3\sin^2\theta\cos^2\phi - 1}{r^3} \right) \qquad 1.40$$

and

$$\frac{\partial^2 \Delta V}{\partial y^2} = \Delta e \left(\frac{3\sin^2\theta\sin^2\phi - 1}{r^3} \right) \qquad 1.41$$

and it now follows that the total value of q at the nucleus due to the i electrons in its vicinity is

$$q = -e \sum_i \int_{\text{all space}} \psi_i^* \left(\frac{3\cos^2\theta_i - 1}{r_i^3} \right) \psi_i \, d\tau_i \qquad 1.42$$

where θ_i, ϕ_i, r_i are the polar co-ordinates of the i^{th} electron with respect tothe principal axes of the electric field gradient tensor. ψ_i is the normalised wavefunction for the i^{th} electron, so that if the atomic or molecular wavefunctions are known then q can be calculated, and hence the nuclear quadrupole coupling constant eqQ can be evaluated from the wavefunctions, provided that the nuclear quadrupole moment is known; the extent of agreement between experimental and calculated values of eqQ can thus serve as a test of the accuracy of proposed ground state molecular wavefunctions near the nucleus.

In practice a number of problems surround any attempt to calculate q , which mainly arise from difficulties in obtaining reliable atomic and molecular wavefunctions. For this reason it is convenient to discuss atoms and molecules separately, since many of the conclusions drawn from work on coupling constants in atoms can be applied to studies of molecular systems and can be used in shaping the form of analysis applied to the latter.

1.5 Quadrupole coupling constants in atoms

In order to calculate q for an atom with hydrogen-like orbitals it follows from equation 1.42 that it is necessary to evaluate the expression $(3\cos^2\theta - 1)r^{-3}$ at the nucleus, averaged over the electronic distribution. It follows immediately from this equation that no spherically symmetric distribution of charges can make any contribution to q, so that s electrons, and electrons in filled shells, should give

rise to no electric field gradient at the nucleus. By contrast an electron in a hydrogen-like $2p$ orbital should produce a large field gradient at its nucleus; for a $2p_z$ orbital the e.f.g. is in fact given by

$$q_{2p_z} = -\frac{1}{30}\left(\frac{eZ^3}{a_o^3}\right) \qquad 1.43$$

whereas an electron in an analogous $2p_x$ or $2p_y$ orbital produces an e.f.g. at the nucleus of

$$q_{2p_x} = q_{2p_y} = +\frac{1}{60}\left(\frac{eZ^3}{a_o^3}\right) \qquad 1.44$$

Since the field gradient exerted at the nucleus by a single electron in a p orbital depends on Z^3, quadrupole resonance frequencies should in general be larger for nuclei of high atomic number. It is also apparent that, because of the inverse dependence on r^3, electron density close to the nucleus should make the largest contribution to q ; d- and f- electrons thus make little contribution to the field gradient in comparison to those in p-orbitals of the same principal quantum number. For example the ratios of the contributions to q from a $4p_z$ electron, a $4d_{z^2}$ electron and a $4f_{z^3}$ electron are $1 : \frac{1}{7} : \frac{1}{21}$.

From the above discussion, and the simple form of the expressions for q in equations 1.43 and 1.44, it would appear that it should be easy to obtain good agreement between calculated and experimental values of the quadrupole coupling constant. That this is not so is due to the presence of correlation effects, and to the phenomenon known as Sternheimer polarisation. The correlation effects which occur are analogous to those encountered in considering hyperfine

interactions in electron paramagnetic resonance spectroscopy. Thus if the atom has a single p electron in the valence shell this will give rise to an e.f.g. of the magnitude given in equation 1.43 or 1.44 ; simultaneously however the valence electron distorts the inner shells producing a further field gradient at the nucleus, the magnitude of which is identical to that predicted by the Sternheimer effect.

The latter effect is visualised as follows. The quadrupole moment of the nucleus here polarises the inner shells, and the resulting quadrupolar distortion of their charge distribution interacts with the electric field gradient of the p electron. If the p electron itself were expected to give rise to a field gradient of V_{zz}^{o} then the e,f.g. in the presence of the Sternheimer effect becomes $V_{zz}^{o}\ (1 - \gamma)$ where γ, a constant, is known as the Sternheimer polarisation factor of the atom.

Thus the electric field gradient predicted by, for example, equation 1.44 must be multiplied by the factor $(1 - \gamma)$ in order to give an accurate prediction of the field gradient in all atoms except hydrogen.

The evaluation of γ is an even more vital factor in the calculation of the e.f.g. in an ionic crystal, since γ is very large when the charges producing the distortion are external to the atom or ion containing the quadrupolar nucleus; in an instance of this sort uncertainty in the value of γ can give rise to the major error in the calculation.

1.6 Quadrupole coupling constants in molecules

From the discussion above it is clear that the theoretical calculation of the field gradient at a nucleus in even a relatively simple molecule is an extremely difficult task. Although some encouraging results can be obtained for diatomic molecules, in other cases considerable simplifications have to be introduced, and the way in which this problem is normally approached is considered below.

The electric field gradient at a nucleus in a molecule can be expressed in the form

$$q_{ZZ} = -e \int \psi^* \frac{(3\cos^2\theta - 1)}{r^3} \psi \, d\tau + e \sum_i Z_i \frac{(3\cos^2\theta_i - 1)}{R_i^3} \qquad 1.45$$

Here Z_i is the total charge on nucleus i in the molecule, at distance R_i from the one under consideration, and ψ is the wavefunction for the complete electron distribution about the nucleus. The magnitude and symmetry of the e.f.g. are determined largely by the electrons in the neighbourhood of the nucleus. The nuclear term in equation 1.45 is much smaller and is usually neglected.

In molecular orbital theory, the molecule can be described by a set of N doubly occupied orthogonal molecular orbitals, each of which can be written in the form of a linear combination of n orthogonal atomic orbitals. The $j^{\underline{th}}$ member of this set is

$$\psi_j = \sum_i^n c_{ij} \phi_i \qquad 1.46$$

and in general inner shell orbitals are completely neglected. When this equation is substituted into the first term of equation 1.45 the contribution to q at the first nucleus from all but

the inner closed shells of electrons, becomes

$$q_{el} = -e \int \left(\sum_{i}^{n} c_{ij} \phi_i \right)^* \left(\frac{3\cos^2\theta - 1}{r^3} \right)_1 \left(\sum_{i}^{n} c_{ij} \phi_i \right) d\tau \qquad 1.47$$

The subscript 1 indicates that the term to which it applies is to be evaluated at nucleus 1, since it is this nucleus whose quadrupole coupling constant is of interest to us. On expanding out equation 1.47 three types of integral are encountered. There are one-centre integrals of the form

$$c_{1j}^* c_{1j} \int \phi_1^* \left(\frac{3\cos^2\theta - 1}{r^3} \right)_1 \phi_1 \, d\tau$$

two-centre integrals such as

$$c_{1j}^* c_{2j} \int \phi_1^* \left(\frac{3\cos^2\theta - 1}{r^3} \right)_1 \phi_2 \, d\tau$$

involving atoms 1 and 2 say, and three-centre integrals of the form

$$c_{2j}^* c_{3j} \int \phi_2^* \left(\frac{3\cos^2\theta - 1}{r^3} \right)_1 \phi_3 \, d\tau$$

involving atoms 1,2 and 3. Evaluation of the two - and three - centre integrals is fairly difficult so that in general some approximations have to be made.

The most common method of overcoming these computational problems is that introduced by Townes and Dailey. This employs what is essentially a localized-orbital approach. Thus for a terminal nucleus, such as chlorine - 35 in a compound R-Cl, we consider only orbitals on chlorine and on the atom to which it is bonded. All three-centre integrals are then zero; all two-centre integrals are set against the nuclear contribution of the bonded atom, and normally polarization effects are assumed to be the same as those in the chlorine atom. We now find that the

magnitude of the electric field gradient depends entirely on the populations of the chlorine 3p orbitals.

The situation is particularly simple if the directions of the principal axes of the e.f.g. can be identified with the molecular symmetry and the p orbitals specified by the same axis system. In this case, in a molecule such as R-Cl, q_{zz} lies along the bond direction and the chlorine bonding orbital can be taken to be a 3s - 3p hybrid of the form

$$\psi_1 = a\psi_{3s} + (1 - a^2)^{\frac{1}{2}} \psi_{3p_z} \qquad 1.48$$

where a^2 is the s character of the bonding orbital; the population of this orbital is set equal to b. The non-bonding orbital, whose population is conventionally designated n, is now of the form

$$\psi_2 = (1 - a^2)^{\frac{1}{2}} \psi_{3s} - a\psi_{3p_z} \qquad 1.49$$

while the π orbitals take the form

$$\begin{aligned} \psi_3 &= \psi_{3p_x} \\ \psi_4 &= \psi_{3p_y} \end{aligned} \qquad 1.50$$

The populations of the π orbitals are p_x and p_y respectively.

It can now be easily shown that there is a relationship between the quadrupole coupling constant for this molecule (R-Cl) and that for the chlorine atom, such that

$$\frac{(eqQ/h)\ \text{mol}}{(eqQ/h)\ \text{atom}} = -\left\{b(1 - a^2) + na^2\right\} + \tfrac{1}{2}(P_x + P_y) \qquad 1.51$$

where the ^{35}Cl nuclear quadrupole coupling constant in the chlorine atom is known experimentally to be -109.7 MHz. If it is now assumed that the p_x orbital can take part in π bonding, but that the p_y orbital cannot interact in this way, then this expression becomes

$$\frac{(eqQ/h)mol}{(eqQ/h)atom} = (1 - a^2)(2 - b) - \frac{\pi}{2} \qquad 1.52$$

This expression can be recast by employing a valence-bond rather than a molecular orbital picture, in which case

$$\frac{(eqQ/h)\ mol}{(eqQ/h)\ atom} = (1 - a^2)(1 - i) - \frac{\pi}{2} \qquad 1.53$$

Here i is the ionic character of the R-Cl bond which is introduced by expressing the wavefunction of the bonding orbital in the valance-bond form

$$\psi_b = (1 - i)\,\tfrac{1}{2}\,\psi(R - Cl) + i\,\tfrac{1}{2}\,\psi(R^+ Cl^-) \qquad 1.54$$

The ionic form R^+Cl^- will of course make no contribution to the quadrupole coupling constant since the chloride ion has spherical symmetry. The other new quantity in equation 1.53, namely π, is normally referred to as the "π- character" of the bond, since it measures the extent of π bonding in the system. It is defined by setting the population of ψ_3, the p_x orbital, equal to $2 - \pi$; in the absence of π-bonding this orbital becomes non-bonding, and so must have a population of 2. The presence of this π bonding results in the loss of the cylindrical symmetry, so that the asymmetry parameter is non-zero, and is related to the π character of the bond by the expression

$$\eta = \frac{3}{2}\,\pi \cdot \frac{(eqQ/h)\ atom}{(eqQ/h)\ mol} \qquad 1.55$$

Equations 1.53 and 1.55 can now be used to analyze the experimental data obtained from nuclear quadrupole resonance spectroscopy in terms of simple bonding parameters. There are however at least three parameters in these expressions (a, i and π) and only the two experimental quantities eqQ and η, so that interpretation of results is not straightforward

unless some simplifying assumptions can be made. Nevertheless the theory is extremely useful in helping to rationalise n.q.r. data, especially when comparisons are to be made among several related compounds.

1.7 Environmental effects in nuclear quadrupole resonance spectroscopy

In all of the preceding discussion it has been tacitly assumed that in nuclear quadrupole resonance the molecule under study can be treated as an isolated entity. Thus the above theory interprets eqQ and η in terms of the intramolecular bonding, and neglects any influence exerted by neighbouring molecules. However, since pure n.q.r. spectroscopy is only applicable to solids, it follows that the spectrum observed for any molecule, even one present in a simple molecular crystal, must be perturbed to some extent by its environment. A number of important consequences follow from this simple statement.

Perhaps the most obvious effect of the crystalline state on n.q.r. is that nuclei which are chemically identical in the isolated molecule may often lie in crystallographically inequivalent sites in the solid, and so have slightly different resonance frequencies. The spread of frequencies observed is normally relatively small, generally less than 500 K Hz. in ^{35}Cl quadrupole resonance. If care is taken to ensure that all the signals have been detected, the n.q.r. spectrum may thus give an indication of the molecular point symmetry in the crystal, so that n.q.r. provides a sensitive method of detecting phase changes.

It is generally found that quadrupole coupling constants

determined in the solid state by n.q.r. are lower by up to 10% than measurements made in the gas phase by microwave spectroscopy. This is true even when the compound in question forms a simple molecular crystal in which the intermolecular forces present are non-specific, so that strong interactions such as hydrogen bonding are absent. The effect is assumed to be partly due to the fact that in the solid each molecule sits in an electric field created by the surrounding dipoles; in order for this to cause a fall in eqQ the dipoles must be oriented so as to tend to make the molecule more ionic. Although this interaction of dipoles is undoubtedly present, there is no reason to suppose that it should always act in the same sense, so we would expect that in some systems it could lead to a rise in eqQ on going from the gas to the solid phase.

To explain the almost universal lowering of the quadrupole coupling constant on going to the solid state it must be remembered that the molecules in the crystal are not static, but are vibrating. Molecular motions in solids have a profound effect on quadrupole resonances, since torsional modes of molecules in the solid cause the nuclei to be agitated at a rate which is very fast compared to the quadrupole resonance frequencies of the nuclei. This affects the relaxation times and also usually averages the quadrupole coupling constant to a lower value than that for the static molecule, explaining the drop in eqQ on going to the solid state which we have noted above. Furthermore the n.q.r. frequency now becomes a function of temperature, falling further as the amplitudes of the torsional motions increase with increasing temperature.

When almost free rotation sets in, as in a solid at an elevated temperature just below its melting point, or when complete tumbling is present and collision frequencies are high, as in a liquid or in a gas under high pressure, then the electric field gradient is time averaged to zero and n.q.r. can no longer be observed.

The sensitivity of nuclear quadrupole resonance to the various solid state effects described here makes the technique an extremely useful probe of the structural environment in molecular solids, and of the nature of the vibrational modes which occur therein.

1.8 Experimental aspects of nuclear quadrupole resonance spectroscopy

The great majority of nuclear quadrupole resonance experiments carried out to date have employed either a marginal oscillator or a super-regenerative oscillator. Marginal oscillators are preferred at frequencies in the range $1 \leq \nu \leq 10$ M.Hz. The major advantage of this type of system over the super-regenerative oscillator is its good lineshape reproduction and its ability to work at low radio-frequency power levels. This makes it suitable for the study of compounds in which nuclei have long relaxation times.

Super-regenerative oscillators can be used at frequencies from 10 MHz. up to at least 700 MHz., and are believed to be inherently more sensitive than marginal oscillators, but until recently it has been difficult to make wide frequency scans with this type of instrument while simultaneously retaining high

sensitivity. More modern spectrometers incorporate automatic gain control systems which improve oscillator stability and therefore simplify the process of searching for resonances in new compounds. A characteristic of the super-regenerative oscillator is that the periodic quenching of the r.f. carrier leads to the presence of strong sidebands at integral multiples of the quench frequency in the oscillator's frequency spectrum. Signals are detected by using low frequency modulation techniques. The recorded n.q.r. signal thus consists of a family of lines whose separation is equal to the quench frequency, and sometimes this makes it difficult to assign the correct resonance frequency. This problem can be overcome by modulating the quench frequency at a rate which is fast compared to the recording time constant, but slow compared to the spectrometer's detection frequency. In these circumstances the frequencies of the sidebands vary continuously and they are no longer detected. The Decca Radar n.q.r. spectrometer used in this work is of the super-regenerative type and has facilities for suppressing sidebands in this way.

Marginal and super-regenerative oscillators can both be operated with either frequency modulation or Zeeman modulation. The use of frequency modulation however carries the risk that piezoelectric effects may give rise to resonances, so that for initial searches in new compounds, Zeeman modulation is preferred.

Nuclear quadrupole resonance can also be detected by pulse techniques, in which case not only the n.q.r. frequencies but also the spin-lattice and spin-spin relaxation times, T_1 and T_2^*, can be measured. Such studies can potentially yield a great deal of information about relaxation phenomena and hence molecular

motion in solids.

1.9 Alternative methods of measuring quadrupole coupling constants.

Although pure nuclear quadrupole resonance spectroscopy is the most widely applicable technique by which quadrupole coupling constants can be measured, there are several other methods by which quadrupole coupling constants can be evaluated, and these are briefly discussed here. We have already indicated that such data is available for some atoms and molecules in the gas phase; for atoms this data can be obtained both by careful analysis of atomic emission spectra and by atomic beam resonance methods. Molecules can be studied in the vapour phase by molecular beam resonance techniques, but the most widely used method of measuring coupling constants for gaseous molecules is pure rotational microwave spectroscopy. All these techniques can yield the sign of eqQ, as well as its magnitude, in contrast to quadrupole resonance which only allows us to measure $|eqQ|$.

It is the solid state however to which most quadrupole coupling constant data refers. We have already discussed the use of Zeeman-n.q.r. experiments where the magnetic field is a small perturbation on the quadrupolar energy levels; the converse situation, in which the quadrupolar interaction acts as a perturbation on the nuclear magnetic resonance spectrum can be readily visualised, and allows us to extract values of quadrupole coupling constants from n.m.r. experiments in suitable solids. Naturally in order to perform such an experiment at moderate magnetic fields the quadrupolar interaction must be relatively small, so that this technique is not suitable for

chlorine - 35 except in ionic chlorides; it is however a good method for nuclei with small quadrupole moments, such as deuterium.

If the quadrupolar nucleus of interest is contained in a paramagnetic molecule the pure n.q.r. lines are often too broad to be easily detectable; in such a case it may be possible to extract the quadrupolar interaction from the electron paramagnetic resonance spectrum, particularly for complexes of transition elements. The phenomena of paramagnetic resonance will be treated at length in a later part of this thesis.

The other important method of measuring quadrupole coupling constants, namely Mössbauer spectroscopy, is unique in that it can be used to investigate nuclei which do not possess quadrupole moments in their ground states. This comes about because the Mössbauer effect is concerned with the resonant absorption of a γ ray by a nucleus, causing the nucleus to jump to an excited state whose nuclear spin quantum number I differs from that of the ground state. The method thus allows the measurement of the difference in the quadrupole coupling constants in the ground and first excited states. It is confined to nuclei in which the first excited state is relatively low lying, and is most useful for ^{57}Fe and ^{119}Sn; in each of these nuclei the quadrupole moment is zero in the ground state, so the technique measures the quadrupole coupling constant in the excited state in these nuclei. Since the quadrupolar splitting of Mössbauer spectra is comparable to the natural linewidth, the accuracy with which the quadrupole coupling constant can be measured is much lower than for the other magnetic resonance techniques mentioned above.

CHAPTER II

THE USE OF CHLORINE - 35 NUCLEAR QUADRUPOLE RESONANCE SPECTROSCOPY FOR STRUCTURAL ASSIGNMENTS IN CHLOROCYCLOTRIPHOSPHAZATRIENES ; CHLORINE N.Q.R. SPECTRA OF SOME ACYCLIC PHOSPHORYL AND PHOSPHINE COMPLEXES

2.1 Introduction

A number of studies [1 - 4] of the ^{35}Cl nuclear quadrupole resonance spectra of compounds containing P–Cl bonds have been carried out ; in the majority of these cases the chlorine is bonded to a tetrahedrally co–ordinated phosphorus atom in a phosphoryl, thiophosphoryl or phosphazene system. The latter class of compounds are of particular interest because the structures are such that (d–p)π bonding may be present between phosphorus and nitrogen, and because there are many chlorine–containing derivatives which are suitable for study by n.q.r. spectroscopy. Thus ^{35}Cl nuclear quadrupole resonance studies have been reported on several chlorocyclophosphazenes including the trimer [5,6], $N_3P_3Cl_6$, the tetramer [5,7], $N_4P_4Cl_8$, and the pentamer [8], $N_5P_5Cl_{10}$. More recently an attempt has been made to compare the results for these species with data obtained from spectra of some substituted trimeric derivatives, [9] and it has been found that a linear relationship exists between the ^{35}Cl n.q.r. frequencies and the associated P - Cl bond lengths in these chlorocyclophosphazenes.

The present work incorporates a systematic investigation of the ^{35}Cl nuclear quadrupole resonance spectra of a series of substituted chlorocyclotriphosphazatrienes, the purpose of which is to determine whether n.q.r. spectroscopy can be routinely

used as an aid to structural assignment in these derivatives or whether its usefulness is limited by sensitivity problems or by the presence of crystal-packing effects. Before proceeding to discuss the results of this study, we pause briefly to consider some facets of the relatively unusual bonding arrangement believed to be present in these compounds.

2.2 Structure and bonding in phosphazenes

Perhaps the most striking features of the phosphazenes are first the high thermal stability of both linear and cyclic derivatives, and second, the fact that phosphorus-nitrogen bond distances in these compounds are shorter than expected for pure covalent σ bonds. In fact the phosphorus-nitrogen skeletal bond distances in cyclo - or polyphosphazenes fall in the range $1.47 \leq d \leq 1.62$ Å, compared to the so-called P-N single bond length of 1.77 Å, as derived from x-ray studies of sodium phosphoramidate,[10,11] and the structural data for the cyclic phosphazenes reveals that bond lengths are generally equal around the ring, unless there is an unsymmetrical arrangement of ligands. Skeletal bond angles at phosphorus approximate to 120° while in the cyclic species, ring angles at nitrogen are close to 120° for trimers and are larger than this in larger rings. These facts indicate that the phosphorus-nitrogen bond in mono- , cyclo- or polyphosphazenes differs from a normal covalent σ bond, yet the overall situation does not resemble the familiar $\sigma - \pi$ bonding of organic chemistry, since spectral effects normally associated with organic π -electron systems, such as the bathochromic ultraviolet shifts which accompany increased delocalization, are absent in the phosphazenes.

In order to derive a bonding scheme capable of rationalising

the facts noted above, we take as our starting point the stereochemistry common to linear and cyclic species in which tetracoordinate phosphorus is linked to dicoordinate nitrogen. It is assumed that the atomic orbitals can be separated into non-interacting sets so that the π orbitals can be treated separately from the σ orbitals. The σ bond framework can now be readily constructed on the basis of the stereochemistry mentioned above ; in a cyclic compound two $2sp^2$ hybrids at each nitrogen and two 3 sp^3 hybrids at each phosphorus are used to define σ bonding around the ring. The two remaining sp^3 hybrid orbitals at each phosphorus are of course used to form bonds to the "ligands". Some distortion of the sp^3 "tetrahedron" is required at phosphorus in order to adapt to the normal ring angle of 120°. The third trigonal hybrid orbital at nitrogen is directed radially and contains a lone pair of electrons while the remaining valence electron at nitrogen is contained in the P_z orbital at right angles to the ring plane.

To explain the bond shortening alluded to above it is now necessary to include some form of π interaction. Such an interaction could take place between the electrons in the nitrogen $2p_z$ orbitals and empty phosphorus $4p_z$ orbitals, if the ligands attached to phosphorus are sufficiently electronegative to cause some contraction of orbitals at phosphorus. This $(p - p)\pi$ bonding model rationalises a number of the special features of phosphazene systems, including the fact that P – N bond strengths increase with ligand electronegativity ; defects of this scheme are that it cannot explain why ring puckering does not seem to affect stability, nor why the barrier to torsion of a phosphorus–

nitrogen bond in a linear phosphazene is low. [12]

In an attempt to overcome these defects the above picture is often modified by introducing the possibility of phosphorus d–orbital participation in the π – bonding. [13,14,15] Unfortunately there are as many arguments against d–orbital contributions to bonding in phosphorus compounds as there are in favour, [16] but in spite of this the concept of (d–p)π bonding in phosphazenes provides the most satisfactory working hypothesis for rationalising the structure and chemistry of these compounds. To build up the bonding scheme including d–orbital involvement the σ bond framework is first constructed as above ; π bonding is assumed to take place in the following two ways.

Firstly, π bonds can be formed between phosphorus and nitrogen by promotion of the remaining valence electron at phosphorus to the 3d level, to occupy either the $3d_{xz}$ or $3d_{yz}$ orbital. Theoretical calculations [17] suggest that the $3d_{xz}$ orbital is contracted from its normal diffuse state in the free atom by the electrostatic field of the ligands, while the $3d_{yz}$ orbital remains fairly diffuse in the complex, so that it is often assumed that the $3d_{xz}$ orbital is more readily available for bonding interactions than the $3d_{yz}$ orbital. A consequence of this approach is that the π system formed, by interaction of this phosphorus $3d_{xz}$ orbital with a nitrogen $2p_z$ orbital is heteromorphic and cyclically delocalized. [18] Other authors have argued that the $3d_{xz}$ and $3d_{yz}$ orbitals should participate equally in the π bond [14] with the result that delocalisation is less extensive. The bonding system which results from interaction of the nitrogen $2p_z$ orbital with the $3d_{xz}$ or with a linear combination of the $3d_{xz}$ and $3d_{yz}$ orbitals at phosphorus is antisymmetric with respect to reflection in the molecular plane and is referred to simply as

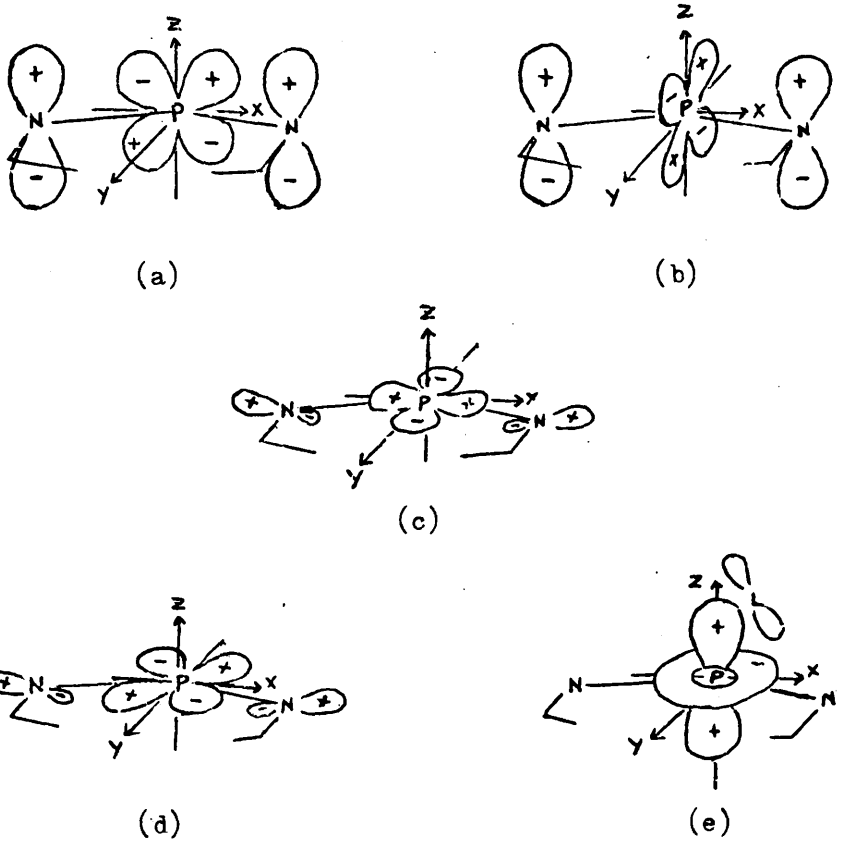

Figure 2.1

Overlap schemes for π -bonding of (a) d_{xz} and (b) d_{yz} with p_z ; (c) π' - bonding of $d_{x^2-y^2}$ and (d) d_{xy} with an sp_y hybrid ; (e) π - bonding of d_{z^2} with a ligand p-orbital.

the " π - system". The orbital overlaps involved are illustrated in Figure 2.1 .

The second interaction which can give rise to π - bonding occurs essentially in the ring plane ; it involves the donation of the lone pair of electrons in the radial nitrogen $2sp^2$ orbital into an empty $3d_{xy}$ or $3d_{x^2-y^2}$ orbital at phosphorus. The resulting " π' - system" is symmetric with respect to reflection in the molecular plane. Again the orbitals which interact to form the " π' - system" are shown in Figure 2.1.

The physical and chemical data available for these complexes can be rationalised in terms of this fairly complex bonding scheme, and the chlorine nuclear quadrupole resonance spectra of some of these complexes are discussed below.

2.3 Chlorine - 35 nuclear quadrupole resonance spectra of substituted chlorocyclotriphosphazatrienes

Chlorine - 35 nuclear quadrupole resonance spectra of a series of substituted chlorocyclotriphosphazatrienes have been investigated in order to assess the usefulness of this technique in obtaining structural information on these derivatives, and the results obtained are presented in Table 2.1 , together with previously reported data [5,6] for $N_3P_3Cl_6$ which is included for comparison. In some cases the observed signals were weak, and spectra were not always observable at both 77K and 293K. Strictly speaking when comparisons are to be made between several compounds, the quadrupole coupling constants are the quantities which should be considered ; however Lucken has shown [19] that the asymmetry parameter in $N_3P_3Cl_6$ is less than 0.02, so that for these compounds $|eqQ/h|$ is effectively equal to twice the observed frequency. It is thus simpler to make

comparisons between the observed ^{35}Cl n.q.r. frequencies, bearing in mind however that these are to be regarded as representative of the quadrupole coupling constants in the molecules considered.

The spectra observed for the monoamino-derivatives $N_3P_3Cl_5NMe_2$ and $N_3P_3Cl_5NC_5H_{10}$ show signals in two distinct regions. Those at higher frequency fall in the range $26.8 \leqslant \nu \leqslant 28.6$ M.Hz., and by comparison with the data for $N_3P_3Cl_6$ these signals must be associated with the $\equiv PCl_2$ groups.[9] The lower frequency signals, falling within the range $24.3 \leqslant \nu \leqslant 25.0$ M.Hz. are thus associated with the $\equiv PCl\,NR_2$ groups. The latter species are expected to have longer P-Cl bonds than the $\equiv PCl_2$ groupings, since the crystal structures of the geminal[20] and the cis non-geminal[21] isomers of $N_3P_3Cl_3(NMe_2)_3$ show that P-Cl bond lengths in $\equiv PCl\,NMe_2$ groups are approximately 2.05Å compared to the usual length of 2.00Å in a $\equiv PCl_2$ group. Thus the results for the monoamino derivatives confirm the trend noted by other workers[9] that the lower ^{35}Cl n.q.r. frequencies in the cyclophosphazenes are associated with the longer P-Cl bonds. We have already seen in the previous chapter that the presence of π - bonding to chlorine is expected to lead to a fall in the ^{35}Cl n.q.r. frequency ; since the lowest frequencies in the phosphazenes are found associated with the longest P-Cl bonds it follows that π bonding between phosphorus and chlorine must be relatively small in these molecules. In these compounds a decrease in the ^{35}Cl n.q.r. frequency and an associated increase in P-Cl bond length can thus both be ascribed to an increase in the degree of ionic character in the P-Cl bond.

These differences between $\equiv PCl_2$ and $\equiv PClNR_2$ groups indicate

TABLE 2.1

Chlorine - 35 n.q.r. data for amino - and phenyl derivatives of $N_3P_3Cl_6$

Compound	m.p. (t/°C)	Structure [a]	n.q.r. frequency (M.Hz.) at 77K	n.q.r. frequency (M.Hz.) at 293K	Reference
$N_3P_3Cl_6$	113		28.3175, 28.3279 28.5982, 28.6842	27.608, 27.684 27.812, 27.880	5,6
$N_3P_3Cl_5NMe_2$	12–14	2,2,4,4,6 : 6	24.930, 24.976 27.463, 27.845 28.406, 28.550 28.116[b]	liquid	d
$N_3P_3Cl_5NC_5H_{10}$	68	2,2,4,4,6 : 6	24.950, 25.000 27.749, 27.806 28.096, 28.154 28.355, 28.408	24.346 26.827, 26.902 27.162, 27.411	e
$N_3P_3Cl_4(NMe_2)_2$	103	2-trans-4,6,6 : 2,4	24.14 , 24.67 27.45	23.50, 23.95 26.40, 26.64	e
$N_3P_3Cl_4(NC_5H_{10})_2$	104–105	2-trans-4,6,6 : 2,4	23.726, 23.770 24.176, 24.218 27.927	23.129[b], 23.185[b] 27.122 (all at 300K)	e
$N_3P_3Cl_4(NMe_2)_2$	86	2-cis-4,6,6 : 2,4	24.073 27.388, 28.139	23.583 26.614, 27.067	d

Compound	m.p. (t/°C)	Structure [a]	n.q.r. frequency (M.Hz.) at 77K	at 293K	Reference
$N_3P_3Cl_4(NC_5H_{10})_2$	129	2-cis-4,6,6 :2,4	c	23.789, 23.964 26.947, 27.080	d
$N_3P_3Cl_5(N = PMe_3)$		2,2,4,4,6 : 6	c	23.917 26.246, 26.879 26.996, 27.415	d
$N_3P_3Cl_5(N = PPh_3)$	215	2,2,4,4,6 : 6	25.120 27.462, 27.636 27.810	24.572 26.662, 26.906 26.994, 27.095	f
$N_3P_3Cl_4(N = PPh_3)_2$	199-200	2,2,4,4 : 6,6	27.44 , 27.75	c	e
$N_3P_3Cl_3Ph_3$	158-159	2-trans-4,6 : 2,4,6	c	23.867, 24.331 24.787	d
$N_3P_3Cl_3Ph_3$	191-192	2-cis-4-cis-6 : 2,4,6	c	23.965, 24.126 24.331, 24.383 24.522	d
$N_3P_3Cl_3Ph_3 \cdot C_6H_6$	-	2-cis-4-cis-6 : 2,4,6	24.277, 24.320 24.668, 24.716 25.052, 25.092	23.893, 24.326 24.385	d

a For nomenclature see R.A. Shaw, B.W. Fitzsimmons and B.C. Smith, Chem. Rev., 1962, 62, 247

b These signals are very weak

c No signals detectable

d This work

e W.H.Dalgleish, R. Keat, A.L. Porte, D.A. Tong, M. Ul-Hasan and R.A. Shaw, J. Chem. Soc. Dalton, 1975, 309

f M.Biddlestone and R.A. Shaw, J. Chem. Soc. Dalton, 1973, 2740

that positional isomers might readily be distinguished by quadrupole resonance, and this is found to be the case. However, it is not clear which of the $\equiv PCl_2$ signals for the monoamino derivatives are assignable to chlorine atoms in a cis - or trans - relationship to the amino group, and an ability to distinguish these signals is obviously important in making structural assignments to geometrical isomers. One argument which might be used to assign these $\equiv PCl_2$ signals derives from studies of halogen atom replacement reactions in cyclophosphazenes where the fact that aminolysis reactions involving dimethylamine or piperidine proceed mainly by non-geminal substitution has been explained by assuming that a "cis-effect" is important in determining the reaction path.[22] The idea underlying the "cis-effect" is that an electron supplying substituent, such as an $-NMe_2$ group, may transfer electron density preferentially to a chlorine atom which is cis - to the dimethylamino group. This would have the effect of making chlorine atoms cis - to the dimethylamino group more labile, and for an ideal S_N2 mechanism would lead to mainly non-geminal trans-substitution patterns ; in terms of n.q.r. frequencies the "cis-effect" predicts that chlorines cis - to an $-NMe_2$ or $-NC_5H_{10}$ group should be more ionic, and hence resonate at a lower frequency, than chlorines trans - to such a substituent. The data summarised in Table 2.1 does not however support the general occurrence of such a "cis-effect".

This difficulty in assigning $\equiv PCl_2$ signals is exemplified by the bisdimethylamino derivatives shown overleaf. Thus the cis-bisdimethylamino - derivative (I) may

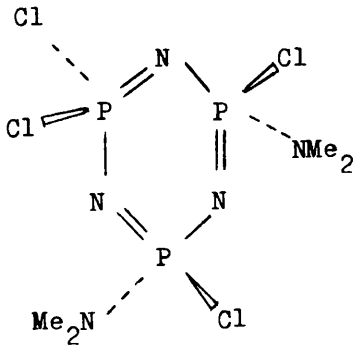

(I)

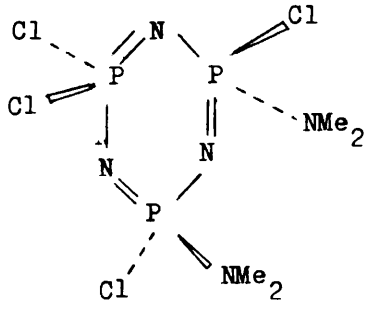

(II)

be expected to have two chemically distinct types of chlorine atom in the $\equiv PCl_2$ group, whereas the trans-bisdimethylamino-derivative (II) should have only one. As expected two $\equiv PCl_2$ signals are indeed observed for the cis-isomers covering a range of 0.5 and 0.2 MHz. for dimethylamino- and piperidino-derivatives respectively. Only one $\equiv PCl_2$ signal is found for the transpiperidino- species as anticipated from its structure, but there are two such signals for the trans-bisdimethylamino- derivative, presumably because of crystal packing effects; however the separation of these two signals is only about half that in the cis-isomer, so that the isomers can be distinguished by n.q.r. so long as both spectra are available. A peculiarity of the trans-bispiperidino-derivative is that the difference between the mean $\equiv PCl_2$ and $\equiv PClR$ frequencies is 3.9 MHz, but for all the other bisamino- derivatives it lies between 2.8 and 3.1 MHz at 293K. This structural feature may imply that steric interactions are leading to a lowering of symmetry here and this is

consistent with the presence of an unusually large splitting of the band corresponding to the P = N stretching vibration in the infra-red spectrum of this compound, both in the solid state and in solution.

Although the problem of assigning $\equiv PCl_2$ resonances to chlorine atoms cis- and trans- to a substituent make it difficult to distinguish geometrical isomers by means of n.q.r. spectroscopy at atmospheric pressure, it has been found that, at least in certain cases, it is possible to distinguish geometrical isomers by studying the effects of pressure changes on chlorine nuclear quadrupole resonance frequencies. This topic is discussed in detail in Chapter IV.

Two other features of the spectra of the amino-derivatives are worthy of mention. First we note that, despite the relatively small amount of data available, it is clear that the $\equiv PClR$ frequencies are characterised by a smaller temperature dependence than the $\equiv PCl_2$ frequencies. The second point is that there is a clear trend for both $\equiv PCl_2$ and $\equiv PClR$ resonances to move to lower frequencies with increasing degree of aminolysis; this implies that the electron-releasing effect of the amino-groups is not localised on the phosphorus atom to which they are bonded, but is transmitted around the ring framework affecting all the chlorine atoms to some extent. This is to be expected in view of the fact that both σ and π bonding occur around the ring, and is consistent with the ability of one substituent to influence the position of attack of a second reagent, as in the "cis-effect".

Data is also reported in Table 2.1 concerning the ^{35}Cl n.q.r. spectra of two triphenylphosphazenyl cyclotriphosphazatrienes and one analogous trimethyl derivative; as before signals are observed in two distinct frequency regions. Resonances of chlorine atoms in

$\equiv PCl_2$ groups occur within the range $26.2 \leq \nu \leq 27.8$ M.Hz., that is slightly lower in frequency than the corresponding signals in phosphazenes with amino substituents, while resonance frequencies for $PCl(N{=}PPh_3)$ and $PCl(N{=}PMe_3)$ groups fall in the range $23.9 \leq \nu \leq 25.2$ M.Hz. The slight lowering of ^{35}Cl n.q.r. frequencies on going from amino - to phosphazenyl substituents probably reflects the greater electron donating ability of the two-coordinate nitrogen atom in the phosphazenyl substituents.

Table 2.1 also shows the results of some studies of the quadrupole resonance spectra of some phenyl substituted cyclotriphosphazatrienes. The geminal phenyl derivatives $N_3P_3Cl_{6-n}Ph_n$ (n = 2 and 4) have been shown [9] to give ^{35}Cl n.q.r. signals in the range $26.3 \leq \nu \leq 28.3$ M.Hz. at 77K. Although the non-geminal cis - and trans- triphenyl derivatives $N_3P_3Cl_3Ph_3$ gave no signals at this temperature, the results obtained at 293K clearly show that $\equiv PCl_2$ and $\equiv PClPh$ groups have characteristic frequency ranges, with the latter group covering $23.8 \leq \nu \leq 24.8$MHz. The resonance frequencies observed for trans-$N_3P_3Cl_3Ph_3$ are spread over a wider range (1 M.Hz.) than those for cis- $N_3P_3Cl_3Ph_3$ (0.6 M.Hz.) as expected from the chemical inequivalence of the chlorine atoms in the former. The range observed for the cis-isomer may be extended by the presence of more than one molecule in the asymmetric unit, as is suggested by the fact that five signals are observed for this molecule. The presence of a benzene molecule within the crystal lattice has little effect on the frequency range observed for the cis-isomer. There is however an increase in the number of signals observed when the clathrate complex is cooled from room temperature to 77K, implying either the occurrence of a phase change between these temperatures or simply a freezing out of

vibrational motion of the guest benzene molecules within the lattice.

Since the ^{35}Cl resonance frequencies for compounds of related structure containing - NMe_2, - Ph, - N = PPh_3 or - N = PMe_3 groups fall into similar frequency ranges, it is reasonable to assume [9] that the P - Cl bonds are of a similar length. This contention is consistent with the observation that the P - Cl bond lengths are equal within experimental error in the nongeminal (2,4,6,8 : 2,4,6,8 structures) tetrameric derivatives $N_4P_4Cl_4R_4$ where R = Ph [23] and NMe_2 [24].

The results obtained for the cyclotriphosphazatrienes can be briefly summarised in that chlorine - 35 n.q.r. frequencies characteristic of $\equiv PCl_2$, $\equiv PClNR_2$, $\equiv PClPh$ and $\equiv PCl$ (N = PR_3) groups occur in the ranges 26 - 29, 22 - 25, 23 - 25 and 23.5 - 25.5 M.Hz. respectively at both 77K and 293K. The characteristic frequency ranges of the last three functional groups overlap so these groups cannot be distinguished by this technique. It is possible to distinguish cis- and trans- isomers by chlorine - 35 n.q.r. spectroscopy, by comparison of the range of frequencies observed, but in general this is only possible when results for both isomers are available. It turns out that, as discussed later in Chapter IV, a study of the chlorine - 35 n.q.r. spectrum as a function of applied hydrostatic pressure can, at least in some cases, make it possible to assign $\equiv PCl_2$ resonances to chlorines cis- and trans- to an amino substituent, and so potentially provides a simple method of distinguishing geometrical isomers in cyclotriphosphazenes.

2.4 Acyclic phosphoryl and phosphine complexes

In addition to the cyclophosphazenes discussed above, the nuclear quadrupole resonance spectra of a small number of acyclic compounds containing P - Cl bonds have also been investigated; the results of these studies are reported in this section. The data obtained for three of these compounds is tabulated in Table 2.2, together with data for similar species reported by other workers. In general we find that the results can be fairly simply rationalised in terms of the amount of electron donation or withdrawal expected from the substituents present, so that, as previously noted for the cyclophosphazenes, phosphorus-chlorine π -bonding may be assumed to be absent.

The frequencies found for the triphenyl phosphazenyl - phosphoryl chloride, $Ph_3P = N - P(O)\ Cl_2$ show that, as we have noted in the cyclophosphazenes, there is again a marked fall in the ^{35}Cl n.q.r. frequency on replacing one chlorine atom by an electron releasing phosphazenyl residue. This compound has of course an extended π -system, so that the P-N "single" bond will have some multiple bond character. The fall in frequency on going from $P(O)Cl_3$ to $Ph_3P = N - P(O)Cl_2$ is of the order of 3 M.Hz. once we have allowed for the different temperatures used in making the measurements. This compares with a drop in frequency of about 2.5 M.Hz. on replacing one chlorine in $P(O)Cl_3$ by a dimethylamino - group,[25] and confirms the greater electron donorability of the phosphazenyl group than the dimethyl - amino group, which we noted earlier.

Table 2.2

^{35}Cl n.q.r. data for acyclic phosphoryl and phosphine compounds containing P – Cl bonds.

Compound	^{35}Cl n.q.r. frequency (M.Hz.)	Temperature (K)	Reference
Phophorus V derivatives			
$P(O)Cl_3$	28.938, 28.986	77	2
$Ph_3P{=}N{-}P(O)Cl_2$	25.088, 25.463	293	a
$\left[Cl_2P(O)\right]_2 CH_2$	26.755, 26.771 26.997, 27.008	293	a
Phosphorus III derivatives			
PCl_3	26.107, 26.202	77	30
$PCl_2(NMe_2)$	23.135, 24.450 (α phase) 23.692, 23.892 24.098, 24.314 (β phase)	77	25
$PCl(NMe_2)_2$	18.508	77	25
$(Cl_2P)_2 N Bu^t$	24.428, 24.851 25.123, 25.136	293	a

a This work

As expected, the n.q.r. frequencies of $\left[Cl_2P(O)\right]_2CH_2$ are intermediate between those of $P(O)Cl_3$ and $Ph_3P=N-P(O)Cl_2$. The structure of $\left[Cl_2P(O)\right]_2CH_2$ in the solid state [26] is unusual in that the molecules are linked together through $\geqslant C-H - - - - O=P\leqslant$ hydrogen bonds into infinite chains in the Z-direction. The P-Cl bonds are not very different in character from those in $P(O)Cl_3$, as shown by the fairly similar P-Cl bond lengths (1.994 and 1.997 Å in $\left[Cl_2P(O)\right]_2CH_2$ compared with either 1.989 or 1.993 Å in $P(O)Cl_3$ as measured by microwave spectroscopy [27] and electron diffraction [28] respectively) and by the similarity of the ^{35}Cl n.q.r. frequencies after allowing for the temperature difference of the measurements. Since the P - Cl bond length [29] in $Ph_3P=N-P(O)Cl_2$ is 2.025(1)Å, it follows that there is an approximate relationship between P - Cl bond length and ^{35}Cl n.q.r. frequency for these phosphoryl compounds, which is in the same sense as the linear relationship found in the chlorocyclophosphazenes. [9]

The ^{35}Cl n.q.r. spectrum of the phosphorus (III) complex $(Cl_2P)_2NBu^t$ is also reported in Table 2.2. Very much less n.q.r. data is available for phosphorus (III) halides than for the phosphazene and phosphoryl systems. Thus ^{35}Cl nuclear quadrupole resonance spectra have been recorded only for PCl_3 itself,[30] the fluorine [31] derivatives PF_nCl_{3-n} (n = 1,2) and for CH_3PCl_2, [32,33,34] $(C_2H_5)PCl_2$, [33,34] and $PhPCl_2$ [32] as well as for two chlorophosphinoamines; [25] data for some of these is included in Table 2.2 for comparison purposes.

Once again we find that the effect of replacing chlorine by amino substituents is to allow the remaining chlorine atoms in the molecule to pull more electron density to themselves, resulting in a fall in the observed frequency. The frequencies found for

$(Cl_2P)_2$ N Bu^t are in close agreement with the values which would be predicted from the data on other amino- derivatives quoted in Table 2.2 since an - $N(Bu^t)PCl_2$ substituent would be expected to donate rather less electron density than a dimethylamino residue, resulting in a slightly higher resonance frequency in $(Cl_2P)_2$ NBu^t than in $PCl_2(NMe_2)$.

The series of mixed chlorofluorides, PF_nCl_{3-n} (n = 1,2) do not follow these simple electronegativity trends. This is not surprising since fluorine is so strongly electronegative that its presence is likely to cause some change in the hybridisation at phosphorus, and may even allow chlorine to engage in π- bonding to phosphorus, so that the bonding pattern in these mixed halides must be markedly different from that in the amino-substituted compounds $PCl_2(NMe_2)$ and $(Cl_2P)_2$ NBu^t.

One other compound has been studied in the present work, namely $Cl_2P(O)$ - N(Me)-PCl_2 whose n.q.r. frequencies should be in line with the data obtained above for phosphoryl and phosphine derivatives. Very strong signals were observed for this compound at room temperature, so that both ^{35}Cl and ^{37}Cl n.q.r. spectra could be recorded, although most of the ^{37} Cl peaks could not be resolved at 77K. The data obtained for this species is summarised in Table 2.3. The ^{35}Cl spectrum at room temperature consists of two groups of two peaks, each of these signals being split into a doublet at 77K. The increase in signal multiplicity on cooling is indicative of a phase change or, in view of the relative flexibility of the linear molecule, of a freezing out of some torsional motion of the system on cooling. If we restrict attention to the room temperature spectrum in order to assign the signals

Table 2.3

^{35}Cl and ^{37}Cl n.q.r. data for $Cl_2P(O) - N(Me) - PCl_2$

n.q.r. frequencies (M.Hz.) at 77K		n.q.r. frequencies (M.Hz.) at 293K[c]		Ratio $\frac{\nu(^{37}Cl)}{\nu(^{35}Cl)}$ [b]
^{37}Cl	^{35}Cl	^{37}Cl	^{35}Cl	at 293K
21.470	25.321			
	25.392	19.522	24.704	0.790
a	25.750	19.870	25.164	0.789
	25.833			
	27.135			
	27.201	21.018	26.644	0.789
	27.917	21.480	27.229	0.789
	27.987			

a Other ^{37}Cl signals were too weak at 77K to be distinguished from the background electronic noise

b This should be compared with the ratio of the nuclear quadrupole moments, $\frac{Q(^{37}Cl)}{Q(^{35}Cl)} = 0.788$

c Intensities of ^{35}Cl signals are three times those of the corresponding ^{37}Cl resonances.

observed, then we can say with certainty that the two high frequency signals (26.644 and 27.229 M.Hz.) are associated with chlorine atoms in the $-P(O)Cl_2$ fragment, since the frequencies are typical of those found for chlorines in this type of environment. The remaining resonances, at 24.704 and 25.164 M.Hz., are now assigned to chlorines in the $-PCl_2$ group, and the data shown in Table 2.2 confirms that this assignment is reasonable.

It is very noticeable that the quadrupole resonance spectra of the acyclic compounds which have been investigated here exhibit the same trends at the cyclic phosphazenes discussed earlier, showing the essential similarity of the type of bonding influences present in all these systems.

2.5 Experimental

All n.q.r. spectra were recorded using a Decca Radar nuclear quadrupole resonance spectrometer which employs a super-regenerative oscillator operating within the frequency range $5 \leq \nu \leq 55$ M.Hz. Resonances were recorded using bi-directional Zeeman modulation, and frequencies were measured by interpolation between calibration markers automatically printed on the recorder chart at 25K.Hz. intervals.

The samples to be studied were sealed in thin walled glass ampoules. Spectra could be recorded at ambient temperature and, by immersing the complete probe, containing the sample, in liquid nitrogen, at 77K.

The compounds were synthesised by literature methods. Thus the dimethylamino-cyclotriphosphazatrienes are readily prepared [35]

by the reaction of $N_3P_3Cl_6$ with dimethylamine in ether solution; isomers can be separated by chromatographic techniques. A similar technique [22] was used to prepare the piperidino derivatives of $N_3P_3Cl_6$, while the phenyl substituted chlorophosphazenes were made by reacting phenyltetrachlorophosphorane with ammonium chloride in an inert solvent such as chlorobenzene. [36] The phosphazenyl-cyclophosphazenes were synthesised [37,38] by reacting the appropriate monophosphazene with $N_3P_3Cl_6$.

As for the linear compounds investigated, $[Cl_2P(O)]_2 CH_2$ was prepared as described by Maier, [39] by reacting a mixture of $[(EtO)_2P(O)]_2 CH_2$ and $[(HO)_2P(O)]_2 CH_2$ with a large excess of PCl_5; the preparation of $(Cl_2P)_2N Bu^t$ involves the reaction of PCl_3 with the primary amine hydrochloride salt. [40] $Ph_3P = N-P(O)Cl_2$ was synthesised [41] from the species $[Ph_3P = NPCl_3]^+Cl^-$, while $Cl_2P(O) - N(Me) - PCl_2$ is prepared by reacting phosphoryl (V) chloride with hexamethyldisilazane, $(Me_3 Si)_2 NH$ to give $Cl_2P(O)N(Me)-SiMe_3$ which can then be refluxed with PCl_3 to give the product. [42]

A number of compounds were studied in which signals were not detected. These were $N_3P_3Cl_4 (NHEt)_2$ trans, $N_3P_3Cl_3(NEt_2)_3$ trans, $N_3P_3Cl_2(NC_5H_{10})_4$ cis, and $[Cl_2P(S)]_2 NPh$.

2.6 Summary

The results obtained may be summarised by saying that in the chlorocyclotriphosphazatrienes $\equiv PCl_2$ groups may be distinguished from $\equiv PClR$ species (R = N (alkyl)$_2$, aryl or a phosphazenyl substituent) since the ^{35}Cl n.q.r. frequencies fall into distinct frequency ranges. Unfortunately the frequencies characteristic of $\equiv PClR$, $\equiv PClNR_2$ and $\equiv PCl(N = PR_3)$ groups overlap so that they cannot be distinguished simply by ^{35}Cl n.q.r. spectroscopy. Despite this difficulty, the technique provides a very useful probe of cyclic phosphazene systems

and provides a relatively simple method of distinguishing cis - and trans-isomers, so long as spectra can be obtained for both derivatives.

The studies of the acyclic phosphoryl and phosphine compounds reveal that the major influence on the observed n.q.r. frequency appears to be the degree of ionic character of the P–Cl bond; the trend in frequencies for a series of derivatives can be simply rationalised in terms of the relative electron-donating or withdrawing powers of the substituents.

In the next chapter the quadrupole resonance studies are extended to some chlorocyclodiphosphazanes, and the spectra of these compounds are investigated over a wide range of temperatures and pressures. The results of the studies reported in Chapter III imply that the changes in n.q.r. frequencies caused by temperature and pressure changes should be characteristic of the P–Cl bending modes of vibration occurring in the solid, and these ideas are applied to some cyclotriphosphazatrienes in Chapter IV.

CHAPTER III

CHLORINE - 35 NUCLEAR QUADRUPOLE RESONANCE SPECTRA OF THE CHLOROCYCLODIPHOSPHAZANES, $(Cl_3PNR)_2$, AND OF THE CHLOROOXOCYCLODIPHOSPHAZANES, $(Cl(O)PNR)_2$

3.1 Introduction

Nuclear quadrupole resonance spectroscopy has been extensively used to probe the environment of ^{35}Cl nuclei bonded to phosphorus. In the majority of these studies however the phosphorus atom is in its most common structural environment, that is tetrahedrally coordinated. Studies of ^{35}Cl n.q.r. spectra of chlorine atoms bonded to phosphorus in a trigonal bipyramidal environment are less common, but have been carried out[1] for the phosphorus (V) chlorofluorides, $PCl_{5-n}F_n$ where n = 1, 2 or 3, for molecular phosphorus pentachloride[2], for the phenylchlorophosphoranes[3], $PCl_{5-n}Ph_n$, where n = 1 or 2, and for the cyclodiphosphazanes,[4,5] $(Cl_3PNR)_2$ where R = CH_3, C_2H_5 or Ph. The latter group of compounds are dimers of the N substituted phosphinimines, $Cl_3P = NR$. It is found that a high electron density at nitrogen is necessary for dimerisation, so that dimers are formed if the parent amine is a strong base. When electron-attracting groups are attached to nitrogen the phosphinimine is the more stable species.[6] The cyclodiphosphazanes can be depolymerised to the phosphinimines, $Cl_3P = NR$, by refluxing in a suitable inert solvent.[7,8,9]

Crystal structure analyses[10,11] of 1,1,1,3,3,3-hexachloro-2,4-dimethylcyclodiphosphazane, $(Cl_3PNCH_3)_2$, show that this molecule has the centrosymmetric structure (I) in which hybridisation at phosphorus is based on a trigonal bipyramid, and the ring nitrogen atoms occupy both axial and equatorial sites. Coordination

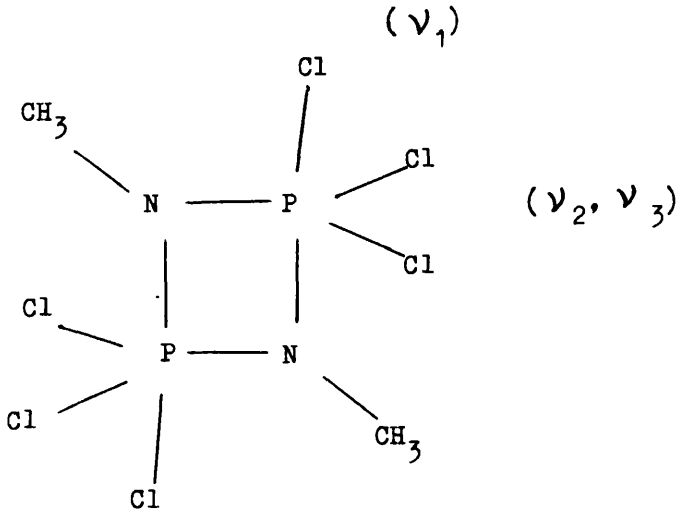

(I)

around nitrogen is planar. The axial P-Cl bonds, at 2.15Å , are significantly longer than the equatorial P-Cl bonds (2.02Å). There is a similar difference in the P-N skeletal bond lengths, since the equatorial P-N bonds are contracted by 0.15Å from the length of a "normal" P-N single bond. Thermochemical data [12] also confirm that axial P-N bonds are weaker than the corresponding equatorial bonds, by about 9 K.cal. The far infrared spectrum in solution (30-450cm^{-1}) for $(Cl_3PNMe)_2$ has been recorded[13] and a normal coordinate analysis has been carried out[13] on it and on the closely related molecule $(F_3PNCH_3)_2$.

This body of data implies that the bonding in the cyclodiphosphazanes is fairly complex. The fact that the formation of these dimeric species is favoured by the presence of electron withdrawing groups at phosphorus might be taken to indicate that contraction of the d-orbitals on phosphorus is necessary to allow them to participate in bonding, before the dimer becomes more stable

Table 3.1

Chlorine - 35 nuclear quadrupole resonance data for $(Cl_3PNR)_2$ where R = CH_3, C_2H_5 or Ph.

R	Position of Cl	Frequency (M.Hz.) 77K	293K	Difference Frequency (M.Hz.)
CH_3	axial (ν_1)	25.823	25.617	0.206
	equatorial (ν_2)	30.007	29.587	0.420
	(ν_3)	30.351	29.778	0.573
C_2H_5	axial (ν_1)	26.186	26.033	0.153
	equatorial (ν_2)	30.456	30.010	0.446
	(ν_3)	30.540	30.096	0.446
Ph	axial (ν_1)	26.375	26.139	0.236
	equatorial (ν_2)	30.579	30.081	0.498
	(ν_3)	30.790	30.122	0.668

$\nu_{77} = 25.823$
$\nu_{293} = 25.617$
$\Delta\nu = 0.206$

$\nu_{77} = 26.186$
$\nu_{293} = 26.033$
$\Delta\nu = 0.153$

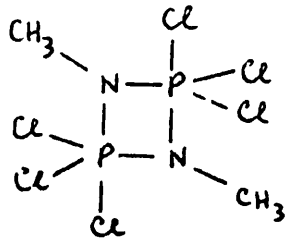

$\nu_{77} = 30.007$
$\nu_{293} = 29.587$
$\Delta\nu = 0.420$

$\nu_{77} = 30.351$
$\nu_{293} = 29.778$
$\Delta\nu = 0.573$

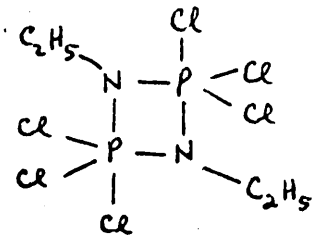

$\nu_{77} = 30.456$
$\nu_{293} = 30.010$
$\Delta\nu = 0.446$

$\nu_{77} = 30.540$
$\nu_{293} = 30.096$
$\Delta\nu = 0.446$

$\nu_{77} = 26.375$
$\nu_{293} = 26.139$
$\Delta\nu = 0.236$

$\nu_{77} = 29.242$
$\nu_{77} = 29.274$

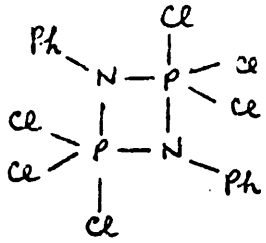

$\nu_{77} = 30.579$
$\nu_{293} = 30.081$
$\Delta\nu = 0.498$

$\nu_{77} = 30.790$
$\nu_{293} = 30.122$
$\Delta\nu = 0.668$

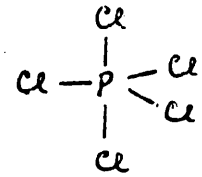

$\nu_{77} = 33.751$

Figure 3.1 Chlorine – 35 n.q.r. frequencies and difference frequencies for $(Cl_3 PNR)_2$ where R = CH_3, C_2H_5 or Ph, and for molecular PCl_5. All frequencies are given in M.Hz.

than the monomeric phosphinimine. This is in agreement with the fact that dimerisation is favoured if the parent amine is a strong base. Thus the picture which emerges is one in which some π interaction is possible between the nitrogen lone pair orbital and the empty phosphorus d orbitals. Support for this picture comes from the unusual coordination around nitrogen; the three bonds at each nitrogen are coplanar, leaving the nitrogen lone pairs, in $2p_z$ orbitals at right angles to the plane of the ring, free to participate in supplementary π bonding. Again this concept is in keeping with the crystal structure data which shows that equatorial bonds are considerably shortened from the single bond length, whereas the axial bonds, which in the trigonal bipyramid are often considered to utilise a phosphorus hybrid involving the d_{z^2} orbital, has the same length as a "conventional" P-N single bond. The structure of the cyclodiphosphazanes can thus be rationalised most simply in terms of an alternation of σ and π bonding around the ring.

Chlorine -35 nuclear quadrupole resonance spectra[4] of the cyclodiphosphazanes $(Cl_3PNR)_2$ where R = CH_3, C_2H_5 or Ph, show that all three molecules are centrosymmetric and that axial chlorine atoms can be readily distinguished from equatorial chlorine atoms in the bipyramid, first by the large differences in their characteristic quadrupole resonance frequencies and second, by the characteristic differences that are observed when the resonance frequencies at 77K are compared with the corresponding frequencies at 293K. These characteristic frequencies and difference frequencies are listed in Table 3.1 and Figure 3.1, and a typical spectrum obtained for $(Cl_3PNCH_3)_2$ is shown in Figure 3.2.

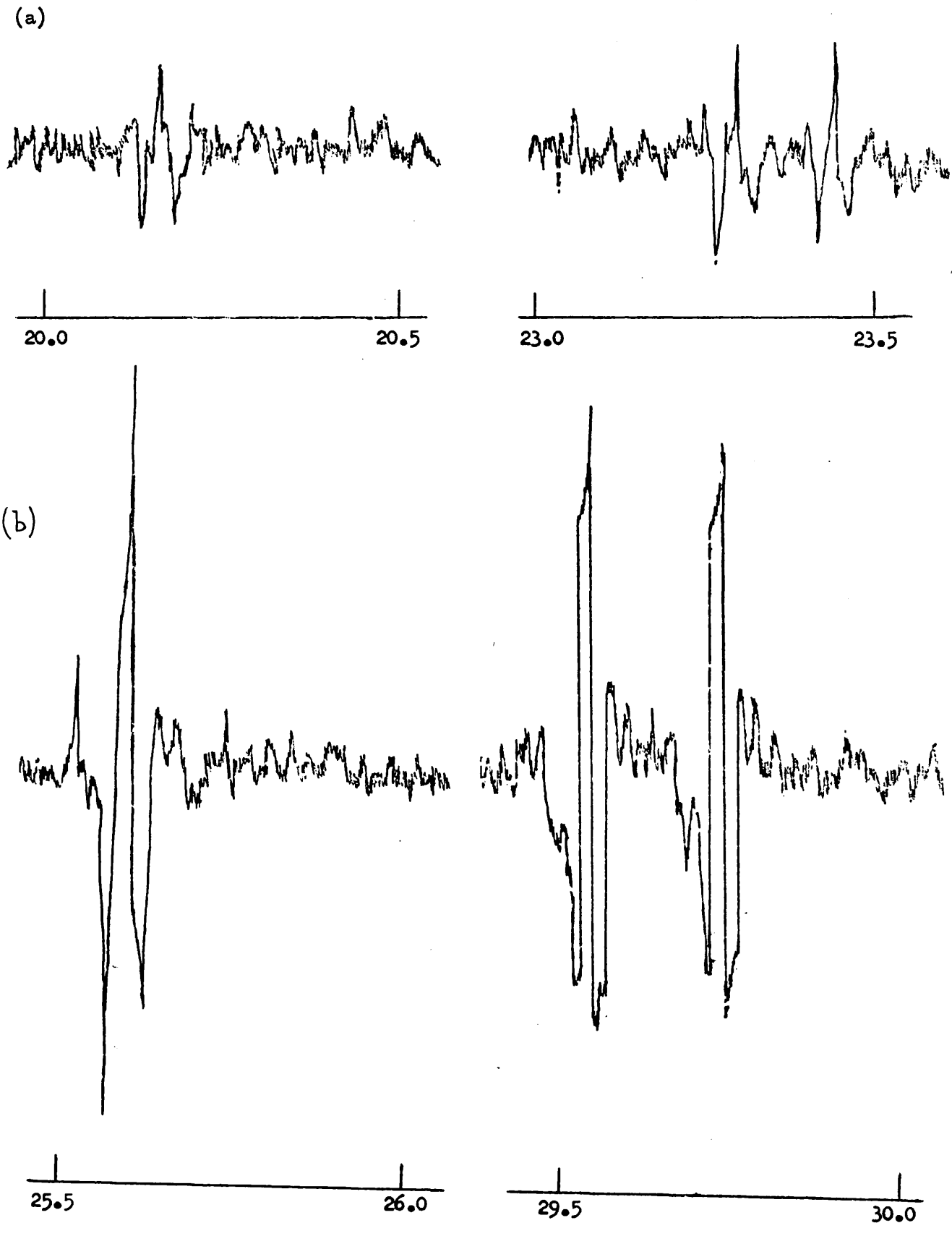

Figure 3.2 Chlorine – 37(a) and chlorine – 35(b) n.q.r. spectra of $(Cl_3PNCH_3)_2$ at room temperature, recorded using Zeeman modulation. Frequencies are in M.Hz.

The origin of these very characteristic effects is not fully understood, so these quadrupole resonance spectra have been examined in detail. The effects on the chlorine - 35 nuclear quadrupole resonance spectra of the cyclodiphosphazanes when they are subjected to (I) magnetic fields within the range $0 \leqslant H \leqslant 30$ gauss, (II) to pressures within the range $1 \leqslant P \leqslant 1500$ Kg. cm^{-2} and (III) to temperatures within the range $77 \leqslant T \leqslant 350$K are reported in the following sections.

3.2. The nuclear quadrupole resonance spectrum of $(Cl_3PNCH_3)_2$ in an applied magnetic field.

It has not been possible to grow large enough single crystals of any of the cyclodiphosphazanes to enable the "zero-splitting locus" [14] or the "frequency-field" [15] methods to be used to determine the asymmetry parameters in these compounds, and so our Zeeman studies have been limited to polycrystalline samples of $(Cl_3PNCH_3)_2$. When the orientation of a single crystal in a magnetic field is altered, then the transition energies and transition probabilities of each of the four allowed chlorine - 35 transitions are altered, [16] so that the spectrum obtained from a polycrystalline sample consists of a superposition of the spectra associated with each orientation, weighted in proportion to the probability of finding the crystallite at that particular orientation. The forms of this spectrum and of its derivative have been worked out by Morino and Toyama, [17] for the case in which the weak magnetic field is parallel to the radio-frequency field used to excite the transitions, and they have shown that the resulting lineshape is sensitive to the value of η. Other workers have demonstrated [18] that when the r.f. and Zeeman fields are perpendicular, the resonance lineshape and position are

insensitive to η . Thus the asymmetry parameter can be estimated from n.q.r. spectra of a polycrystalline sample in a weak static magnetic field, provided that the Zeeman field is parallel to the r.f. field. The use of a polycrystalline sample means of course that this method cannot provide information about the orientation of the principal axes of the electric field gradient relative to the crystal axes, and this places the technique at a disadvantage compared with the single crystal methods.

In calculating the lineshape expected from a polycrystalline sample, Morino and Toyama employ a number of simplifying assumptions. As already mentioned the Zeeman and radiofrequency magnetic fields are constrained to be parallel to each other and are also assumed to be homogeneous over the sample volume; the absorption line is taken to be very sharp in the absence of a static field, and the sample is assumed to consist of a large number of crystallites oriented at random. Morino and Toyama now proceed to calculate the lineshape by essentially a first-order perturbation theory approach;[17] in the parallel fields the splitting frequency, $\nu_{\pm}(\theta,\phi)$ and the intensity, $P_{\pm}(\theta,\phi)$ of each Zeeman component are found to be

$$\left|\nu_{\pm}(\theta,\phi)\right| = \tfrac{1}{2}\nu_L \left|(4-3\cos^2\theta)^{\frac{1}{2}} \mp 3\left|\cos\theta\right|\right| \qquad 3.1$$

$$P_{\pm}(\theta,\phi) = \tfrac{3}{8}\sin^2\theta\left[1 \pm \frac{\left|\cos\theta\right|}{(4-3\cos^2\theta)^{\frac{1}{2}}}\right] \qquad 3.2$$

for the case $\eta = 0$. The "splitting" frequency $\nu_{\pm}(\theta,\phi)$ is defined as the difference between the pure n.q.r. frequency and the transition frequency in the weak static field, the + and − signs indicating the inner (α) and outer (β) pairs of the Zeeman components respectively. In these expressions θ and ϕ denote

the polar co-ordinates of the Zeeman field with respect to the principal axes of the e.f.g. at each nuclear site. Intensities are measured on an arbitrary scale, and ν_L is the Larmor frequency for the nuclei in the applied field. The shape function describing the envelope of the absorption line broadened by the static field is now simply shown to be

$$I(\nu) = \frac{N}{12\nu_L}(4 - f^2) \qquad \text{for } |f| \leq 1$$

and

$$I(\nu) = \frac{N}{24\nu_L}\left[(4 - f^2) + |f|\left\{3(4-f^2)\right\}^{\frac{1}{2}}\right] \qquad \text{for } 1 < |f| \leq 2 \qquad 3.3$$

where N is a normalisation constant and $f = \nu \pm / \nu_L$

This approach can be extended to the case $\eta \neq 0$, to give a new expression for the shape function of the form

$$I(\nu) = \frac{N}{2\pi\nu_L}\left[\frac{|\epsilon|}{(1 + |\epsilon|)}\right] \cdot F\left\{\frac{\pi}{2}, \frac{2|\epsilon|^{\frac{1}{2}}}{(1 + |\epsilon|)}\right\}$$

where

$$\epsilon = \frac{|f| - 1}{\eta} = \frac{|\nu| - \nu_L}{\eta\nu_L}$$

and

$$F(\phi, k) = \int_0^{\phi} \frac{dx}{(1-k^2 \sin^2 x)^{\frac{1}{2}}} \qquad 3.4$$

The behaviour of the shape function can now be plotted out, and the resulting curve is illustrated in Figure 3.3 together with its derivative. The singularities in the absorption curve occur at $\pm(1 \pm \eta)\nu_L$, so that an estimate of η can be made by measuring the frequencies of these four points. The spectrum is normally analysed by measuring the linewidth parameter δ_1, shown in Figure 3.3; since this corresponds to the "peak to peak linewidth" for the $\pm \nu_L$ regions of the derivative spectrum, the ratio $\delta_1 / 2\nu_L$ should equal the asymmetry parameter, so long as the original linewidth is negligible. In practice η is normally measured by plotting

$\delta_1/2\nu_L$ against the reciprocal of the magnetic field strength, and extrapolating to infinite field, since the original linewidth becomes progressively less important as field strength increases.[17] The extrapolation procedure is aided by the fact that in the low field limit $\delta_1/2\nu_L$ is asymptotic to $\Delta\nu/2\nu_L$ where $\Delta\nu$ is the original (zero-field) linewidth and also by the fact it reaches a minimum at some intermediate field, before approaching the $(H^{-1}) = 0$ axis along the curve $(\eta - \Delta\nu/2\nu_L)$, so long as the original line is gaussian in form.[17,19] The magnitude of magnetic field needed to make the splitting due to the asymmetry greater than the original linewidth is given by the expression

$$H > \frac{2\pi\Delta\nu}{\eta|\gamma|} \qquad 3.5$$

Measurement of asymmetries by this method is thus relatively straightforward, although the very marked broadening of the signal in the presence of the Zeeman field restricts the method to compounds which have strong zero-field quadrupole resonance signals. The other major limitation of this particular technique is that since the calculation outlined above proceeds by a perturbation method, the lineshape illustrated in Figure 3.3 is strictly applicable only for $\eta < 0.2$. In order to use Zeeman - n.q.r. spectroscopy to calculate η for a species in which the asymmetry may be quite large an alternative approach is required; several workers have recently tried to provide this by simulating powder patterns for Zeeman - n.q.r. spectroscopy using numerical techniques, and some promising results have been obtained.[19-22]

In the present work the technique adopted in analysing the Zeeman spectra is essentially that of Morino and Toyama. The

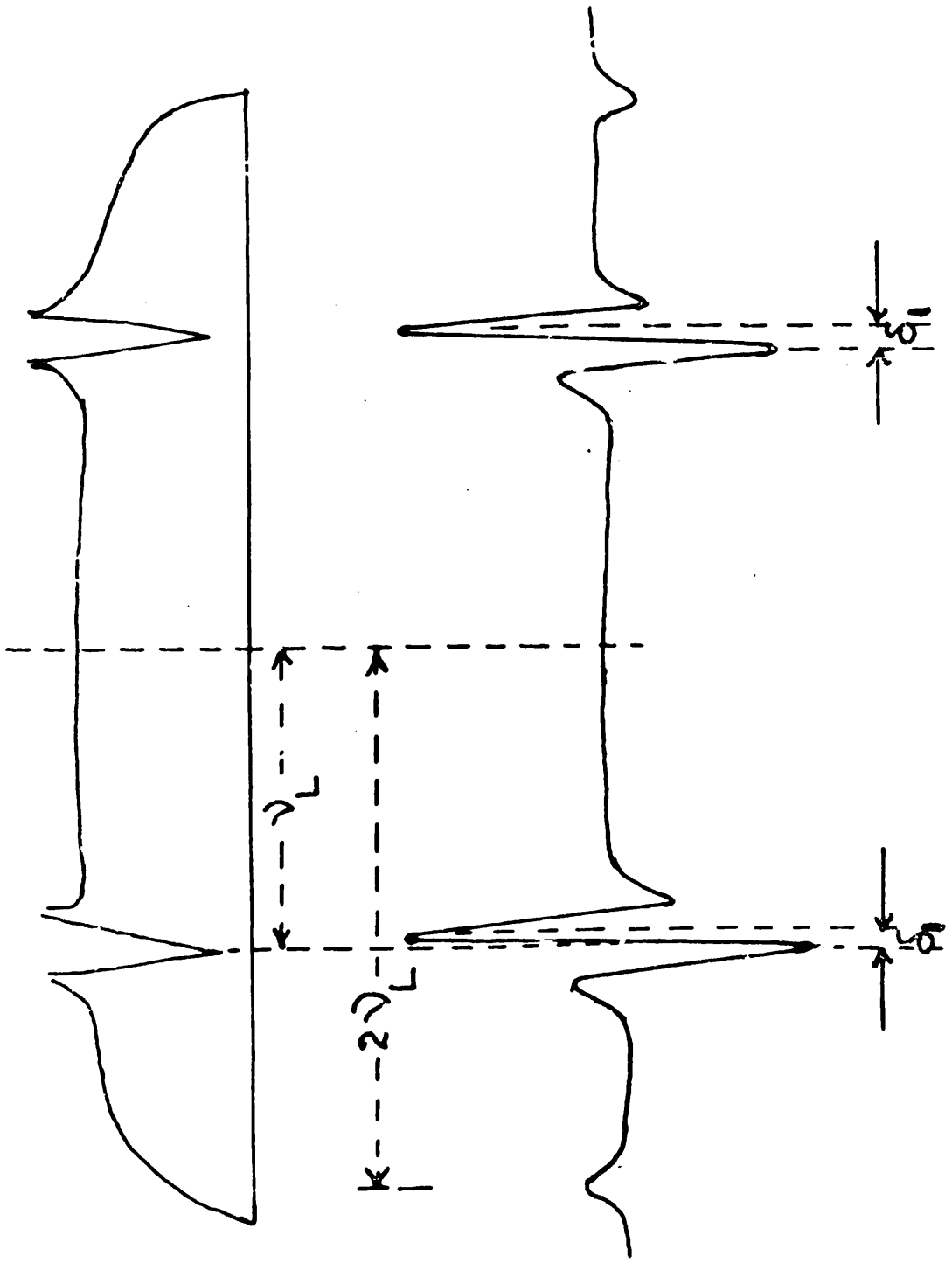

Figure 3.3 N.q.r. absorption spectrum, and corresponding first derivative spectrum of a polycrystalline sample subjected to a magnetic field : the asymmetry parameter, η , is assumed to be small.

chlorine - 35 n.q.r. spectrum of $(Cl_3PNCH_3)_2$ has been studied in weak magnetic fields of up to 30 gauss, generated by a Helmholtz coil arrangement, and all spectra were detected and recorded using the spectrometer system previously described, together with a time averaging computer. The experimental aspects of these measurements are discussed more fully in Appendix A.

A typical spectrum obtained from one of the equatorial nuclei, ν_2, when H = 21.5 gauss, and after 1225 passes through the spectrum, is shown in Figure 3.4. It illustrates the characteristic peaks predicted by Morino and Toyama in the $\pm \nu_L$ region, but because of overlapping with neighbouring sidebands and noise problems, we have never been able to identify with certainty the peaks at $\pm 2\nu_L$ in these derivative spectra. However the results are good enough to enable the peak-to-peak separation δ_1 to be measured, and the procedure described above of graphing $\delta_1 (2\nu_L)^{-1}$ against (H^{-1}) then enables the asymmetry parameter to be measured. The δ_1 values obtained in this way are given in Tables 3.2 and 3.3 for the ν_1 and ν_2 resonances respectively, and the corresponding graphs of $\delta_1 (2\nu_L)^{-1}$ against (H^{-1}) are shown in Figures 3.5 and 3.6 The effect of the magnetic field on the equatorial resonance ν_3 is identical to the corresponding effect on ν_2. The asymmetry parameters obtained in this way for $(Cl_3PNCH_3)_2$ are summarised in Table 3.4, together with values of the quadrupole coupling constants derived from the observed frequencies and η values.

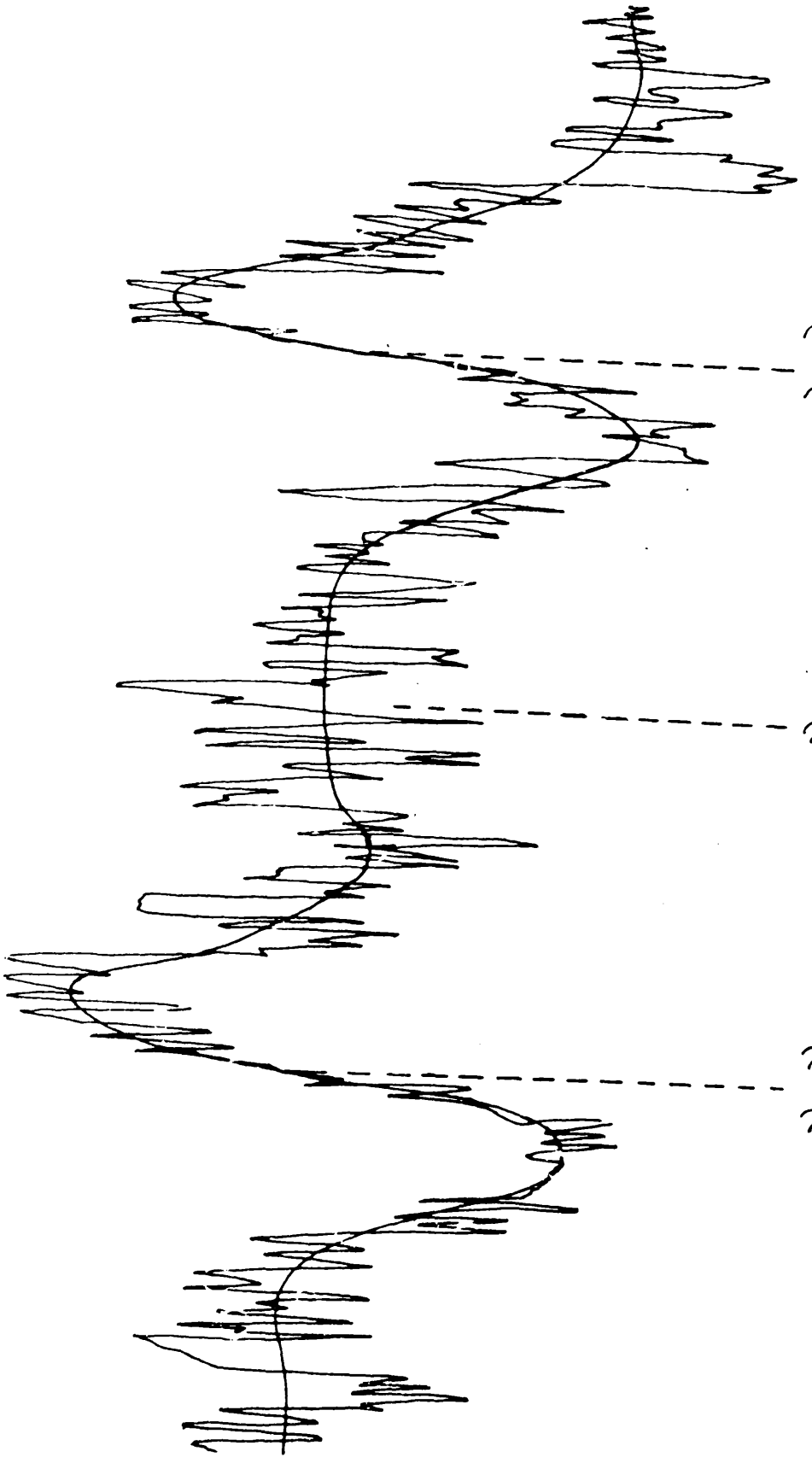

Figure 3.4. First derivative of one of the sidebands of the ν_2 resonance in $(Cl_3PNCH_3)_2$ subjected to a magnetic field of 21.5 gauss.

Table 3.2

Lineshape parameters δ_1 and $\delta_1/2\nu_L$ obtained by analysis of the ν_1 resonance signal of a polycrystalline sample of $(Cl_3PNCH_3)_2$ in weak magnetic fields.

Magnetic field (gauss)	Larmor frequency for ^{35}Cl (K.Hz.)	δ_1 (K.Hz.)	$\frac{\delta_1}{2\nu_L}$
2.75	1.145	0.429	0.188
3.80	1.584	0.396	0.125
4.21	1.758	0.488	0.139
5.10	2.128	0.456	0.107
7.49	3.125	0.521	0.083
7.92	3.306	0.517	0.078
11.09	4.630	0.648	0.070
11.13	4.644	0.514	0.055
14.53	6.062	0.779	0.064
15.89	6.629	0.758	0.057
17.63	7.353	0.784	0.053
26.50	11.045	1.038	0.047

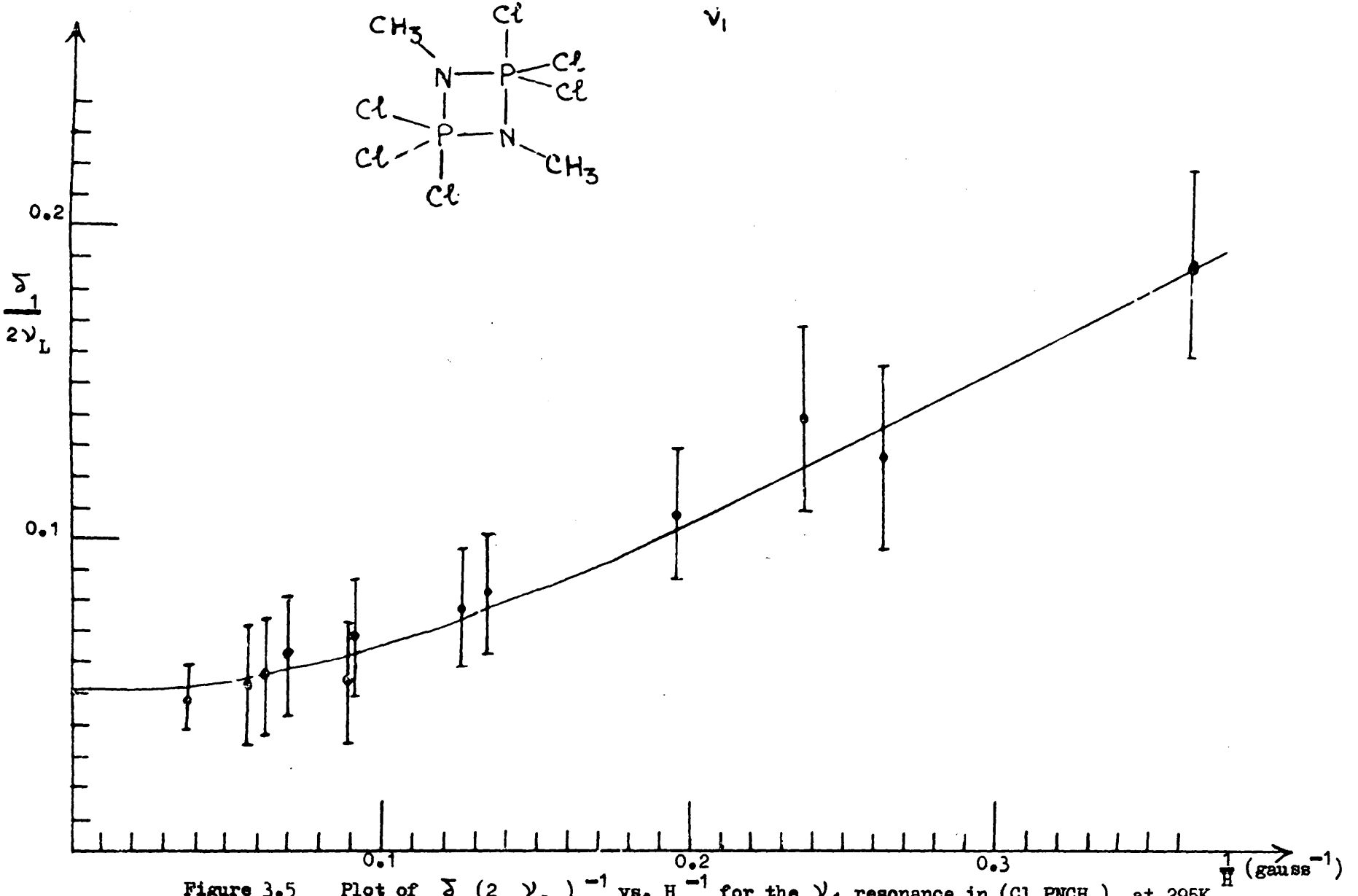

Figure 3.5 Plot of $\delta_1 (2\ \nu_L)^{-1}$ vs. H^{-1} for the ν_1 resonance in $(Cl_3PNCH_3)_2$ at 295K

Table 3.3

Lineshape parameters δ_1 and $\delta_1/2\nu_L$ obtained by analysis of the ν_2 resonance signal of a polycrystalline sample of $(Cl_3PNCH_3)_2$ in weak magnetic fields.

Magnetic field (gauss)	Larmor frequency for ^{35}Cl (K.Hz.)	δ_1 (K.Hz.)	$\delta_1/2\nu_L$
3.56	1.484	0.807	0.272
4.37	1.821	0.918	0.252
6.10	2.543	0.895	0.176
8.20	3.418	1.073	0.157
8.48	3.535	1.039	0.147
9.80	4.085	1.160	0.142
10.00	4.168	1.275	0.153
11.90	4.960	1.299	0.131
15.15	6.315	1.389	0.110
15.39	6.415	1.552	0.121
18.18	7.577	1.591	0.105
22.22	9.261	1.686	0.091
23.81	9.924	2.044	0.103
26.50	11.045	2.695	0.122

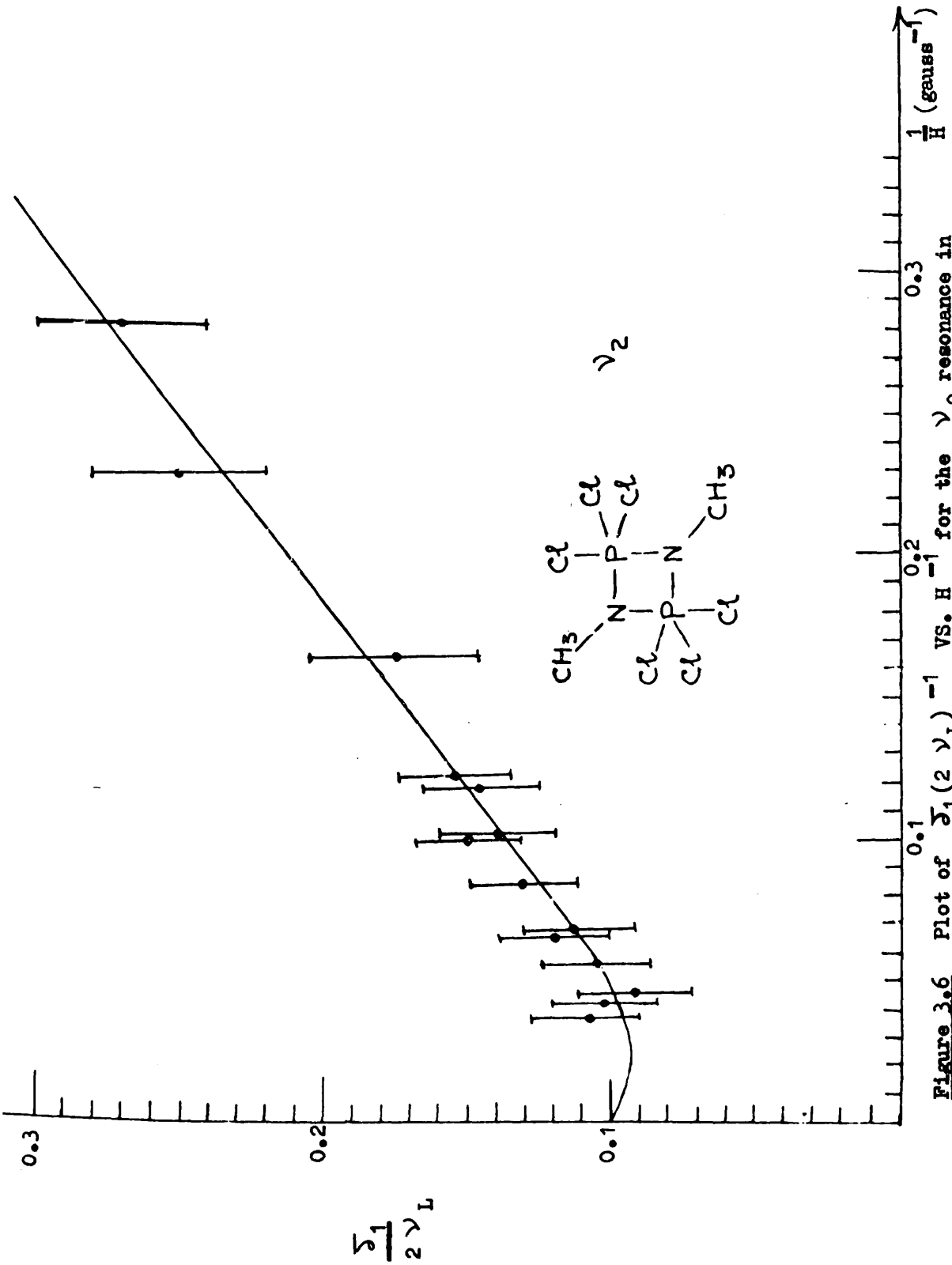

Figure 3.6 Plot of $\delta_1(2\nu_L)^{-1}$ vs. H^{-1} for the ν_2 resonance in $(Cl_3PNCH_3)_2$ at 295K.

Table 3.4

Chlorine - 35 n.q.r. frequencies, asymmetry parameters and quadrupole coupling constants for $(Cl_3PNMe)_2$ at 293K

Resonance	^{35}Cl n.q.r. Frequency (M.Hz.)	η	$\left(\frac{eqQ}{h}\right) = \frac{2\nu}{\left(1 + \frac{\eta^2}{3}\right)^{\frac{1}{2}}}$ (M.Hz.)
axial ν_1	25.617 ± 0.001	0.05 ± 0.01	51.21 ± 0.01
equatorial ν_2	29.587 ± 0.001	0.10 ± 0.02	59.08 ± 0.03
equatorial ν_3	29.778 ± 0.001	0.10 ± 0.02	59.46 ± 0.03

These results can be employed in an approximate analysis of the type of bonding present in this molecule by means of the method developed by Townes and Dailey.[23] We have already derived the equations needed to perform an analysis of this sort, but we repeat them at this point for clarity. Thus, if the chlorine-phosphorus bond is formed from a chlorine 3s - 3p hybrid orbital of s-character a, defined as in equation 1.48, it can be shown that [24,25]

$$\frac{(eqQ/h)\ mol}{(eqQ/h)\ atom} = (1 - a^2)(2 - b) - \frac{\pi}{2}$$

$$= (1 - a^2)(1 - i) - \frac{\pi}{2} \qquad 3.6$$

where b is the population of the chlorine bonding orbital and i is the ionic character of the bond, defined by equation 1.54; π is fixed by taking the population of the chlorine $3p_x$ orbital to have fallen from 2 to $(2 - \pi)$ because of the presence of phosphorus - chlorine $(d \leftarrow p)\pi$ bonding. Thus π can be found from

$$\eta = \frac{3}{2}\pi \frac{(eqQ/h)\ atom}{(eqQ/h)_{molecule}} \qquad 3.7$$

Values of π and i calculated by this approximate method are summarised in Table 3.5. In performing these calculations the s - character of the bonding orbital has been arbitrarily set equal to 0.15, after Townes and Dailey, and $|(eqQ/h)\ \text{atom}|$ for chlorine has been set equal to 109.7 M.Hz.[26]

Table 3.5

Resonance		P–Cl bond length(Å)	π	i
axial	ν_1	2.15	0.02	0.51
equatorial	ν_2	2.02	0.04	0.43
equatorial	ν_3	2.02	0.04	0.43

In view of the sweeping approximations involved in deriving the Townes-Dailey theory, the individual values in Table 3.5 should not be endowed with great significance. Nevertheless the results do indicate that π - bonding is of very minor importance; π - character does not contribute any more than 2 - 3% to the nature of the P - Cl bonds in this molecule. The differences in the frequencies found for axial and equatorial chlorine atoms originate in the fact that the axial P - Cl bond is more ionic than the equatorial P - Cl bond. This is consistent with the accepted picture of bonding in a trigonal bipyramidal environment in which the central atom, phosphorus in this case, uses sp^2 hybrid orbitals to form equatorial bonds, and either a pure p orbital or a p - d hybrid, to form axial bonds.

3.3 Chlorine - 35 n.q.r. spectra of $(Cl_3PNCH_3)_2$ and $(Cl_3PNPh)_2$ subjected to hydrostatic pressure

The chlorine - 35 nuclear quadrupole resonance spectra of $(Cl_3PNCH_3)_2$ and $(Cl_3PNPh)_2$ have been examined whilst these compounds were subjected to hydrostatic pressures within the range $1 \leq P \leq 1500$ Kg. cm $^{-2}$ at 295K, generated inside a pressure chamber of conventional design which contained the sample coil. Various aspects of the experimental arrangement employed, and of high pressure studies in general, are discussed later in this chapter, and in Appendix B.

Plots of the three chlorine - 35 nuclear quadrupole resonance frequencies for $(Cl_3PNCH_3)_2$ as a function of pressure are shown in Figure 3.7. The axial chlorine nucleus can again be quite clearly distinguished from the equatorial nuclei, this time on the basis of the response of the resonance frequencies to applied pressure ; the axial resonance frequency is surprisingly reduced as the pressure is increased, whereas the equatorial frequencies increase with increase in pressure. The variation in frequency is effectively linear in the "low-pressure" region for each of the three signals, and in each case there is a distinct change in the pressure dependence at approximately 650 Kg. cm^{-2} , possibly indicating that the pressure forces some slight change in the packing of the molecules in the solid. This is not too surprising since the distance between equatorial chlorine atoms in adjacent molecules is less than the sum of the van der Waals' radii[11] and some "slipping" of the molecules relative to each other seems inevitable.

Figure 3.8 shows that very similar changes are observed when $(Cl_3PNPh)_2$ is subjected to pressure. Again the axial chlorine nucleus can be distinguished from the equatorial nuclei, and again there is a distinct change in the pressure dependence at approximately

650 Kg.cm $^{-2}$. The close similarity of the results obtained for these two compounds implies that the solid state structures are very similar in the region of the $=PCl_3$ fragments, and that the differences in packing forced by the bulk of the phenyl group affects the magnitude of the pressure dependence of each frequency slightly, but leaves the overall pattern unchanged.

These results can be accurately described by expressing the frequencies in terms of a polynomial in pressure and the least squares fits of the experimental data for each resonance in $(Cl_3PNCH_3)_2$ and $(Cl_3PNPh)_2$ are given in Table 3.6.

3.4 The effects of temperature changes on chlorine - 35 n.q.r. spectra of chlorocyclodiphosphazanes.

(1) Constant pressure conditions

Nuclear quadrupole resonance spectra of several chlorocyclodiphosphazanes have been examined over the temperature range $77 \leq T \leq 350K$ at atmospheric pressure. To ensure a uniform temperature over the whole sample the temperature was held constant for at least thirty minutes before recording each spectrum. The temperature was varied by means of a nitrogen gas-flow system which is described in Appendix C. The observed variation of frequencies with temperature for $(Cl_3PNCH_3)_2$ is shown in Figure 3.9 ; the curves shown are smooth and there is no sign of any sudden discontinuity such as one might expect to see if a phase change occurred. The linewidth and intensity of each resonance are also independent of temperature. Similar curves are obtained for $(Cl_3PNC_2H_5)_2$ and $(Cl_3PNPh)_2$ and these are illustrated in Figures 3.10 and 3.11 respectively. The temperature dependence of the resonance frequencies is very similar in all three compounds; in each case

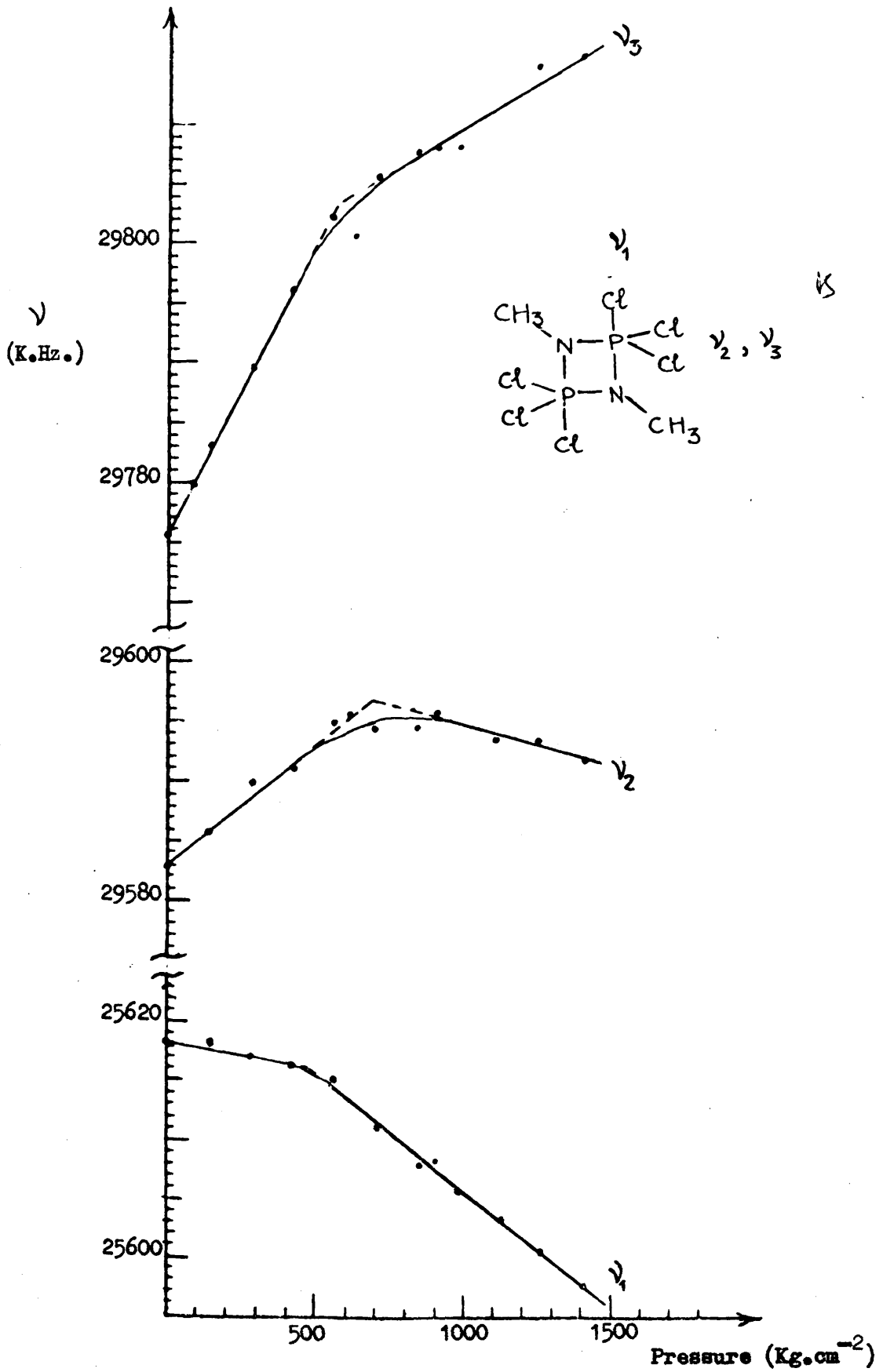

Figure 3.7 Plot of chlorine – 35 n.q.r. frequencies vs. applied pressure for $(Cl_3PNCH_3)_2$ at 295K.

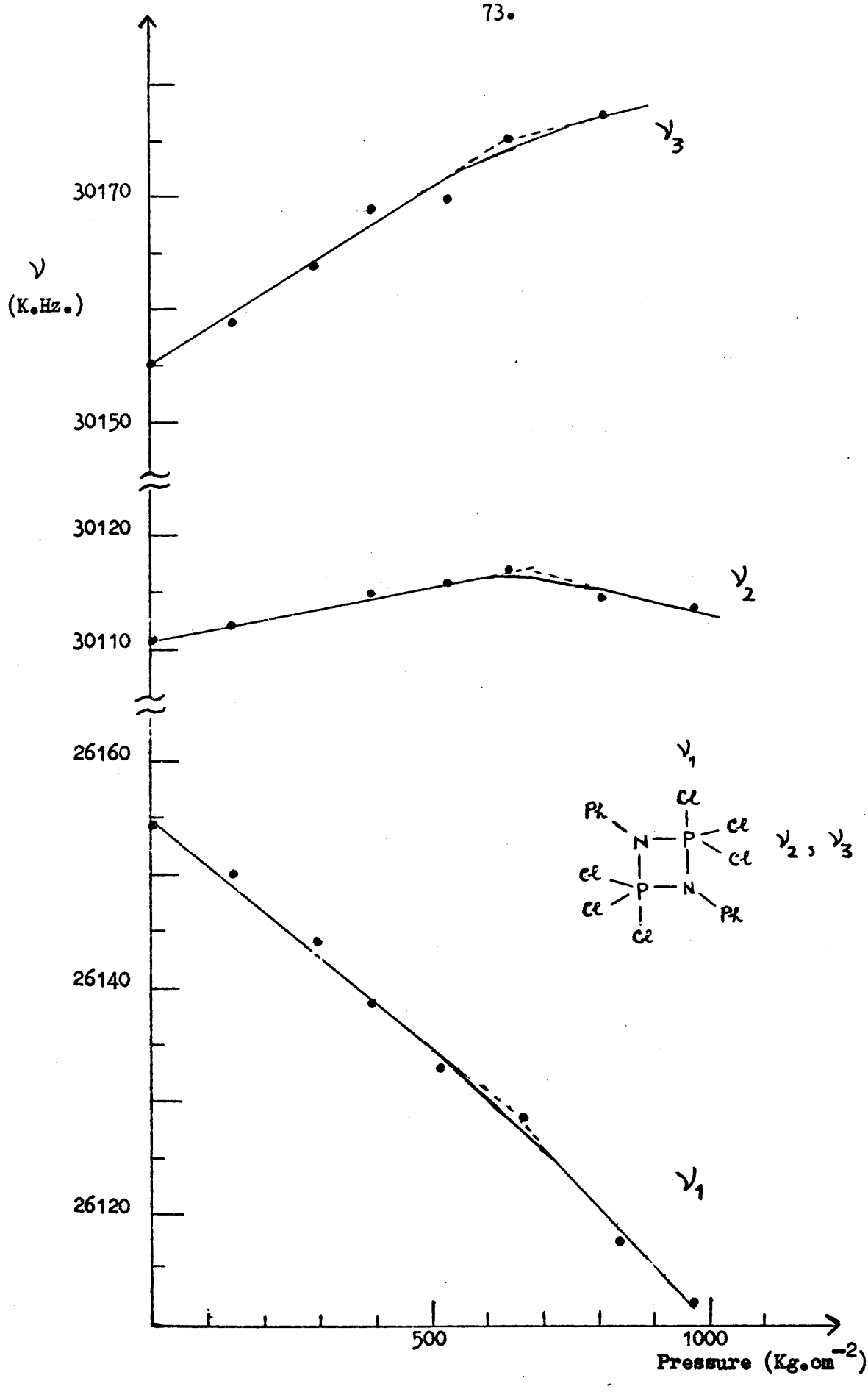

Figure 3.8 Plot of chlorine – 35 n.q.r. frequencies vs. applied pressure for $(Cl_3PNPh)_2$ at 295K.

Table 3.6

Polynomial equations, obtained using the least squares criterion, which describe the variation of ^{35}Cl n.q.r. frequencies with applied pressure within the range $1 < P \leqslant 1500$ Kg. cm $^{-2}$ (at 295K). In each case ν is in M.Hz. and P in Kg. cm $^{-2}$.

Compound	Resonance	Equation	Standard Deviation in ν
$(Cl_3PNCH_3)_2$	ν_1	$\nu = 25.6190 - 5.7471 \times 10^{-6}P - 7.4344 \times 10^{-9}P^2$	1.027×10^{-3}
	ν_2	$\nu = 29.5828 + 2.6607 \times 10^{-5}P - 1.4788 \times 10^{-8}P^2$	1.376×10^{-3}
	ν_3	$\nu = 29.7760 + 5.3499 \times 10^{-5}P - 1.8401 \times 10^{-8}P^2$	1.486×10^{-3}
$(Cl_3PNPh)_2$	ν_1	$\nu = 26.1551 - 3.6641 \times 10^{-5}P - 8.6495 \times 10^{-9}P^2$	7.024×10^{-4}
	ν_2	$\nu = 30.1106 + 1.6857 \times 10^{-5}P - 1.4322 \times 10^{-8}P^2$	9.101×10^{-4}
	ν_3	$\nu = 30.1543 + 3.8250 \times 10^{-5}P - 1.1819 \times 10^{-8}P^2$	1.405×10^{-3}

the frequency of the axial chlorine is least affected by the temperature change.

We can see from Figures 3.9 and 3.11 that in both $(Cl_3PNCH_3)_2$ and $(Cl_3PNPh)_2$ the two equatorial frequencies have measurably different temperature coefficients, so that the resonances move closer together with increasing temperature. The effects of the vibrations and thermal expansion in these compounds thus combine to gradually overcome the solid state effects which make the equatorial chlorines' resonance frequencies inequivalent. The situation is different for $(Cl_3PNC_2H_5)_2$ since here, as shown in Figure 3.10 the two equatorial resonances are equally affected by the temperature changes over the entire temperature range investigated. This is also illustrated by the temperature increments quoted in Table 3.1, and the difference in the behaviour of the ethyl derivative may well be a result of differences in crystal packing between the ethyl compound and the other species studied.

Figure 3.12 shows the corresponding variation of frequency with temperature for the chlorooxocyclodiphosphazane $\left[Cl(O)PNCH_3\right]_2$ whose tertiarybutyl analogue has recently been shown to possess a centre of symmetry.[27] An attempt to carry out detailed n.q.r. studies on $\left[Cl(O)PNPh\right]_2$ has been unsuccessful since the resonance signal in this compound is very weak at room temperature, and fades out altogether at temperatures below 250K. Between 250K and room temperature the variation in frequency found for $\left[Cl(O)PNPh\right]_2$ is virtually identical to that for $\left[Cl(O)PNCH_3\right]_2$. The frequencies measured for these two compounds at room temperature are given in Table 3.7.

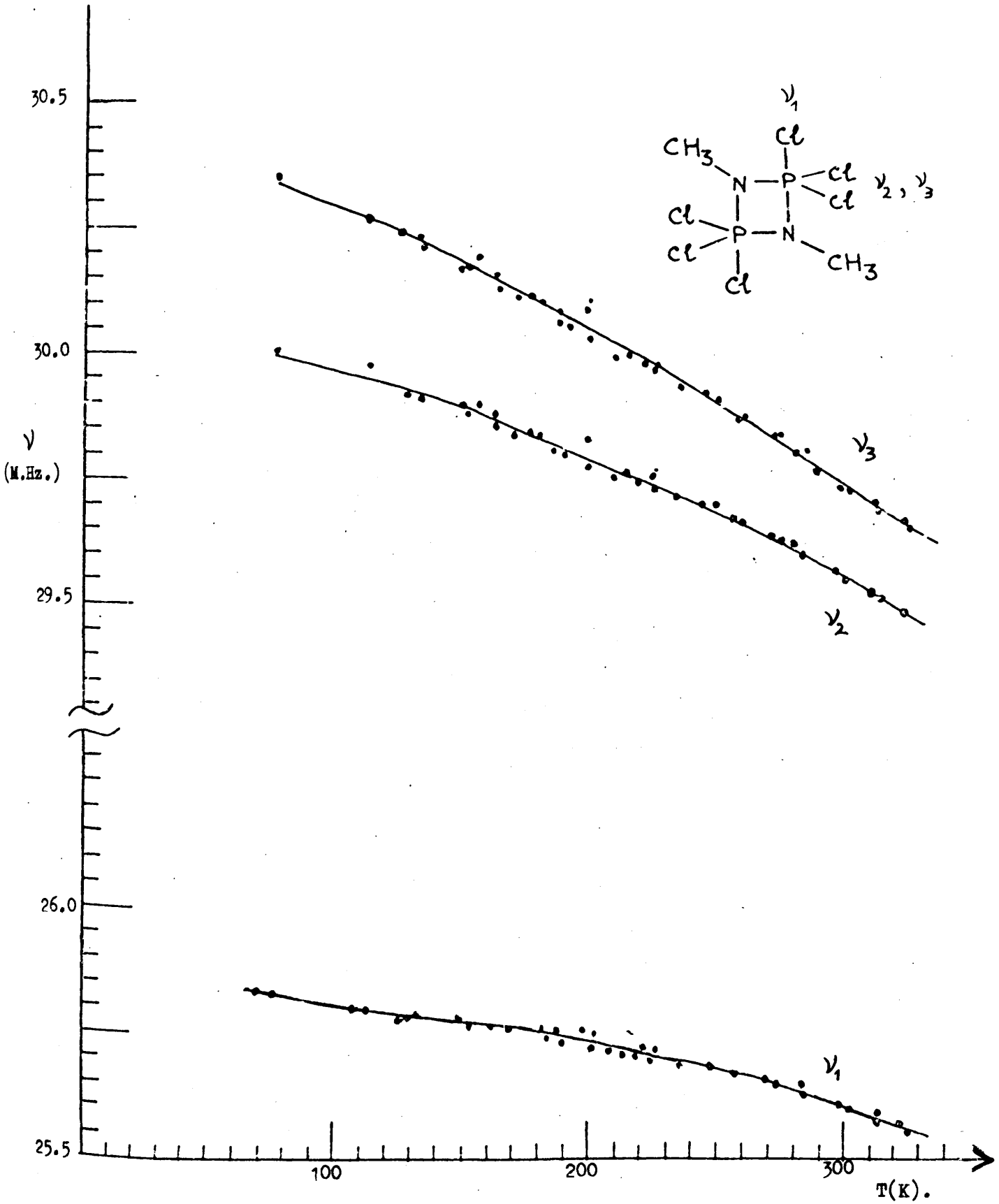

Figure 3.9 Plot of chlorine - 35 n.q.r. frequencies vs. temperature for $(Cl_3PNCH_3)_2$.

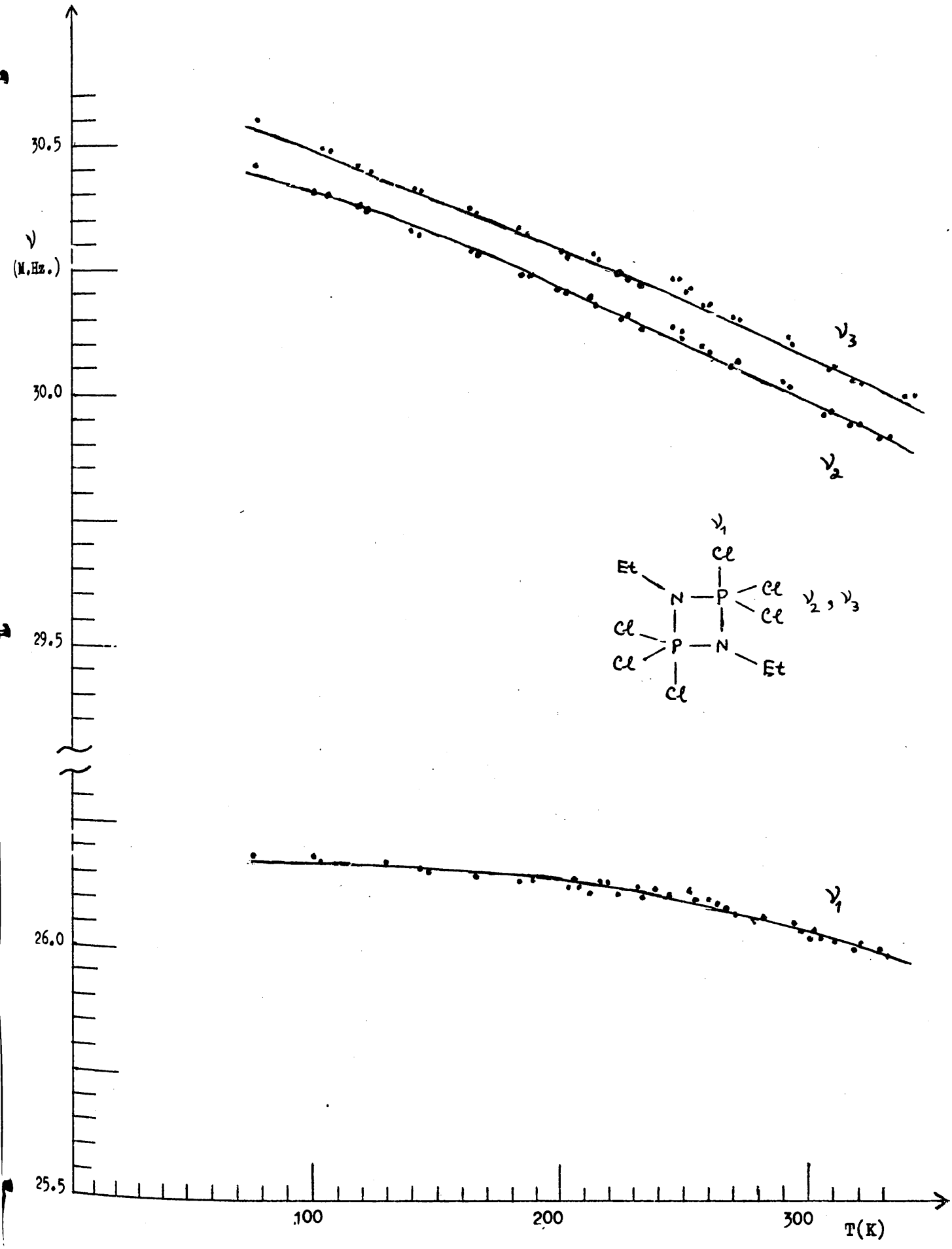

Figure 3.10 Plot of chlorine - 35 n.q.r. frequencies vs. temperature for $(Cl_3PNC_2H_5)_2$

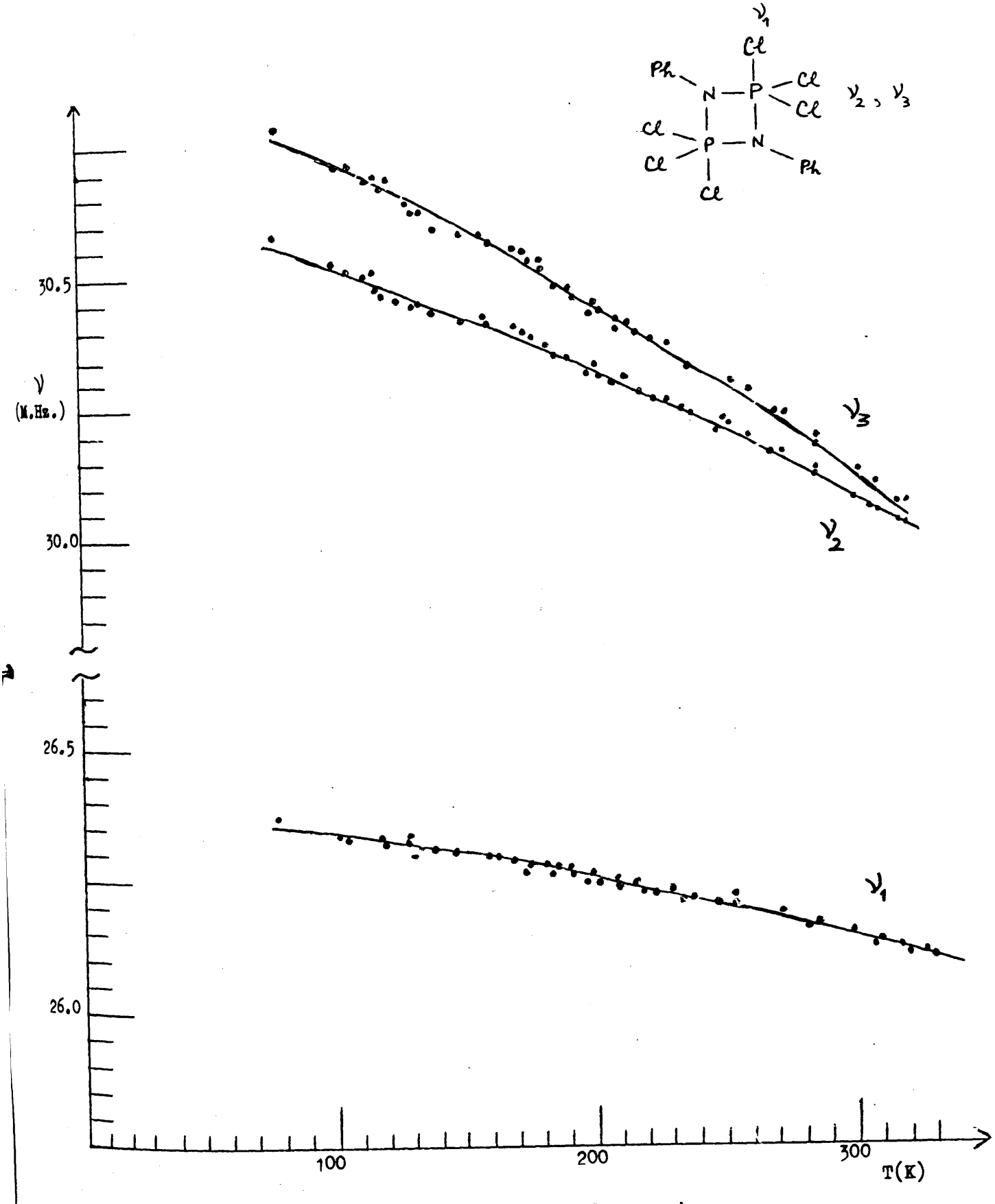

Figure 3.11 Plot of chlorine - 35 n.q.r. frequencies vs. temperature for $(Cl_3PNPh)_2$.

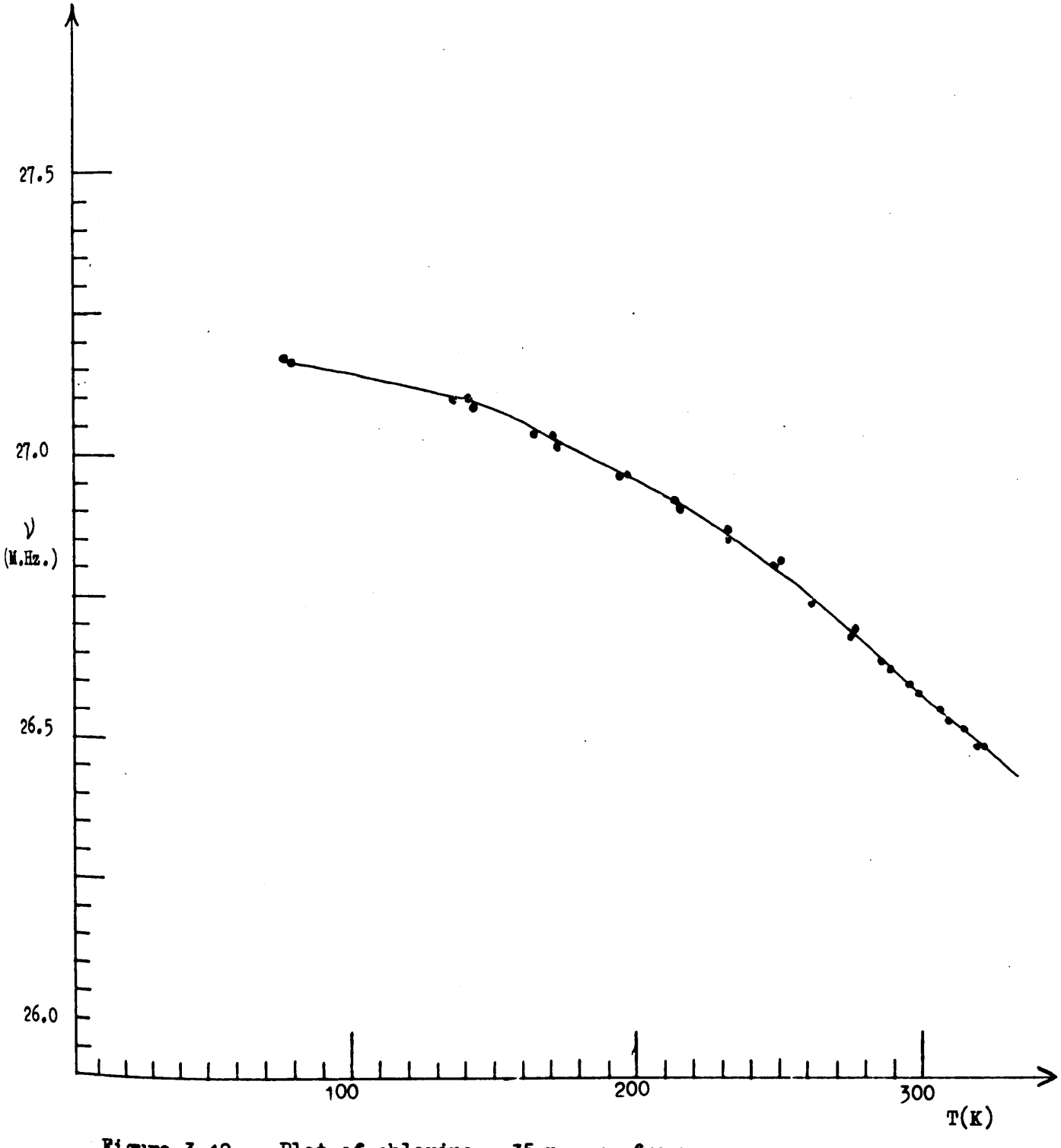

Figure 3.12 Plot of chlorine - 35 n.q.r. frequency vs. temperature for $[Cl(O)PNCH_3]_2$.

Table 3.7

Chlorine - 35 n.q.r. data for $[Cl(O)PNCH_3]_2$ and $[Cl(O)PNPh]_2$

Compound	Frequency (M.Hz.)		Difference Frequency (M.Hz.)
	77K	293K	
$[Cl(O)PNCH_3]_2$	27.168	26.621	0.547
$[Cl(O)PNPh]_2$	-	26.530	-

The chlorine atoms in $[Cl(O)PNR]_2$, when R = CH_3 or Ph cannot be distinguished from the axial chlorine atoms in $(Cl_3PNR)_2$, where R is CH_3, C_2H_5 or Ph, by simply comparing their chlorine quadrupole resonance frequencies at any given temperature, but the two functional groups can easily be distinguished from one another by making use of the marked, and characteristic, differences in the changes in these frequencies when the temperature is changed.

The observed variations of the resonance frequencies with temperature can be fitted to expressions of the form

$$\nu = a + bT + \frac{c}{T} \qquad 3.8$$

as predicted by the theories developed by Bayer [28] and by Kushida et al.[29,30] which are discussed in a later section of this chapter. The least squares fits of the experimental data for $(Cl_3PNR)_2$ where R = CH_3, C_2H_5 and Ph, and for $[Cl(O)PNCH_3]_2$ $(Cl_3PNR)_2$ on 3.8 are listed in Table 3.8.

(ii) Constant volume conditions

The almost universal reduction in eqQ on going from vapour phase measurements to solid state data clearly shows that even in

Table 3.8

Coefficients calculated by fitting the best curves of the form

$$\nu = a + bT + \frac{c}{T}$$

to the experimental curves of n.q.r. frequency vs. temperature

Compound	Resonance	a	b	c
$(Cl_3PNCH_3)_2$	ν_1	26.075×10^6	-1406	-1.265×10^7
	ν_2	30.399×10^6	-2598	-1.598×10^7
	ν_3	30.768×10^6	-3210	-1.434×10^7
$(Cl_3PNC_2H_5)_2$	ν_1	26.450×10^6	-1211	-1.486×10^7
	ν_2	30.700×10^6	-2279	-6.388×10^6
	ν_3	30.755×10^6	-2212	-4.216×10^6
$(Cl_3PNPh)_2$	ν_1	26.526×10^6	-1219	-5.399×10^6
	ν_2	30.866×10^6	-2469	-9.663×10^6
	ν_3	31.148×10^6	-3272	-9.801×10^6
$[Cl(O)PNCH_3]_2$		27.990×10^6	-4263	-3.864×10^7

(a values are in Hz. , b in $Hz.K^{-1}$, c in Hz.K., standard deviations in b values are 100 Hz K^{-1}. Standard deviations in c values are 2×10^6 Hz.K.)

a simple molecular crystal intermolecular interactions can appreciably influence the observed quadrupole coupling constant. It follows that thermal expansion of a simple molecular solid will alter the intermolecular contribution to the electric field gradient at the quadrupolar nuclei, and so will contribute towards the changes in quadrupole resonance frequencies with temperature which we have detailed above.

The experimental data obtained in the previous section, for the variation of quadrupole resonance frequency with temperature at constant, atmospheric, pressure, and listed in Table 3.8, can be used to derive values of the differential coefficient $\left(\frac{\partial \nu}{\partial T}\right)_{p = 1\ Kg.cm^{-2}}$; values of these coefficients are listed in Table 3.9 for each resonance in $(Cl_3PNCH_3)_2$ and $(Cl_3PNPh)_2$. The table also includes values of $\left(\frac{\partial \nu}{\partial P}\right)_{T = 295K}$ obtained from the data on pressure effects in Table 3.6. These results can be combined to estimate the rate of change of frequency with temperature under conditions of constant volume, in the form of the differential coefficient $\left(\frac{\partial \nu}{\partial T}\right)_V$, by using the relationship[31]

$$\left(\frac{\partial \nu}{\partial T}\right)_V = \left(\frac{\partial \nu}{\partial T}\right)_P + \left(\frac{\alpha}{\beta}\right)\left(\frac{\partial \nu}{\partial P}\right)_T \qquad 3.9$$

and the resulting values of $\left(\frac{\partial \nu}{\partial T}\right)_V$ are included in Table 3.9. Equation 3.9 is strictly correct only if the vibrational frequencies in these solids are not functions of temperature or pressure; there is however some limited evidence that vibrational modes in some molecular solids can vary with temperature,[32] although such an effect in the present case is expected to be small. A further restriction on equation 3.9 is that it is exact only for an

Table 3.9

Differential coefficients for $(Cl_3PNCH_3)_2$ and for $(Cl_3PNPh)_2$

Compound	Resonance	$\left(\frac{\partial \nu}{\partial T}\right)_{P=1Kg.cm^{-2}, T=295K}$	$\left(\frac{\partial \nu}{\partial P}\right)_{T=295K}$	$\left(\frac{\partial \nu}{\partial T}\right)_V$
$(Cl_3PNCH_3)_2$	ν_1	-1266	- 5.7	-1397
	ν_2	-2420	+26.6	-1808
	ν_3	-3050	+53.5	-1819
$(Cl_3PNPh)_2$	ν_1	-1159	-36.6	-2000
	ν_2	-2362	+16.8	-1976
	ν_3	-3163	+38.2	-2284

$\left(\frac{\partial \nu}{\partial T}\right)_P$ values are in units of $Hz.K^{-1}$. $\left(\frac{\partial \nu}{\partial P}\right)_T$ values are in units of $Hz.Kg^{-1}\ cm^2$. $\left(\frac{\partial \nu}{\partial T}\right)_V$ values are in units of $Hz.K^{-1}$.

isotropic solid. Although the use of this expression must introduce some errors, it is believed that their effects on the estimated values of $\left(\frac{\partial \nu}{\partial T}\right)_V$ are small in the series of compounds considered here.

In equation 3.9, α is the volume coefficient of thermal expansion, and β is the isothermal compressibility of the solid. Very little data concerning thermal expansion and compressibility of covalent phosphorus compounds is available and we have therefore used approximate estimates of α and β obtained from the available literature data for other molecular crystals in equation 3.9 in order to calculate $\left(\frac{\partial \nu}{\partial T}\right)_V$. For organic compounds of moderate polarity in which hydrogen bonding is absent, the volume compressibility, β, is typically [33-36] of the order of 11×10^{-6} Kg^{-1} cm^2. Typical organic compounds in which hydrogen bonding is absent have volume coefficients of thermal expansion, α, of the order of 260×10^{-6} K^{-1} and the values for the molecular species $POCl_3$, $POBr_3$ and PBr_3 are similar.[33,37] We have therefore assumed that for the chlorocyclodiphosphazanes $\left(\frac{\alpha}{\beta}\right) \cong 23$ $Kg.cm^2K^{-1}$.

3.5 The origin of the characteristic effects of temperature changes on the chlorine - 35 resonance frequencies in chlorocyclodiphosphazanes.

The effects of temperature on nuclear quadrupole resonance frequencies are explained by the Bayer-Kushida theory [28-30] in terms of the vibrational motions which occur in the solid. These cause the effective electric field gradient and asymmetry parameter for each chlorine nucleus to change with vibration amplitude and the parameters eq and η averaged over these motions can be related [38-40] to the angular displacements θ_x, θ_y and θ_z about the

principal axes X, Y and Z of the electric field gradient tensor by the equations

$$eq \simeq eq_o \left[1 - \frac{3}{2} \left(\langle \theta_x^2 \rangle + \langle \theta_y^2 \rangle \right) + \frac{1}{2} \eta_o \left(\langle \theta_y^2 \rangle - \langle \theta_x^2 \rangle \right) \right] \quad 3.10$$

$$\eta \simeq \frac{qo}{q} \left\{ \eta \left[1 - \frac{1}{2} \left(\langle \theta_x^2 \rangle + \langle \theta_y^2 \rangle \right) - 2 \langle \theta_z^2 \rangle \right] + \frac{3}{2} \left(\langle \theta_y^2 \rangle - \langle \theta_x^2 \rangle \right) \right\} \quad 3.11$$

In the chlorocyclodiphosphazanes the asymmetry parameters are small so that η can be taken to be constant in these equations and the last term in equation 3.10 can be neglected.

Any small amplitude external co-ordinate θ_i can be expanded as a linear combination of the normal co-ordinates ξ_j by

$$\theta_i = \sum_j A_{ij} \xi_j \quad 3.12$$

and if it is assumed that only librational and torsional motions are involved, and that these are harmonic, then it can be shown that

$$\nu = \nu_o \left\{ 1 - \frac{3}{2} \sum_{j=1}^{N} A_{ij} \left[\frac{h}{4\pi^2 I_j \nu_j} \right] \left[\frac{1}{2} + \frac{1}{\exp(h\nu_j / kT) - 1} \right] \right\} \quad 3.13$$

where the coefficient A_{ij} gives the relative weight of the contribution made by the j^{th} mode to the nuclear motion, ν_j is the frequency of the mode, and I_j is the effective moment of inertia about the axis associated with the motion. ν_o is the nuclear quadrupole resonance frequency which would be obtained for the rigid lattice in the absence of even zero-point vibrations. The lattice vibrations can be grouped into high - and low - frequency modes according to whether their frequencies are greater or smaller than

$$\nu = \frac{k T_M}{h} \quad 3.14$$

where T_M is the lowest temperature used in the experiments. If the contributions to ν from the high frequency modes are set equal to $\Omega(T)$, and A_{ij} is taken to be 1, then

$$\nu = \nu_o \left\{ 1 - \frac{3kT}{8\pi^2} \sum_{j=1}^{M} \frac{1}{I_j \nu_j^2} - \frac{h^2}{32\pi^2 kT} \sum_{j=1}^{M} \frac{1}{I_j} + \Omega(T) \right\} \quad 3.15$$

where

$$\Omega(T) = -\frac{3}{2} \sum_{j=M+1}^{N} \frac{h}{4\pi^2 I_j \nu_j} \left(\frac{1}{2} + \frac{1}{\exp(h\nu_j / kT) - 1} \right) \quad 3.16$$

and the summations are taken over the j modes which contribute to θ_i. Neglecting the $\Omega(T)$ term completely, equation 3.15 can be re-cast into the form

$$\nu = a + b'T + \frac{c'}{T} \quad 3.17$$

where

$$a = \nu_o$$

$$b' = -\frac{3k\nu_o}{8\pi^2} \sum_{j=1}^{M} \frac{1}{I_j \nu_j^2} \quad 3.18$$

$$c' = -\frac{h^2 \nu_o}{32\pi^2 k} \sum_{j=1}^{M} \frac{1}{I_j}$$

and it now follows that at room temperature the rate of change of n.q.r. frequency with temperature under constant volume conditions is given by

$$\left(\frac{\partial \nu}{\partial T}\right)_V \simeq -\frac{3k\nu_o}{8\pi^2} \sum_{j=1}^{M} \frac{1}{I_j \nu_j^2} \quad 3.19$$

It is now relatively simple to correlate the behaviour of the n.q.r. frequency with temperature at constant volume with the observed vibrational spectra for the cyclodiphosphazanes. All modes of vibration should be included in the sum when computing values of $\left(\frac{\partial \nu}{\partial T}\right)_V$, but if one mode is assumed to be dominant in influencing the quadrupole resonance frequencies then it can be

identified if its computed contribution to $\left(\frac{\partial \nu}{\partial T}\right)_V$ is consistent with the experimental data discussed earlier and summarised in Table 3.9. The low frequency normal modes given in reference 13 are summarised in Table 3.10 ; each of these modes has been tested in this way and only the 64 cm^{-1}, $= PCl_3$ torsional-bending modes are consistent with the experimental data. A postulated rigid librational motion at 41 cm^{-1}, which would not be infra - red active but could be Raman active, could also account for the data in Table 3.9; as would also a linear combination of this libration and the $= PCl_3$ bending modes. All other vibrational modes observed in this molecule [7,13] occur at 122 cm^{-1} or higher frequencies, and so can be neglected. The experimental and calculated values of $\left(\frac{\partial \nu}{\partial T}\right)_V$ for $(Cl_3PNCH_3)_2$ are listed in Table 3.11.

Figure 3.13 is a projection of the structure of $(Cl_3PNCH_3)_2$ in which the shapes of the atoms have been weighted by the anisotropic thermal parameters given in reference 11, and it shows quite clearly that the main contribution to the motion of the atoms in this solid is made by the $= PCl_3$ torsional-bending modes : rigid librational motions are of minor importance.

3.6 Conclusions

In the chlorocyclodiphosphazanes the quadrupole resonance results clearly indicate that the n.q.r. frequencies are determined essentially by the degree of ionic character of the P–Cl bonds; the characteristic effects of temperature on these frequencies are a consequence of the nature of the bending modes of vibration involving the P – Cl fragments in these molecules. The

Table 3.10

Vibrational frequencies of $(Cl_3PNCH_3)_2$, together with assignments based on an approximate normal co-ordinate analysis. Data is taken from reference 13, and only the low frequency modes are shown.

Frequency No.	Calculated Frequency (cm^{-1})	Nearest Observed Frequency (cm^{-1})	Approx. form of vibration from PED
5	263	268	Ring distortion and PCl stretch
6	71	-	PCl_2 bend
9	218	204	skeletal
10	133	-	PCl_3 bend
12	130	-	skeletal
14	201	204	PCl_3 bend
15	99	-	PCl_3 bend
16	62	62	PCl_3 bend
19	128	122	skeletal
20	98	122	PCl_3 bend
21	56	62	ring puckering
25	195	212	skeletal
26	125	122	PCl_2 bend
29	130	122	PCl_3 bend
30	74	62	PCl_3 bend

Table 3.11

Coefficients of rate of change of N.Q.R. frequency with temperature for each resonance in $(Cl_3PNCH_3)_2$. The $\left(\frac{\partial\nu}{\partial T}\right)_V$ values found from the temperature and pressure dependent studies are listed, together with calculated values which are determined by assuming that only the vibrational frequencies listed contribute to the temperature dependence of the N.Q.R. frequencies. All values given are in units of $Hz.K^{-1}$.

	ν_1	ν_2	ν_3
Experimental $\left(\frac{\partial\nu}{\partial T}\right)_V$	-1397	-1808	-1819
Calculated $\left(\frac{\partial\nu}{\partial T}\right)_V$ assuming that the only vibrational modes which contribute are:			
(i) $64cm^{-1}$ PCl_3 bending modes	-1392	-1845	-1868
(ii) $41cm^{-1}$ librational motion of the entire molecule.	-1543	-1799	-1820

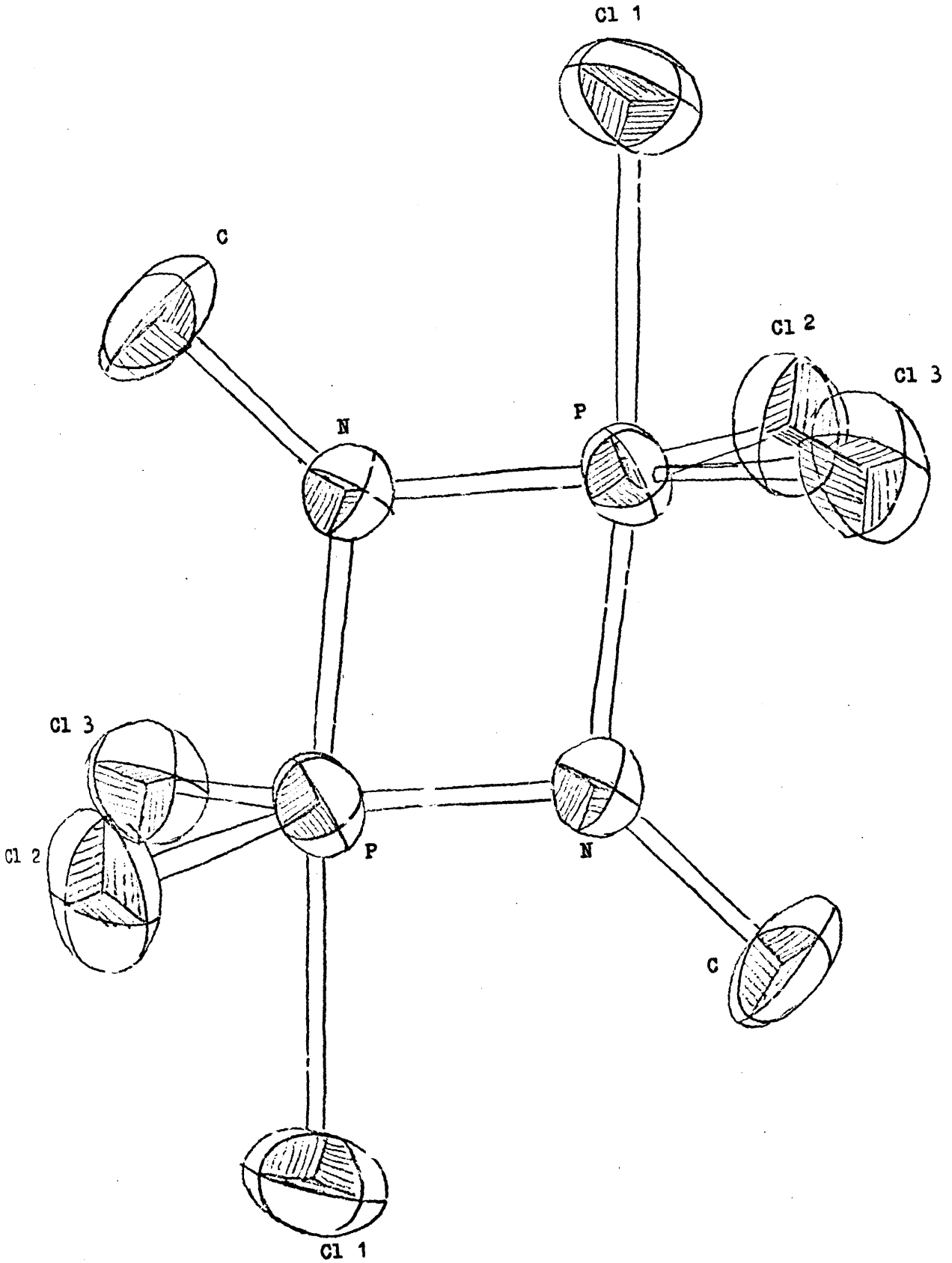

Figure 3.13 Projection of the structure of $(Cl_3PNCH_3)_2$

characteristic effects of pressure on the quadrupole resonance frequencies can now also be qualitatively accounted for since compression of these solids must reduce the amplitudes of these vibrational modes so tending to increase n.q.r. frequencies, and may also affect the P–Cl bond characters to some extent by altering intermolecular distances and angles, thus increasing the "solid-state shift" of the quadrupole coupling constants from the values expected in the free molecule.

The amplitudes of the nuclear displacements during the P–Cl bending modes depend on the magnitudes of the restoring force constants, and these in their turn depend on the details of the electron distribution at the central phosphorus atom. It follows that the effects on the chlorine – 35 nuclear quadrupole resonance frequencies in other P – Cl systems when they are subjected to pressure changes or to temperature changes should be characteristic of these systems.

In view of the approximations inherent in the Bayer–Kushida theory however, such correlations should be restricted to covalent compounds which form simple molecular solids since in these circumstances the influences on the quadrupole resonance frequencies and on their temperature dependence are primarily intramolecular in origin. In ionic compounds, in which interionic interactions can be dominant, changes in n.q.r. frequencies due to temperature or pressure changes are more likely to be characteristic of the ionic lattice than of bonding within each ion since vibrational modes should be more strongly coupled.

In molecular crystals however, localised bending modes which are characteristic of the bond A – B say will contribute significantly to the temperature dependence of the n.q.r. frequency of B if the force constant for the bond A – B is relatively weak

and if the atoms A and B are fairly heavy, so that the bending mode frequencies are low ; otherwise the librational modes will dominate the temperature effects in n.q.r. This implies that in other groups of compounds which have similar bonding to that in the P–Cl fragments in the cyclodiphosphazanes, and larger atomic masses than a phosphorus – chlorine system, the bending modes should be even more important in controlling the effects of temperature and pressure on n.q.r. frequencies.

3.7 Experimental

All quadrupole resonance spectra were recorded using a Decca Radar n.q.r. spectrometer. In the Zeeman experiments the sample coil of the spectrometer was placed with its axis parallel to the field generated by a pair of Helmholtz coils which produce a magnetic field of 134 gauss. amp $^{-1}$. Frequency modulation was used in these experiments. Since even a very small magnetic field considerably broadens the resonances it was necessary to couple the spectrometer output to a Technical Measurement Corporation C1024 time averaging computer. The Decca spectrometer frequency calibrates the spectra so that internal estimates of the magnitudes of the applied field and of the chlorine – 35 Larmor frequency, ν_L are obtained from the spectra. No attempt was made in this work to cancel the earth's magnetic field at the sample. Details of the manner of operation of the spectrometer with the time averaging computer are given in Appendix A.

The investigations of the pressure dependence of the n.q.r. spectra of $(Cl_3PNCH_3)_2$ and $(Cl_3PNPh)_2$ were carried out using a pressure vessel of conventional design which contained the sample coil; further details of the pressure chamber are to be found

in Appendix B. Pressures were measured by means of a standard pressure gauge and are accurate to $\pm$ 2 Kg. cm^{-2}. The calibration of the gauge was checked by studying the quadrupole resonance spectrum of Cu_2O as a function of pressure. The high pressure chamber was constructed from an EN58B stainless steel so that it was not possible to use Zeeman modulation, and frequency modulation techniques were therefore used in recording these spectra. A second pressure vessel has been constructed, to enable these studies to be extended to higher pressures, and this vessel is also described in Appendix B.

The experiments in which spectra were examined over the temperature range $77 \leq T \leq 350K$ were carried out using both Zeeman modulation and frequency modulation. The temperature was varied by means of a nitrogen gas-flow system which is described fully in Appendix C, and was measured by means of a copper-constantan thermocouple whose reference junction was maintained at 273K. To ensure a uniform temperature over the whole sample the temperature was held constant for at least thirty minutes before recording each spectrum.

All curve fitting procedures were carried out using the least squares criterion by standard computer programs available on the University of Edinburgh IBM 370/158 computer and the University of Glasgow KDF9 computer. The thermal ellipsoid diagram for $(Cl_3PNCH_3)_2$ shown in Figure 3.13 was produced by "OR TEP" , a fortran thermal - ellipsoid plot program for crystal structure illustrations, using the 370/158 computer.

The compounds investigated were all prepared by published procedures : $(Cl_3PNCH_3)_2$, $(Cl_3PNC_2H_5)_2$ [41] and $(Cl_3PNPh)_2$ [9]

by the reaction of the appropriate amine hydrochloride with PCl_5 , and the chlorooxocyclodiphosphazanes from $(Cl_3PNR)_2$, R = CH_3 , Ph reacting with SO_2 [42,43].

CHAPTER IV

THE EFFECTS OF PRESSURE CHANGES AND TEMPERATURE CHANGES ON THE CHLORINE - 35 NUCLEAR QUADRUPOLE RESONANCE SPECTRA OF THE CHLOROCYCLOTRIPHOSPHAZATRIENES $N_3P_3Cl_6$ AND $N_3P_3Cl_5NHPr^i$

4.1 Introduction

In the preceding chapter it has been shown that in the chlorocyclodiphosphazanes, $(Cl_3PNR)_2$ where R = CH_3, C_2H_5 or Ph, nuclear quadrupole resonance spectroscopy can be used in three ways to distinguish between axial and equatorial chlorine atoms : the chlorine - 35 nuclear quadrupole resonance frequencies are different, the temperature coefficients of these frequencies are different and the pressure coefficients of these frequencies are different. The characteristic frequencies are determined essentially by the differences in the degree of ionic character associated with axial and equatorial bonds in the trigonal bipyramidal environment, while the characteristic effects of temperature and pressure on these frequencies originate essentially in the bending modes of vibration which involve the P-Cl fragments in the chlorocyclodiphosphazanes. The amplitudes of the nuclear displacements during the P-Cl bending modes depend on the P-Cl bond lengths and on the magnitudes of the restoring force constants, and these in their turn depend on the details of the electron distribution at the phosphorus atom. The effects of pressure changes or temperature changes on chlorine - 35 nuclear quadrupole resonance frequencies in P-Cl systems should therefore be characteristic of the functional groups involved, and it should be possible to use measurements of these effects to discriminate

between such functional groups.

In this chapter the chlorine - 35 nuclear quadrupole resonance spectra are investigated in detail for the chlorocyclotriphosphazatrienes $N_3P_3Cl_6$ and $N_3P_3Cl_5NHPr^i$ where $Pr^i = CH(CH_3)_2$, whilst these solids are subjected to (I) pressures within the range $1 \leq P \leq 1000$ Kg.cm $^{-2}$ and (II), to temperature changes within the range $100 \leq T \leq 320$K in order to ascertain whether the variation of n.q.r. frequencies in these derivatives with temperature and pressure are similarly characteristic of the functional groups involved.

The chlorine - 35 nuclear quadrupole resonance spectrum of $N_3P_3Cl_5NHPr^i$ at 295K is illustrated in Figure 4.1 and the resonance frequencies at this temperature are listed in Table 4.1 together with equivalent data for $N_3P_3Cl_6$.[1,2] The species $N_3P_3Cl_6$ is known to be in a very slight chair conformation in the solid [3] and each molecule is bisected by a mirror plane. The number and intensities of the n.q.r. signals are in keeping with this chair conformation, and the relatively narrow range of frequencies (< 0.4 MHz) is consistent with small packing differences in the crystal. No structural data is available for $N_3P_3Cl_5NHPr^i$, but the $\equiv PCl_2$ signals (ν_2 - ν_5) fall within the expected frequency range for a cyclotriphosphazatriene. The $\equiv PClNHPr^i$ resonance frequency, ν_1 , is within the frequency band attributed to amino-substituted cyclophosphazenes in Chapter II of this work. However it is not apparent from the room temperature data which of the $\equiv PCl_2$ resonances should be assigned to chlorine atoms cis - and trans - to the bulky $NHPr^i$ group.

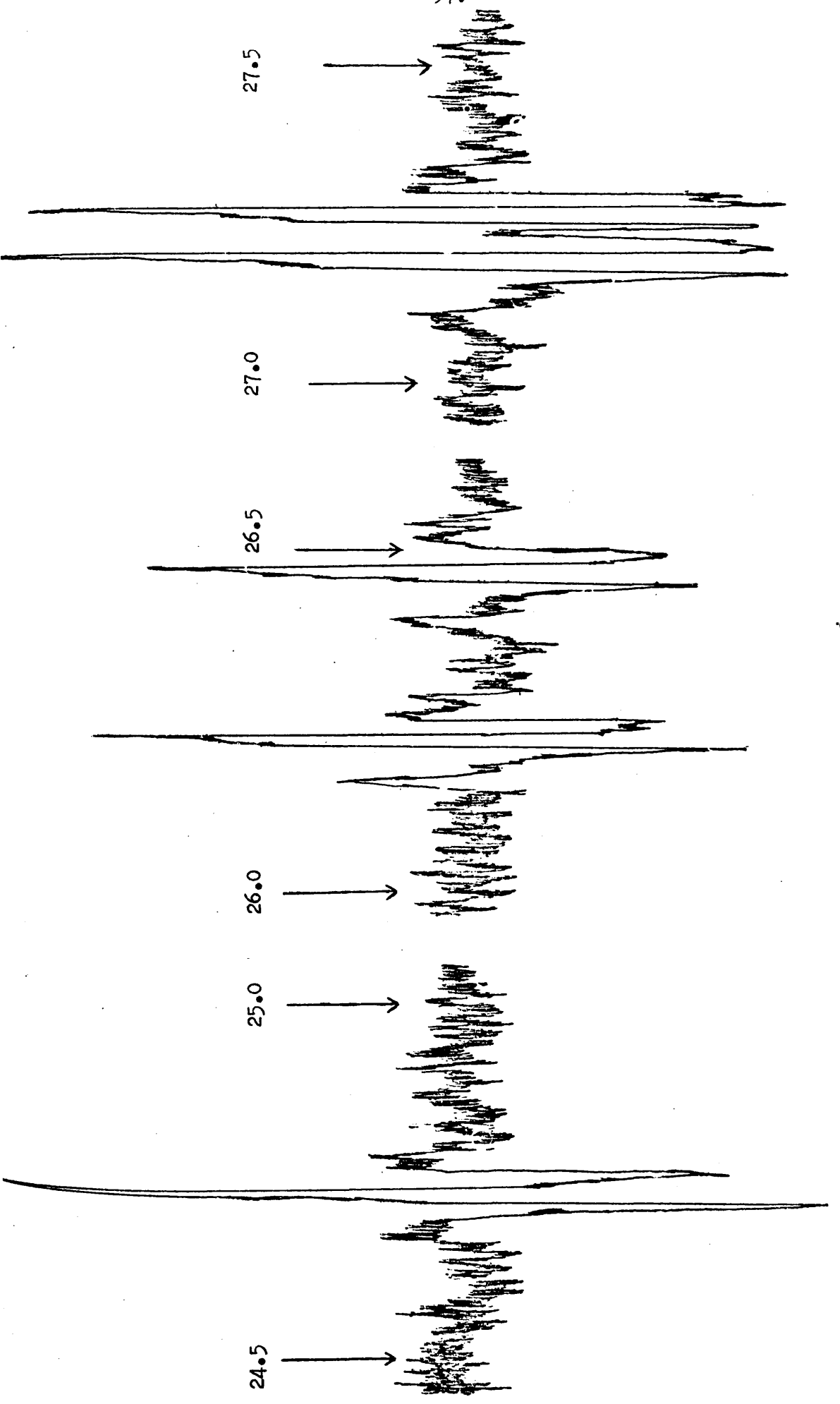

Figure 4.1 Chlorine - 35 n.q.r. spectrum of $N_3P_3Cl_5NHPr^i$ at 295K recorded using Zeeman modulation. Frequencies are given in M.Hz.

Table 4.1

Chlorine - 35 nuclear quadrupole resonance frequencies for the chlorocyclotriphosphazatrienes $N_3P_3Cl_6$ and $N_3P_3Cl_5NHPr^i$ at 295K.

Compound	Resonance	n.q.r. frequency (M.Hz.) [a]
$N_3P_3Cl_6$	ν_1	27.608 [2]
	ν_2	27.684 [1]
	ν_3	27.812 [1]
	ν_4	27.880 [2]
$N_3P_3Cl_5NHPr^i$	ν_1	24.620
	ν_2	26.111
	ν_3	26.352
	ν_4	27.049
	ν_5	27.148

a Superscripts denote relative intensities.

4.2 Chlorine - 35 nuclear quadrupole resonance spectra of $N_3P_3Cl_6$ and $N_3P_3Cl_5NHPr^i$ subjected to hydrostatic pressure

The effects of pressure on the chlorine - 35 nuclear quadrupole resonance frequencies at 295K in $N_3P_3Cl_6$ and in $N_3P_3Cl_5NHPr^i$ are shown in Figures 4.2 and 4.3 respectively, and the corresponding polynomials, relating frequency to the applied pressure are given in Table 4.2. Within the pressure range studied the plot for each resonance is a straight line, that is for these solids $\left(\frac{\partial \nu}{\partial P}\right)_{T = 295K}$ is independent of pressure within the range $1 \leqslant P \leqslant 1000$ Kg.cm^{-2}. The effects of applied pressure on the frequencies of these six-membered ring systems are also quite different from the corresponding effects on the frequencies of the four-membered ring systems which we have already reported, and so can be used to discriminate between the trigonal bipyramidal P - Cl systems in the chlorocyclodiphosphazanes and the tetrahedral P-Cl systems in the chlorocyclotriphosphazatrienes.

The effects of pressure on each of the four observed resonances in $N_3P_3Cl_6$ are very similar and these, in their turn, are very similar to the effects of pressure on ν_1, ν_4 and ν_5 in $N_3P_3Cl_5NHPr^i$. Furthermore, for each of these resonances $\left(\frac{\partial \nu}{\partial P}\right)_{T = 295K}$ is positive. However the effects of pressure on the ν_2 and ν_3 signals in $N_3P_3Cl_5NHPr^i$ are quite different and for these resonances $\left(\frac{\partial \nu}{\partial P}\right)_{T = 295K}$ is negative.

As stated above, in $N_3P_3Cl_5NHPr^i$ the ν_1 frequency must be assigned to the chlorine nucleus in the $\equiv PClNHPr^i$ residue while the four other resonances in this compound cannot be assigned on the basis of the frequencies observed at atmospheric pressure. However,

the results shown in Figures 4.2 and 4.3 and the data in Table 4.2 suggest that ν_2 and ν_3 should be assigned to the chlorine atoms of the $\equiv PCl_2$ groups which lie on the same side of the ring as the bulky $NHPr^i$ functional group; ν_1, ν_4 and ν_5 are assigned to the chlorine atoms which are on the other side of the cyclotriphosphazatriene ring.

The nine chlorine nuclei in these two molecules which find themselves in similar steric environments, namely those in $N_3P_3Cl_5NHPr^i$ on the opposite side of the ring from the bulky amino-substituent together with all six chlorines in $N_3P_3Cl_6$, give rise to chlorine - 35 n.q.r. frequencies which are affected by pressure changes to very similar extents.

4.3 The effects of temperature changes on chlorine - 35 nuclear quadrupole resonance spectra of chlorocyclotriphosphazatrienes

The chlorine - 35 nuclear quadrupole resonance frequencies of $N_3P_3Cl_6$ have already been examined over a wide temperature range [1] and it has been shown that no phase changes occur within the temperature range $77 \leq T \leq 320K$. Its quadrupole resonance frequencies can therefore be related to temperature by means of the equation

$$\nu = a + bT + \frac{c}{T} \qquad 4.1$$

and the values of a, b and c obtained from least squares analyses of data taken from reference 1 are listed in Table 4.3 The chlorine asymmetry parameters in this molecule have also been measured by Lucken [4], and lie within the range $0 \leq \eta \leq 0.02$.

Figure 4.4 shows the effects of temperature changes on

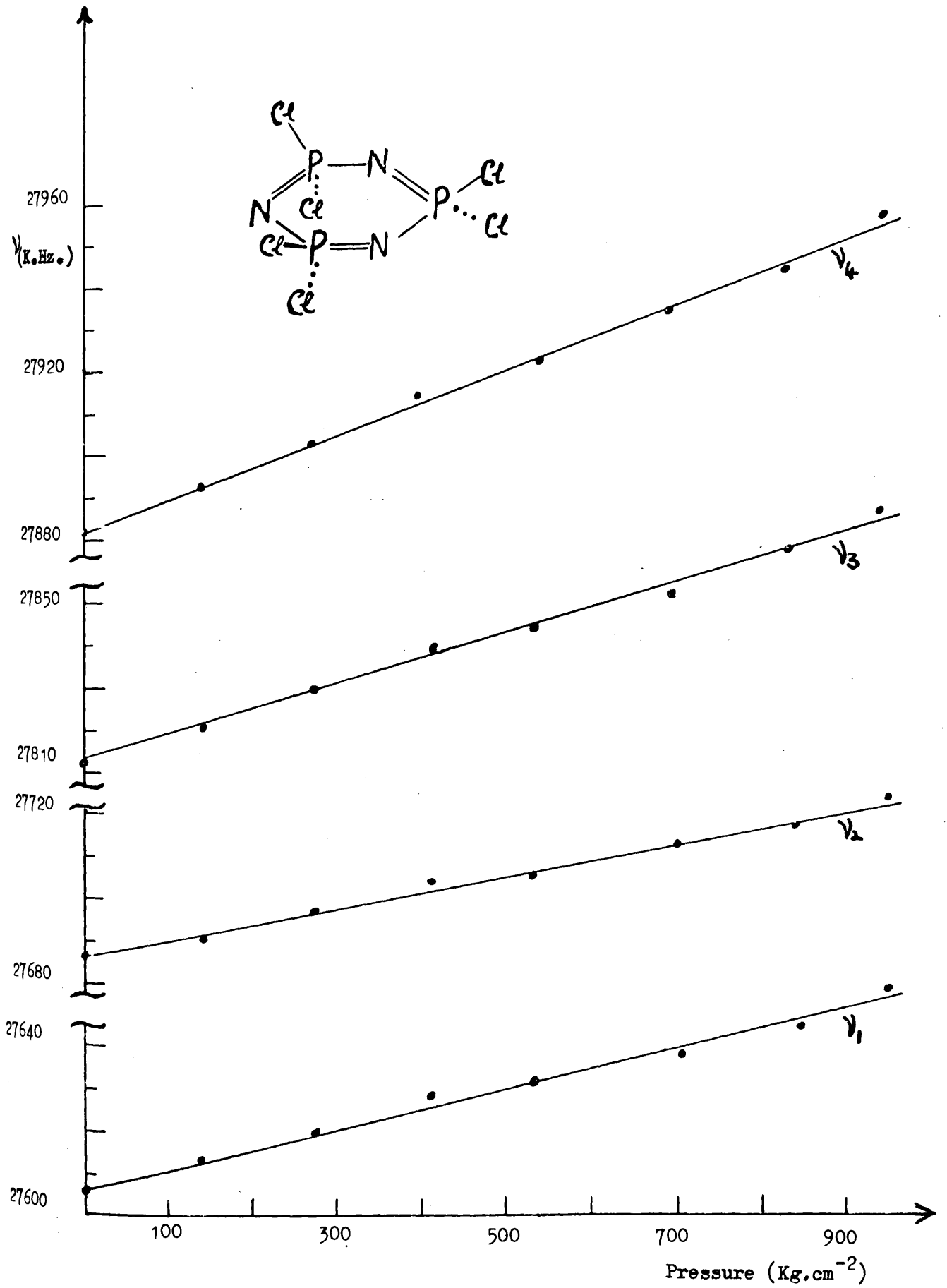

Figure 4.2 Plot of chlorine - 35 n.q.r. frequencies vs. pressure for $N_3P_3Cl_6$ at 295K.

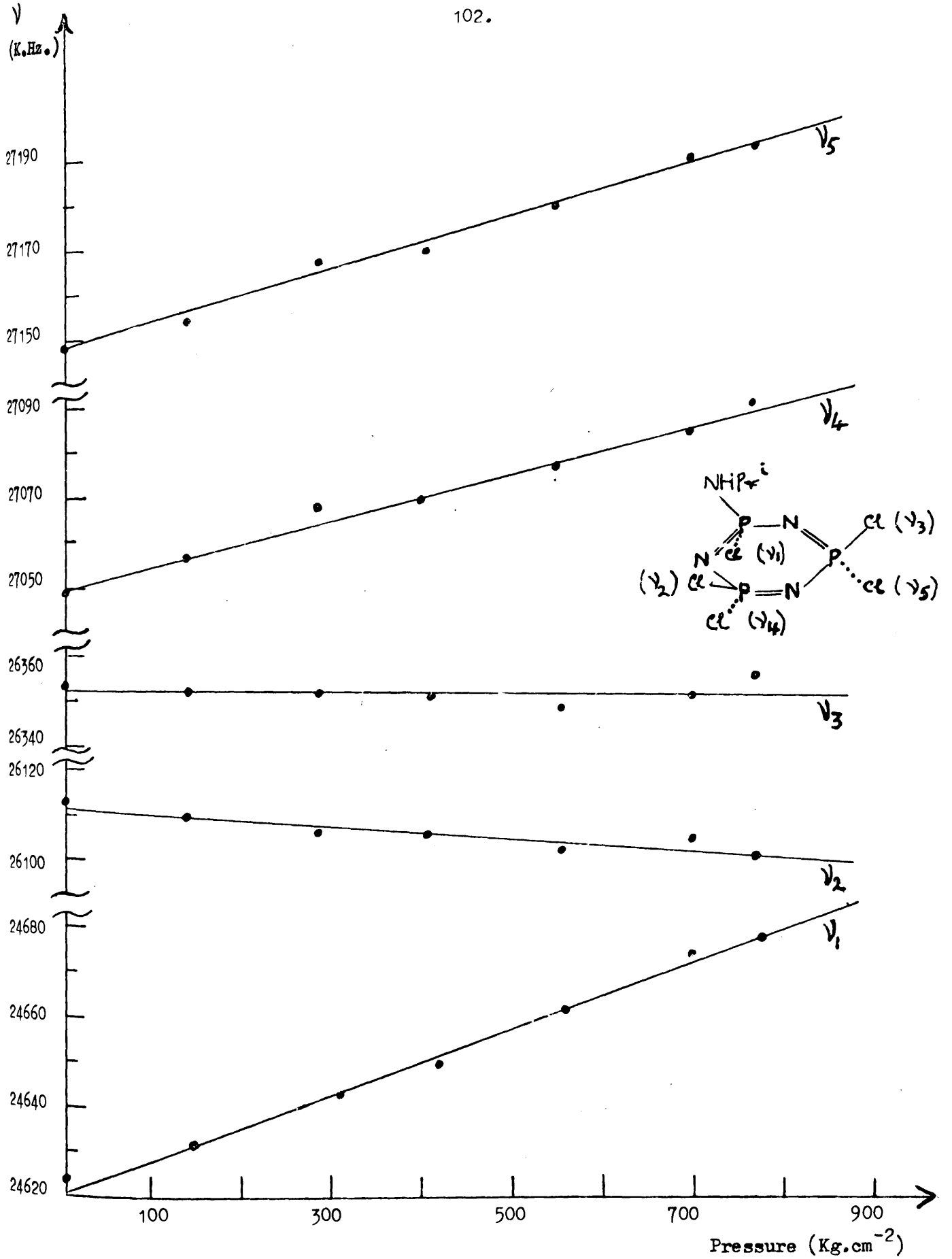

Figure 4.3 Plots of chlorine - 35 n.q.r. frequencies vs. pressure for $N_3P_3Cl_5NHPr^i$ at 295K.

Table 4.2

Polynomial equations, obtained using the least squares criterion, which describe the variation of ^{35}Cl n.q.r. frequencies with applied pressure within the range $1 \leq P \leq 1000 Kg.cm^{-2}$ (at 295K). In each case ν is in M.Hz. and P is in $Kg.cm^{-2}$.

Compound	Resonance	Equation	Standard Deviation
$N_3P_3Cl_6$	ν_1	$\nu = 27.6065 + 4.7282 \times 10^{-5}P$	3.021×10^{-3}
	ν_2	$\nu = 27.6864 + 3.7640 \times 10^{-5}P$	2.257×10^{-3}
	ν_3	$\nu = 27.8122 + 6.0584 \times 10^{-5}P$	2.556×10^{-3}
	ν_4	$\nu = 27.8808 + 7.8028 \times 10^{-5}P$	2.816×10^{-3}
$N_3P_3Cl_5NHPr^i$	ν_1	$\nu = 24.6204 + 7.3367 \times 10^{-5}P$	4.291×10^{-3}
	ν_2	$\nu = 26.1109 - 1.3349 \times 10^{-5}P$	2.331×10^{-3}
	ν_3	$\nu = 26.3516 - 1.4276 \times 10^{-6}P$	2.645×10^{-3}
	ν_4	$\nu = 27.0494 + 5.1251 \times 10^{-5}P$	2.931×10^{-3}
	ν_5	$\nu = 27.1477 + 5.9106 \times 10^{-5}P$	2.028×10^{-3}

the five resonances observed in the chlorine - 35 nuclear quadrupole resonance spectrum of $N_3P_3Cl_5NHPr^i$. It reveals a sharp phase change which occurs in the crystal structure of this compound within the temperature range $230 \leqslant T \leqslant 235K$, and so its resonance frequencies cannot be described by equation 4.1 over the whole temperature range studied ($77 \leqslant T \leqslant 350K$). This phase change might have been predicted from the negative values of $\left(\frac{\partial \nu}{\partial P}\right)_{T = 295K}$ which were observed for ν_2 and ν_3 since isotropic application of pressure to a molecular solid should reduce the vibrational amplitudes of the quadrupolar nuclei, and hence should increase nuclear quadrupole resonance frequencies. In a system where η is negligibly small, a negative value of $\left(\frac{\partial \nu}{\partial P}\right)_T$ implies that shearing movements of electric dipoles occur inside the solid in order to overcome the expected positive contribution from an isotropic application of pressure. If a solid which has a negative value of $\left(\frac{\partial \nu}{\partial P}\right)_T$ at ambient temperature is subjected to a sufficiently high pressure then it must undergo a phase change. The apparatus has obviously been unable to generate pressures which are high enough to force the phase change in $N_3P_3Cl_5NHPr^i$, but the internal pressures generated as the solid is cooled through the temperature range $230 \leqslant T \leqslant 235K$ are high enough to do so.

Values of a, b and c obtained by least squares analyses of the resonance frequencies for $N_3P_3Cl_5NHPr^i$ over the temperature range $240 \leqslant T \leqslant 320K$ are given in Table 4.3. Values of the partial differential coefficients

$$\left(\frac{\partial \nu}{\partial T}\right)_{\substack{P = 1Kg.\ cm^{-2} \\ T = 295K}}, \quad \left(\frac{\partial \nu}{\partial P}\right)_{T = 295K}, \quad \left(\frac{\partial \nu}{\partial T}\right)_{\substack{V \\ T = 295K}}$$

Table 4.3

Coefficients calculated by fitting the best curves of the form

$$\nu = a + b\,T + \frac{c}{T}$$

to the experimental curves of n.q.r. frequency vs. temperature

Compound	Resonance	a	b	c	$\left(\frac{\partial \nu}{\partial P}\right)_{T=295K}$	$\left(\frac{\partial \nu}{\partial T}\right)_{P=1Kg.cm^{-2}, T=295K}$	$\left(\frac{\partial \nu}{\partial T}\right)_{V, T=295K}$
$N_3P_3Cl_6$	ν_1	28.734×10^6	− 3676	-9.959×10^6	+47.3	−3565	−2477
	ν_2	28.658×10^6	− 3189	-6.236×10^6	+37.6	−3120	−2255
	ν_3	28.994×10^6	− 3888	-6.229×10^6	+60.6	−3819	−2425
	ν_4	29.126×10^6	− 3994	-1.052×10^7	+78.0	−3877	−2083
$N_3P_3Cl_5NHPr^i$	ν_1	31.825×10^6	−16007	-7.303×10^8	+73.4	−7615	−5927
	ν_2	30.972×10^6	−11701	-4.139×10^8	−13.4	−6944	−7252
	ν_3	32.477×10^6	−14831	-5.139×10^8	− 1.4	−8926	−8958
	ν_4	33.226×10^6	−14178	-5.876×10^8	+51.3	−7426	−6245
	ν_5	33.238×10^6	−13389	-6.312×10^8	+59.1	−6136	−4776

(a values are in Hz., b in $Hz.K^{-1}$., c in Hz.K., Standard deviations in b values are 100 $Hz.K^{-1}$. Standard deviations in c values are 2×10^6 Hz.K. $\left(\frac{\partial \nu}{\partial P}\right)$ values are in units of $Hz.Kg.^{-1}cm^2$. $\left(\frac{\partial \nu}{\partial T}\right)$ values are in units of $Hz.K^{-1}$.)

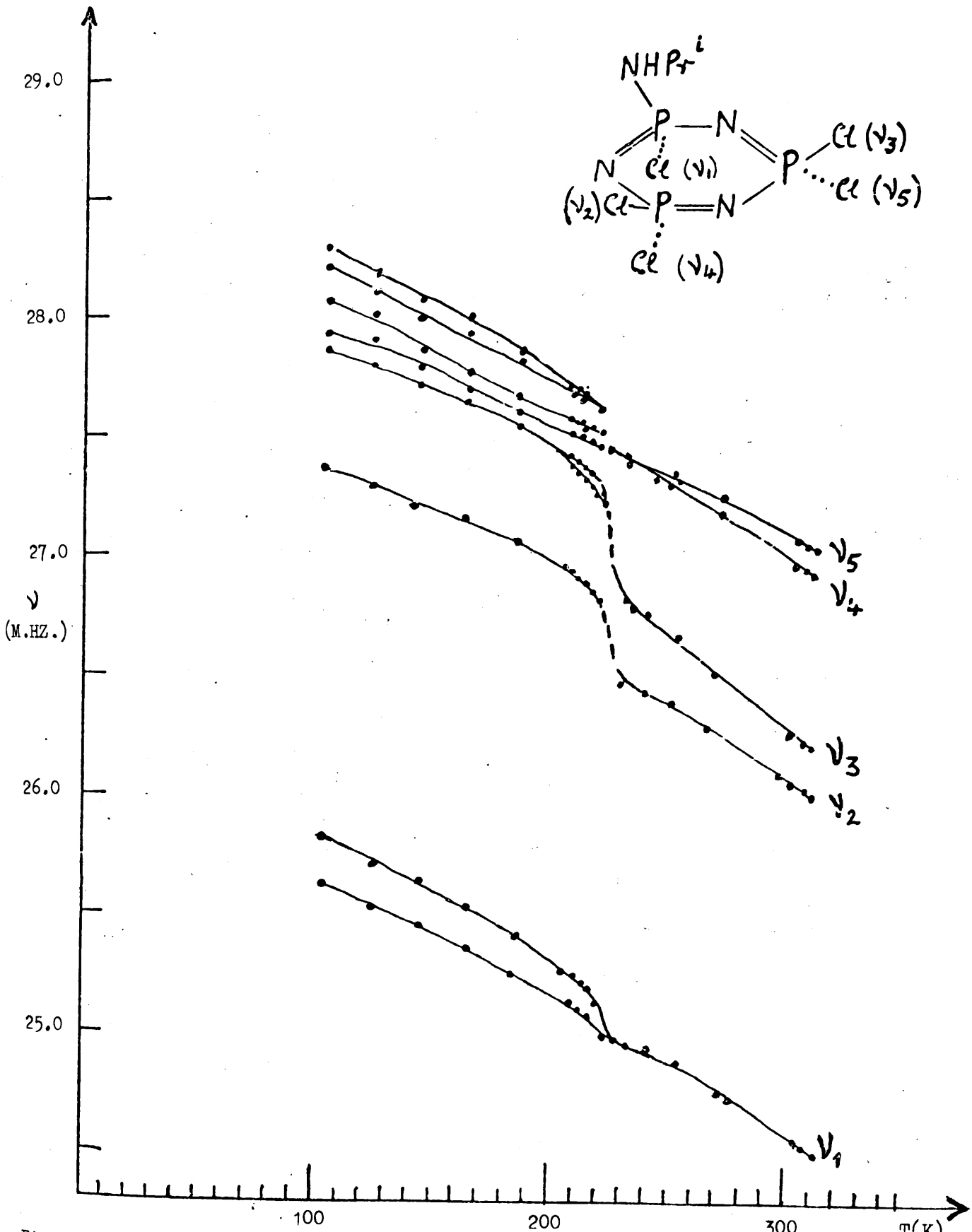

Figure 4.4 Plots of chlorine-35 n.q.r. frequencies vs. temperature for $N_3P_3Cl_5NHPr^i$.

for each resonance in $N_3P_3Cl_6$ and $N_3P_3Cl_5NHPr^i$ are also listed. The table shows that the effects of temperature changes on the quadrupole resonance frequencies of the chlorocyclophosphazatrienes are much larger than the corresponding effects on the chlorocyclodiphosphazanes.

The values of $\left(\frac{\partial \nu}{\partial T}\right)_{V}{}_{T=295K}$, obtained can be compared with values calculated on the assumption that only one mode of vibration influences the n.q.r. frequencies, and this has been done for $N_3P_3Cl_6$ in Table 4.4. A rigid librational motion of the whole molecule at a frequency of $23cm^{-1}$ is consistent with the observed values of $\left(\frac{\partial \nu}{\partial T}\right)_{V}{}_{T=295K}$, as also is a localised $\equiv PCl_2$ bending mode at a frequency in the range $55 < \nu < 60cm^{-1}$, or a linear combination of these two modes. These frequencies are in broad agreement with the observed infra-red spectrum of this compound [5] which shows two groups of low frequency modes within the ranges 23 - 28 cm^{-1} and 42 - 59 cm^{-1}.

In the case of $N_3P_3Cl_5$ $NHPr^i$ the situation seems to be much more complicated. In this case we have considered each nucleus separately and have worked out the frequencies of rigid-body librational motions and of bending modes which are required in order to account for the individual values of $\left(\frac{\partial \nu}{\partial T}\right)_{V}$ which are obtained experimentally. The resultant frequencies are given in the footnote to Table 4.5. As in the pressure experiments the data again appear to fall into two groups, the first being associated with ν_1, ν_4 and ν_5 and the second with ν_2 and ν_3. There is more scatter here, and the vibrational frequencies are lower than those deduced for $N_3P_3Cl_6$. It seems that in $N_3P_3Cl_5$ $NHPr^i$ rigid librational motions of the whole molecule may be more significant, and motions which involve the bulky $NHPr^i$ substituent may be important in accounting for the effects of temperature on the chlorine - 35 nuclear quadrupole resonance frequencies.

Table 4.4

Coefficients of rate of change of N.Q.R. frequency with temperature for each resonance in $N_3P_3Cl_6$. The $\left(\frac{\partial \nu}{\partial T}\right)_V$ values found from the temperature and pressure dependent studies are listed, together with calculated values which are determined by assuming that only the vibrational frequencies listed contribute to the temperature dependence of the N.Q.R. frequencies. All values given are in units of $Hz.K^{-1}$.

	ν_1	ν_2	ν_3	ν_4
Experimental $\left(\frac{\partial \nu}{\partial T}\right)_V$	-2477	-2255	-2425	-2083
Calculated $\left(\frac{\partial \nu}{\partial T}\right)_V$ assuming that the only vibrational modes which contribute are:				
(I) 55 cm^{-1} PCl_2 bending mode	-2439	-2433	-2461	-2472
(II) 23 cm^{-1} librational motion of the entire molecule.	-2371	-2365	-2393	-2403

Table 4.5

Coefficients of rate of change of n.q.r. frequency with temperature for each resonance in $N_3P_3Cl_5NHPr^i$. The $\left(\frac{\partial \nu}{\partial T}\right)_V$ values obtained from temperature and pressure dependent studies are listed, together with calculated values which are determined by assuming that only the vibrational frequencies listed in the footnote contribute to the temperature dependence of the individual n.q.r. frequencies. All values given are in units of $Hz.K^{-1}$.

	ν_1	ν_2	ν_3	ν_4	ν_5
Experimental $\left(\frac{\partial \nu}{\partial T}\right)_V$	-5927	-7252	-8958	-6245	-4776
Calculated $\left(\frac{\partial \nu}{\partial T}\right)_V$ assuming that the only vibrational modes which contribute are:					
(I) bending modes	-5970[a]	-7304[b]	-8965[c]	-6233[a]	-4726[d]
(II) rigid librational motion of the entire molecule	-5782[e]	-7417[f]	-9072[g]	-6036[e]	-4737[h]

[a] Assuming a frequency of 37 cm^{-1} [b] Assuming a frequency of 33 cm^{-1} [c] Assuming a frequency of 30.5cm^{-1}

[d] Assuming a frequency of 42.5 cm^{-1}

[e] Assuming a frequency of 15.5 cm^{-1} [f] Assuming a frequency of 13.5 cm^{-1} [g] Assuming a frequency of 12.5 cm^{-1}

[h] Assuming a frequency of 17.5 cm^{-1}

4.4 Evaluation of apparent vibrational amplitudes from quadrupole resonance data.

The analysis employed here can readily be extended to check whether large amplitude motions are of significance in $N_3P_3Cl_5\ NHPr^i$ by calculating the apparent mean square amplitude of vibration, $\langle\theta^2\rangle$, for each chlorine atom in the molecule. This is possible because it is implicit in the derivation of the Bayer type of analysis that $\langle\theta^2\rangle$ can be written in the form

$$\langle\theta^2\rangle = \frac{h}{4\pi^2\nu_i.I}\left(\frac{1}{2} + \frac{1}{\exp(h\nu_i/kT) - 1}\right) \qquad 4.2$$

where all the symbols used have the meanings defined in the previous chapter; $\langle\theta^2\rangle$ is defined as the time average value of the square of the angle of inclination of the maximum principal axis of the field gradient tensor relative to its equilibrium direction. In the high temperature limit $h\nu_i \ll kT$, so that equation 4.2 simplifies to

$$\begin{aligned}\langle\theta^2\rangle &\simeq \frac{kT}{4\pi^2\nu_i^2\ I} \\ &= \frac{2\ T\ b'}{3\ \nu_o} \\ &= \frac{2\ T}{3\ \nu_o}\left(\frac{\partial\nu}{\partial T}\right)_V \end{aligned} \qquad 4.3$$

where, as before, ν_o is the quadrupole resonance frequency for the static lattice, in the absence of even zero-point vibrations. The values of $\langle\theta^2\rangle$ calculated in this way must contain contributions from all modes which contribute to the temperature dependence of the n.q.r. frequency, not all of which are concerned

Table 4.6

Mean square vibrational amplitudes, $\langle\theta^2\rangle$, for the cyclotriphosphazatrienes $N_3P_3Cl_6$ and $N_3P_3Cl_5NHPr^i$ and for the cyclodiphosphazanes $(Cl_3PNCH_3)_2$ and $(Cl_3PNPh)_2$, calculated from the expression

$$\langle\theta^2\rangle \simeq \frac{2T}{3\nu_o}\left(\frac{\partial\nu}{\partial T}\right)_V \qquad T = 295K$$

Compound	Resonance		$\langle\theta^2\rangle$ (radians)^2
$N_3P_3Cl_6$	ν_1		0.01695
	ν_2		0.01548
	ν_3		0.01645
	ν_4		0.01407
$N_3P_3Cl_5NHPr^i$	ν_1		0.03663
	ν_2		0.04605
	ν_3		0.05425
	ν_4		0.03697
	ν_5		0.02826
$(Cl_3PNCH_3)_2$	ν_1	axial	0.01054
	ν_2	equatorial	0.01170
	ν_3	equatorial	0.01163
$(Cl_3PNPh)_2$	ν_1	axial	0.01483
	ν_2	equatorial	0.01259
	ν_3	equatorial	0.01442

with motion of the nucleus under consideration. It follows that the value of $\langle \theta^2 \rangle$ obtained from quadrupole resonance data will in general be larger than the true mean square amplitude of vibration.

Apparent vibrational amplitudes, $\langle \theta^2 \rangle$, have been calculated as described above from the quadrupole resonance data in Table 4.3 and the results obtained for the cyclotriphosphazatrienes $N_3P_3Cl_6$ and $N_3P_3Cl_5NHPr^i$ are given in Table 4.6 Data for the cyclodiphosphazanes $(Cl_3PNCH_3)_2$ and $(Cl_3PNPh)_2$ is included for comparison.

Once again the two cyclodiphosphazanes $(Cl_3PNCH_3)_2$ and $(Cl_3PNPh)_2$ show very similar behaviour. The apparent vibrational amplitudes calculated for $N_3P_3Cl_6$ are slightly larger, but still within the same range. The situation found for $N_3P_3Cl_5NHPr^i$ is significantly different however. In this case the resonances again fall into two groups, the apparent vibrational amplitudes of the ν_2 and ν_3 signals being much larger than those of ν_1 , ν_4 and ν_5 ; the values for all five resonances in this compound are larger than those found for the other compounds in Table 4.6. The larger apparent vibrational amplitudes for the chlorine nuclei in $N_3P_3Cl_5NHPr^i$ show that large scale vibrational motions, possibly involving the bulky sidechain, are important in this case in affecting the n.q.r. frequencies in the solid. This is not surprising since the compound is above the phase change region and so has a relatively open crystal structure, and at room temperature is quite close to its melting point ($55^{\circ}C$).

4.5 Conclusions

In this chapter the effects of temperature changes and pressure changes on the chlorine - 35 n.q.r. spectra of the chlorocyclotriphosphazatrienes $N_3P_3Cl_6$ and $N_3P_3Cl_5NHPr^i$ have been extensively investigated. It has been found that a sharp phase change occurs in $N_3P_3Cl_5NHPr^i$ over the temperature range $230 \leqslant T \leqslant 235K$, presumably associated with difficulty in accommodating the bulky side-chain in the compact low-temperature lattice. The resonance frequencies in both compounds are linear functions of applied pressure within the range $1 \leqslant P \leqslant 1000$ Kg. cm $^{-2}$, so distinguishing these species from the cyclodiphosphazanes studied earlier. The applied pressure also discriminates between the two kinds of chlorine atoms in the $\equiv PCl_2$ groups in $N_3P_3Cl_5NHPr^i$. Indeed the pressure affects the resonance frequencies of the nine chlorine nuclei in similar environments in these compounds in a very similar manner, and these effects appear to be characteristic of the functional groups involved.

The effects of pressure and temperature changes on the chlorine - 35 quadrupole resonance frequencies in $N_3P_3Cl_6$ can be explained in terms of either a rigid librational motion of the whole molecule at 23 cm $^{-1}$, or a localised $\equiv PCl_2$ bending mode at a frequency in the range $55 < \nu < 60$cm $^{-1}$, or by a linear combination of these two modes; the amplitudes of vibration calculated in this case however imply that, as in the cyclodiphosphazanes, the major influence is that from the localised bending mode. In $N_3P_3Cl_5NHPr^i$ however the vibrational amplitudes of the chlorine atoms appear to be much larger, implying that in this case librational modes in the range $13 < \nu < 18$cm $^{-1}$ may play the dominant role in determining the

influence of pressure and temperature on the n.q.r. frequencies.

4.6 Experimental

The techniques employed in studying the chlorine - 35 n.q.r. spectra as a function of temperature and pressure were identical to those discussed in the previous chapter of this work. Samples of $N_3P_3Cl_6$ were obtained commercially and recrystallised before use; $N_3P_3Cl_5NHPr^i$ was prepared as described in the literature [6], that is by the reaction of $N_3P_3Cl_6$ with isopropylamine in boiling chloroform.

Part II : Electron Paramagnetic Resonance Spectroscopy.

CHAPTER V

ELECTRON PARAMAGNETIC RESONANCE SPECTROSCOPY

5.1 Introduction

In nuclear quadrupole resonance spectroscopy the nuclear levels are split as a result of the interaction of the quadrupole moment of the nucleus with the electric field gradient which it experiences, the latter being determined by the presence of the other charged particles, both electrons and nuclei, in the solid. The situation in electron paramagnetic resonance spectroscopy is fundamentally different from this. In electron paramagnetic resonance spectroscopy the magnetic dipole moment of an unpaired electron interacts with magnetic fields developed by its surroundings. Since the magnetic moment of an electron is determined by both spin and orbital angular momenta, it follows that e.p.r. spectroscopy can be used as a powerful probe for examining the electromagnetic properties of matter.

In the present chapter the interaction of the electronic magnetic moment with a magnetic field is considered and the formalism of the spin Hamiltonian is developed. Attention is focussed on systems in which one unpaired electron interacts with one magnetic nucleus in the molecule.

5.2 The Zeeman interaction

The magnetic moment of an electron depends on its angular momentum G, which in its turn originates in both its intrinsic spin and its orbital motion. Formally the magnetic moment, μ, for an electron in an isolated atom is related to G by the expression

$$\mu = - \gamma_e G \qquad 5.1$$

where γ_e is known as the magnetogyric ratio of the electron and is defined by

$$\gamma_e = \frac{g_e e}{2\,mc} \qquad 5.2$$

In this expression e and m are respectively the charge and mass of the electron, c is the velocity of light, and g_e is the electronic g factor which equals 1 and 2.00232 for the orbital and spin angular momentum respectively.

The Hamiltonian for the magnetic energy associated with the interaction of an unpaired electron and a magnetic field H is given by

$$\begin{aligned} \mathcal{H} &= -\underline{\mu} \cdot \underline{H} \\ &= -\mu_z H \\ &= g_e \beta_e S_z H \end{aligned} \qquad 5.3$$

provided the cartesian z - axis coincides with the direction of H. The electronic Bohr magneton, β_e, is a constant equal to $e\hbar\,(2mc)^{-1}$, and S_z is the spin operator which defines the z-axis component of the electron's angular momentum. In an applied field the value of S_z can be either $-\frac{1}{2}$ or $+\frac{1}{2}$, the energies of the two resultant states being $-\frac{1}{2} g_e \beta_e H$ and $+\frac{1}{2} g_e \beta_e H$ respectively.

If a small orbital contribution to paramagnetism is present the interaction with the field can still be formally described by equation 5.3 if it is assumed that the magnetic moment arises entirely from the spin of the electron and the small orbital contribution is taken into the effective g factor which thus deviates from the spin only value, and becomes orientation dependent. In this approach the experimental results are

accounted for by describing the interaction between the electron and the magnetic field in terms of a Hamiltonian which contains only spin, and not orbital, operators, the Zeeman contribution to this Hamiltonian then becoming

$$\mathcal{H}_z = \beta_e \, \underline{H} \cdot g \cdot \underline{S} \qquad 5.4$$

where g is now a second rank tensor.

Since the concept of the "spin Hamiltonian" is so central to the interpretation of electron paramagnetic resonance spectra, its development, for systems in which the unpaired electron interacts with only one magnetic nucleus, is discussed in some detail in the following sections.

5.3 The spin Hamiltonian

From Kramers theorem we know that the ground state of a molecule with one unpaired electron is a spin doublet in the absence of an applied magnetic field, so that the ground state wavefunctions, in the absence of spin-orbit coupling, may be taken to be real wavefunctions with no orbital magnetic moment. These are denoted by $\phi_o \alpha$ and $\phi_o \beta$. Spin-orbit coupling, defined by the Hamiltonian

$$\mathcal{H}_{LS} = \xi \, \underline{L} \cdot \underline{S} = \xi (L_z S_z + L_x S_x + L_y S_y)$$
$$= \xi \left[L_z S_z + \frac{1}{2} (L_+ S_- + L_- S_+) \right] \qquad 5.5$$

where ξ is the spin-orbit coupling constant, reinstates a small amount of orbital paramagnetism by mixing in excited states $\phi_n \alpha$ and $\phi_n \beta$ into the ground state wavefunction. The new ground state wavefunctions, which are still degenerate, can be found from first order perturbation theory to be

$$
\begin{aligned}
|+\rangle &= |\phi_o\alpha\rangle - \tfrac{1}{2}\zeta \sum_n \frac{\langle\phi_n|L_z|\phi_o\rangle}{E_n - E_o}|\phi_n\alpha\rangle \\
&\quad - \tfrac{1}{2}\zeta \sum_n \frac{\langle\phi_n|L_x + iL_y|\phi_o\rangle}{E_n - E_o}|\phi_n\beta\rangle \\
|-\rangle &= |\phi_o\beta\rangle + \tfrac{1}{2}\zeta \sum_n \frac{\langle\phi_n|L_z|\phi_o\rangle}{E_n - E_o}|\phi_n\beta\rangle \\
&\quad - \tfrac{1}{2}\zeta \sum_n \frac{\langle\phi_n|L_x - iL_y|\phi_o\rangle}{E_n - E_o}|\phi_n\alpha\rangle
\end{aligned}
\qquad 5.6
$$

If the molecule is placed in a magnetic field then the true form of the Zeeman Hamiltonian, which describes the interaction of the unpaired electron with the field, is given by

$$
\begin{aligned}
\mathcal{H}_z &= \beta_e \underline{H}\cdot(g_e \underline{S} + \underline{L}) \\
&= \beta_e H_z (g_e S_z + L_z) + \beta_e H_y (g_e S_y + L_y) + \beta_e H_x (g_e S_x + L_x)
\end{aligned}
\qquad 5.7
$$

where g_e is the spin-only g value of 2.00232. This Zeeman interaction removes the degeneracy of the $|+\rangle$ and $|-\rangle$ basis wavefunctions. The matrix elements obtained when $\mathcal{H}_z$ operates on these functions can now be immediately written down ; for instance

$$
\langle + |\mathcal{H}_z| - \rangle = \beta_e \left[\langle + |g_e S_z + L_z| - \rangle H_z + \langle + |g_e S_y + L_y| - \rangle H_y + \langle + |g_e S_x + L_x| - \rangle H_x \right] \qquad 5.8
$$

These expressions can be considerably simplified since the Hermitian property of angular momentum operators allows the following substitutions to be made

$$
\begin{aligned}
\langle + | g_e S_j + L_j | + \rangle &= -\langle - |g_e S_j + L_j| - \rangle = \tfrac{1}{2} g_{jz} \\
\langle + | g_e S_j + L_j | - \rangle &= \langle - |g_e S_j + L_j| + \rangle^* = \tfrac{1}{2}(g_{jx} + ig_{jy})
\end{aligned}
\qquad 5.9
$$

The form of these substitutions is determined by the fact that diagonal matrix elements represent the expectation values of a real variable, and so must be real, while the off-diagonal matrix elements may be imaginary.

In terms of these substitutions the matrix elements of the Hamiltonian now become

$$\langle + | \mathcal{H}_z | + \rangle = \tfrac{1}{2} g_{zz} \beta_e H_z + \tfrac{1}{2} g_{yz} \beta_e H_y + \tfrac{1}{2} g_{xz} \beta_e H_x$$

$$\langle + | \mathcal{H}_z | - \rangle = \tfrac{1}{2} (g_{zx} - i g_{zy}) \beta_e H_z + \tfrac{1}{2} (g_{yx} - i g_{yy}) \beta_e H_y + \tfrac{1}{2} (g_{xx} - i g_{xy}) \beta_e H_x$$

$$\langle - | \mathcal{H}_z | + \rangle = \tfrac{1}{2} (g_{zx} + i g_{zy}) \beta_e H_z + \tfrac{1}{2} (g_{yx} + i g_{yy}) \beta_e H_y + \tfrac{1}{2} (g_{xx} + i g_{xy}) \beta_e H_x$$

$$\langle - | \mathcal{H}_z | - \rangle = -\tfrac{1}{2} g_{zz} \beta_e H_z - \tfrac{1}{2} g_{yz} \beta_e H_y - \tfrac{1}{2} g_{xz} \beta_e H_x \qquad 5.10$$

The matrix elements here are exactly the same as those which would be obtained by defining a fictitious spin operator S which would act on the states $| + \rangle$ and $| - \rangle$ in the same way as the true spin operator acts on the α and β states, and by using a Hamiltonian of the form

$$\mathcal{H} = \beta_e \underline{H} \cdot g \cdot \underline{S} \qquad 5.11$$

where g is a second rank tensor.

Thus it is possible to obtain expressions for the Zeeman energy of the system by considering the starting states to be pure spin states and by using a Hamiltonian containing only spin operators, known as the spin Hamiltonian. By comparing the elements of the spin Hamiltonian with those of the true Hamiltonian,

it can be shown that in general

$$g_{ij} = g_e \delta_{ij} - 2\lambda \sum_n \frac{\langle \phi_o | L_i | \phi_n \rangle \langle \phi_n | L_j | \phi_o \rangle}{E_n - E_o} \qquad 5.12$$

and it follows from the Hermitian properties of the angular momentum operators that the g - tensor is symmetric.

5.4 The hyperfine interaction

If an unpaired electron is in the vicinity of a nucleus which has a magnetic moment then there is an interaction between the magnetic moment of the electron and that of the nucleus. There are three quite distinct contributions to this interaction.

The first of these is the so-called Fermi contact interaction which is isotropic and arises from the presence of unpaired electron spin density at the magnetic nucleus in cases where the wavefunction of the electron has a finite value at the nucleus or where there is a polarisation of the paired S electrons about the nucleus by the unpaired electron. This interaction may be represented by a Hamiltonian of the form

$$\mathcal{H}_c = \frac{8\pi}{3} g_e g_N \beta_e \beta_N \delta(r_N) \underline{I}.\underline{S} \qquad 5.13$$

where $\delta(r_N)$ is the Dirac delta function which, integrated over the electronic wavefunction, gives the square of the value of the wavefunction at the nucleus.

The second contribution to the hyperfine interaction is an anisotropic contribution which arises from direct dipolar coupling between the spin magnetic moments of the electron and the nucleus. This is essentially the classical interaction of two dipoles $\underline{\mu}_e$ and $\underline{\mu}_N$ separated by a distance $\underline{r}$. The Hamiltonian

representing the energy of this spin-dipolar interaction may be written

$$\mathcal{H}_{SI} = -g_e g_N \beta_e \beta_N \left[r^2 \underline{S}.\underline{I} - 3 (\underline{S}.\underline{r}) (\underline{r}.\underline{I}) \right] r^{-5} \qquad 5.14$$

The final contribution to hyperfine coupling arises from the interaction of the orbital magnetic moment of the electron with the nuclear magnetic dipole and is given by the Hamiltonian

$$\mathcal{H}_{LI} = 2 g_N \beta_e \beta_N r^{-3} \underline{L}.\underline{I} \qquad 5.15$$

It can now readily be shown that the total hyperfine interaction, arising as above, can be represented by a spin Hamiltonian of the form

$$\mathcal{H} = \underline{S}.\underline{A}.\underline{I} \qquad 5.16$$

where A is a symmetrical second rank tensor. Thus the energy of the system, including both Zeeman and hyperfine interactions can be expressed in terms of the spin Hamiltonian

$$\mathcal{H} = \beta_e \underline{H}.\underline{g}.\underline{S} + \underline{S}.\underline{A}.\underline{I} \qquad 5.17$$

5.5 The quadrupolar interaction

As discussed earlier the interaction of a nuclear electric quadrupole moment with the gradient of the electric field at the nucleus results in a mixing of nuclear spin states. In e.p.r. the net effect of a quadrupolar interaction produces a second order shift in the energy levels, and makes normally forbidden transitions in which the electron and nuclear spins change simultaneously become weakly allowed. The quadrupolar interaction does not cause any change in the position of the resonance lines when the steady magnetic field lies parallel to the symmetry axis

of the paramagnetic species, but it does cause such changes when the magnetic field is not parallel to the Z-axis, and in addition the resulting nuclear hyperfine lines are then unequally spaced. The spin Hamiltonian representing this interaction can be written

$$\mathcal{H}_Q = \underline{I} \cdot P \cdot \underline{I} \qquad 5.18$$

where P is the quadrupole coupling tensor, whose components are of the form

$$P_{ij} = \frac{eQV_{ij}}{2I(2I-1)} \qquad 5.19$$

Thus the total spin Hamiltonian for a complex in which one unpaired electron interacts with one nucleus, and in which the orbital contribution to the magnetic moment of the electron is small, can be written as the sum of equations 5.17 and 5.18. If it is possible to choose an axis system which simultaneously diagonalises the g, A and P tensors, then the spin Hamiltonian simplifies to

$$\mathcal{H} = \sum_i \left(\beta_e g_{ii} H_i S_i + A_{ii} S_i I_i + P_{ii} I_i^2 \right) \qquad 5.20$$

where the summation is over the principal axis co-ordinates.

5.6 Solution of the spin Hamiltonian

It is now possible to obtain expressions from the spin Hamiltonian of equation 5.20 for the energy levels, and hence obtain the transition energies, for a single unpaired electron interacting with one magnetic nucleus. In a solution the situation is particularly simple since the rotation of the system averages out the anisotropic contributions to the various tensors so that the spin Hamiltonian becomes

$$\mathcal{H} = g_o \beta_e \underline{H} \cdot \underline{S} + A_o \underline{S} \cdot \underline{I} \qquad 5.21$$

where

$$g_o = \frac{1}{3} \sum_i g_{ii} \qquad \text{and } A_o = \frac{1}{3} \sum_i A_{ii} \qquad 5.22$$

The quadrupolar contribution has of course vanished since the quadrupole tensor is traceless. Eigenvalues of the Hamiltonian in equation 5.21 are given by

$$E_{m_s, m_I} = g_o \beta_e m_s H + A_o m_s m_I + \frac{A_o^2 m_s}{2 g_o \beta_e H} \left[I(I+1) - m_I^2 \right] \qquad 5.23$$

In the solid state the situation is considerably more complex. If we assume that the applied magnetic field H has direction cosines l, m and n with respect to the principal axes of the g – tensor then providing the same set of axes diagonalises all the tensors the Hamiltonian 5.20 can be rewritten as

$$\mathcal{H} = \beta_e (g_{xx} l S_x + g_{yy} m S_y + g_{zz} n S_z) H + \sum_i (A_{ii} S_i I_i + P_{ii} I_i^2) \qquad 5.24$$

where i = x,y,z. The energy levels and transition energies can be found from this expression by first considering the Zeeman interaction alone, and then treating the hyperfine and quadrupolar terms as successive perturbations. The basis states for the problem are of the form $|\alpha, m_I\rangle$ and $|\beta, m_I\rangle$ and we find that the energy matrix can be diagonalised with respect to the Zeeman term by carrying out the transformation

$$\begin{aligned} S_x &= a_{11} S_{x'} + a_{12} S_{y'} + a_{13} S_{z'} \\ S_y &= a_{21} S_{x'} + a_{22} S_{y'} + a_{23} S_{z'} \\ S_z &= a_{31} S_{x'} + a_{32} S_{y'} + a_{33} S_{z'} \end{aligned} \qquad 5.25$$

If the direction cosines of z' with respect to the x,y and z axes are defined to be $g_{xx}\, lg^{-1}$, $g_{yy}\, mg^{-1}$ and $g_{zz}\, ng^{-1}$ then the Zeeman term becomes $\mathcal{H}_z = g\,\beta_e\, HS_{z'}$. The z' axis can now be chosen as the axis of quantisation for the electron spin functions α and β , in which case these states are eigenfunctions of the transformed Zeeman term with energies of $\pm \frac{1}{2} g\,\beta_e\, H$. From the properties of direction cosines it follows that

$$g^2 = g_{xx}^2\, l^2 + g_{yy}^2\, m^2 + g_{zz}^2\, n^2 \qquad 5.26$$

The transformed hyperfine term in the Hamiltonian now becomes

$$= S_x(a_{11}A_{xx}I_x + a_{21}A_{yy}I_y + a_{31}A_{zz}I_z) + S_{y'}(a_{12}A_{xx}I_x + a_{22}A_{yy}I_y + a_{32}A_{zz}I_z)$$
$$+ S_{z'}(a_{13}A_{xx}I_x + a_{23}A_{yy}I_y + a_{33}A_{zz}I_z) + P_{xx}I_x^2 + P_{yy}I_y^2 + P_{zz}I_z^2 \qquad 5.27$$

The hyperfine term can now be treated using non-degenerate perturbation theory, providing it has no off-diagonal matrix elements between states which are degenerate in zero order; this is done by using a transformation of the same type as that above (equation 5.25). Remaining terms, both hyperfine and quadrupolar, can subsequently be treated by second order perturbation theory, and energies of the $|\alpha\ ,\ m_I\rangle$ and $|\beta\ ,\ m_I\rangle$ states can be evaluated, as can the energies of the allowed transitions for which $\Delta m_s = \pm 1$, $\Delta m_I = 0$.

For the special case in which the field lies along a principal axis direction, the transition energies are found to be

$$\Delta E = g_{ii}\ \beta_e H + A_{ii}\ m_I + \frac{(A_{jj}^2 + A_{kk}^2)}{4g_{ii}\ \beta_e H}\left[\ I(I+1) - m_I^2\ \right]$$
$$+ \frac{(P_{kk} - P_{jj})^2}{2A_{ii}}\left[\ 2I\ (\ I+1) - 2m_I^2 - 1\right] m_I \qquad 5.28$$

This expression can be recast in the form needed for the usual experimental arrangement, in which the magnetic field is swept while the microwave frequency, and hence ΔE, is held constant, to give values for the resonant fields as

$$H_i = H_o - a_{ii} m_I - \frac{(a_{jj}^2 + a_{kk}^2)}{4H_i}\left[I(I+1) - m_I^2\right] - \frac{(p_{jj} - p_{kk})^2}{2a_{ii}}\left[2I(I+1) - 2m_I^2 - 1\right] m_I \qquad 5.29$$

where the various parameters are now in units of gauss.

5.7 Lineshapes of electron paramagnetic resonance spectra of magnetically dilute glasses or polycrystalline samples

As long as the sample under investigation in electron paramagnetic resonance spectroscopy is a magnetically dilute single crystal the spectral lines are generally quite sharp so that measurement and analysis of the spectrum is fairly straightforward. However in a glass or in a magnetically dilute polycrystalline sample there are a large number of crystallites randomly oriented with respect to the applied magnetic field. The observed e.p.r. spectrum in these circumstances is then a summation of all possible spectra, each one weighted by the probability of a crystallite being in that particular orientation.

The expected lineshape can be computed by considering the transition probabilities as a function of orientation together with the probability of the molecule having a given orientation relative to the magnetic field direction. Kneubühl has treated the case of a molecule with $S = \frac{1}{2}$, $I = 0$. The lineshape function, $S(H)$, is expressed in terms of the resonant fields H_{11}, H_{22} and H_{33}, which correspond to the principal values of the g factor, g_{11}, g_{22} and g_{33} respectively. Assuming that $H_{33} < H_{22} < H_{11}$ then

in the interval $H_{11} \geqslant H \geqslant H_{22}$, S(H) is given by

$$S(H) = \frac{2H \; H \; H}{\pi H^2 (H_{11}^2 - H_{22}^2)^{\frac{1}{2}} (H^2 - H_{33}^2)^{\frac{1}{2}}} \; K(1') \qquad 5.30$$

whereas in the interval $H_{22} \geqslant H \geqslant H_{33}$,

$$S(H) = \frac{2H \; H \; H}{\pi H^2 (H_{22}^2 - H_{33}^2)^{\frac{1}{2}} (H_{11}^2 - H^2)^{\frac{1}{2}}} \; K(1) \qquad 5.31$$

In these expressions K(1) is the standard elliptic integral given by

$$K(1) = \int_0^{\frac{\pi}{2}} \frac{dx}{(1 - 1^2 \sin^2 x)^{\frac{1}{2}}}$$

$$= \frac{\pi}{2}\left[1 + \left(\frac{1}{2}\right)^2 1^2 + \left(\frac{1 \cdot 3}{2 \cdot 4}\right) 1^4 + - - - -\right] \qquad 5.32$$

and

$$(1')^2 = \frac{1}{1^2} = \frac{(H_{11}^2 - H_{22}^2)(H^2 - H_{33}^2)}{(H_{11}^2 - H^2)(H_{22}^2 - H_{33}^2)} \qquad 5.33$$

Absorption thus occurs between H_{11} and H_{33}. The function S(H) has discontinuities at $H = H_{11}$ and at $H = H_{33}$; it becomes infinite at $H = H_{22}$, where 1 and 1′ both equal one, and the elliptic integrals expand to infinity.

So far it has been assumed that the e.p.r. transitions are infinitely sharp. In fact line broadening does occur, so that if the lines are assumed to be Gaussian in shape, the broadened line has the form S(H′) where

$$S(H') = \int_{H = H_{11}}^{H = H_{33}} S(H) Y (H - H') \, d H \qquad 5.34$$

The Gaussian lineshape function, Y (H − H′) is given by

$$Y (H - H') = (2\pi)^{-\frac{1}{2}} \beta^{-1} \exp\left[-(H - H_o)^2 (2\beta)^{-2}\right] \qquad 5.35$$

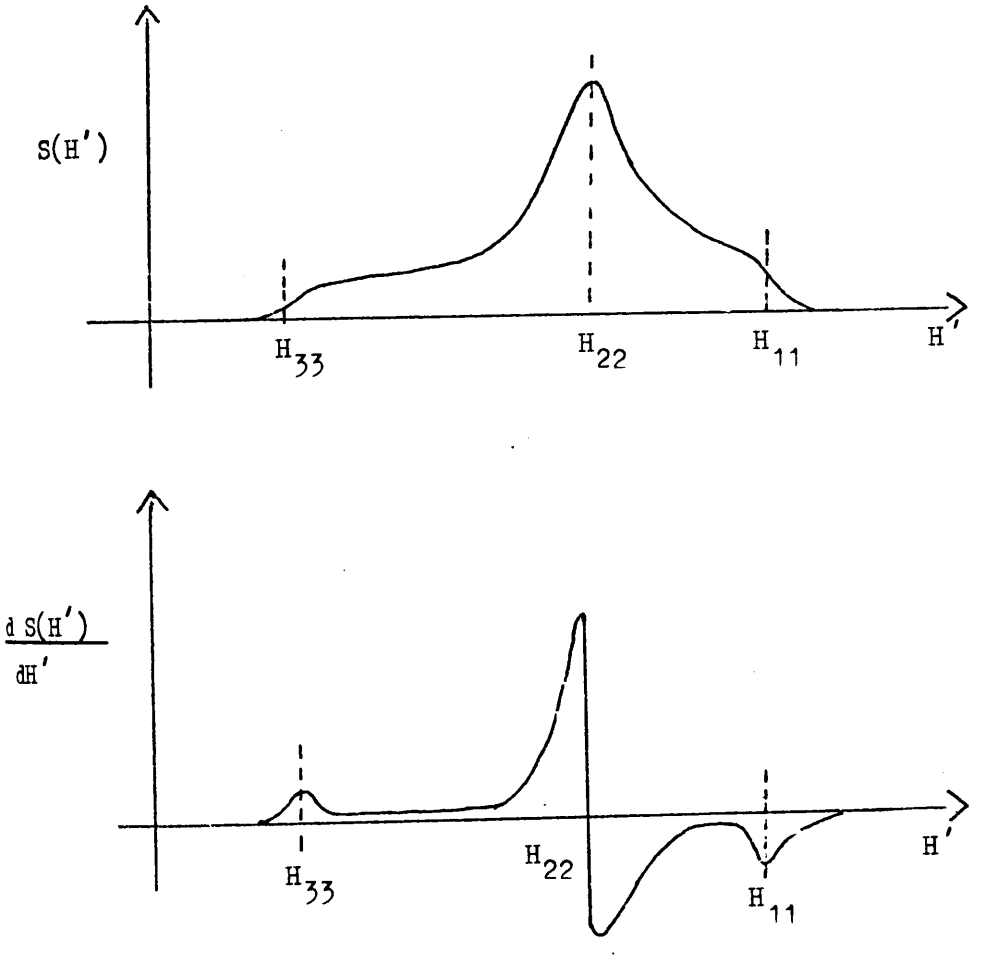

Figure 5.1

and the width of the line is here controlled by the broadening parameter β . The broadened lineshape $S(H')$ is illustrated in Figure 5.1 together with its derivative.

The g - tensor components can easily be obtained from a polycrystalline spectrum of this type by measuring H_{11} , H_{22} and H_{33}. If the electron interacts with a nucleus of spin quantum number I then $(2I + 1)$ patterns of this type will be obtained and it may thence be possible to obtain the principal components of the hyperfine tensor if all the peaks are well resolved. The major disadvantage of this technique is that the orientation of the principal axes of the g and A tensors cannot of course be found ; despite this it is an extremely useful method, particularly for samples which are too reactive to allow successful preparation of doped single crystals.

5.8 Electron paramagnetic resonance spectra and electronic structure

Electron paramagnetic resonance studies of transition metal complexes yield very detailed information about the distribution of the electrons. This information can be derived in two ways. First, the size of the hyperfine coupling between an unpaired electron and a magnetic nucleus decreases rapidly with the distance of the electron from the nucleus. Second, the orbital contribution to paramagnetism is reflected in the deviation of the g-tensor values from the spin-only value, so that e.p.r. spectroscopy gives information about the electron-nuclear distance, and also about the nature of the orbital containing the unpaired electron.

CHAPTER VI

ELECTRON PARAMAGNETIC RESONANCE STUDIES OF BIS - (π - CYCLOPENTADIENYL)-BIS - CHLORO VANADIUM (IV) ; THE SYNTHESIS OF (1.1' - TRIMETHYLENE - DICYCLOPENTADIENYL) - BIS-CHLORO VANADIUM (IV)

6.1 Introduction

Complexes of vanadium (IV) have been fairly extensively investigated by electron paramagnetic resonance spectroscopy. The bulk of this work has been concerned with oxovanadium (IV) species although a small number of studies of d^1 systems in which the vanadium (IV) ion occupies a site of tetrahedral or pseudo-tetrahedral symmetry have been reported. Detailed analyses of the e.p.r. properties of vanadium (IV) in a tetrahedral environment have been carried out for the chloride [1], alkoxide [2-4] and amino [3-5] derivatives VCl_4, $V(OBu^t)_4$ and $V(NR_2)_4$. In each of these complexes the unpaired electron lies essentially in the $3d_{x^2-y^2}$ orbital of the metal "ion".

More recently several studies of the electron paramagnetic resonance properties of the complex bis (π - cyclopentadienyl) - bis-chloro vanadium (IV) , $(\pi\text{-}C_5H_5)_2VCl_2$ and of related pseudotetrahedral complexes have appeared [6-8]; the results obtained by the various workers are at variance with one another. In this chapter the earlier work [9] on this compound is extended in an attempt to resolve this difficulty.

6.2 Electron paramagnetic resonance data for $(\pi - C_5H_5)_2VCl_2$

The electron paramagnetic resonance spectrum obtained from a magnetically dilute glass of $(\pi - C_5H_5)_2VCl_2$ in chloroform

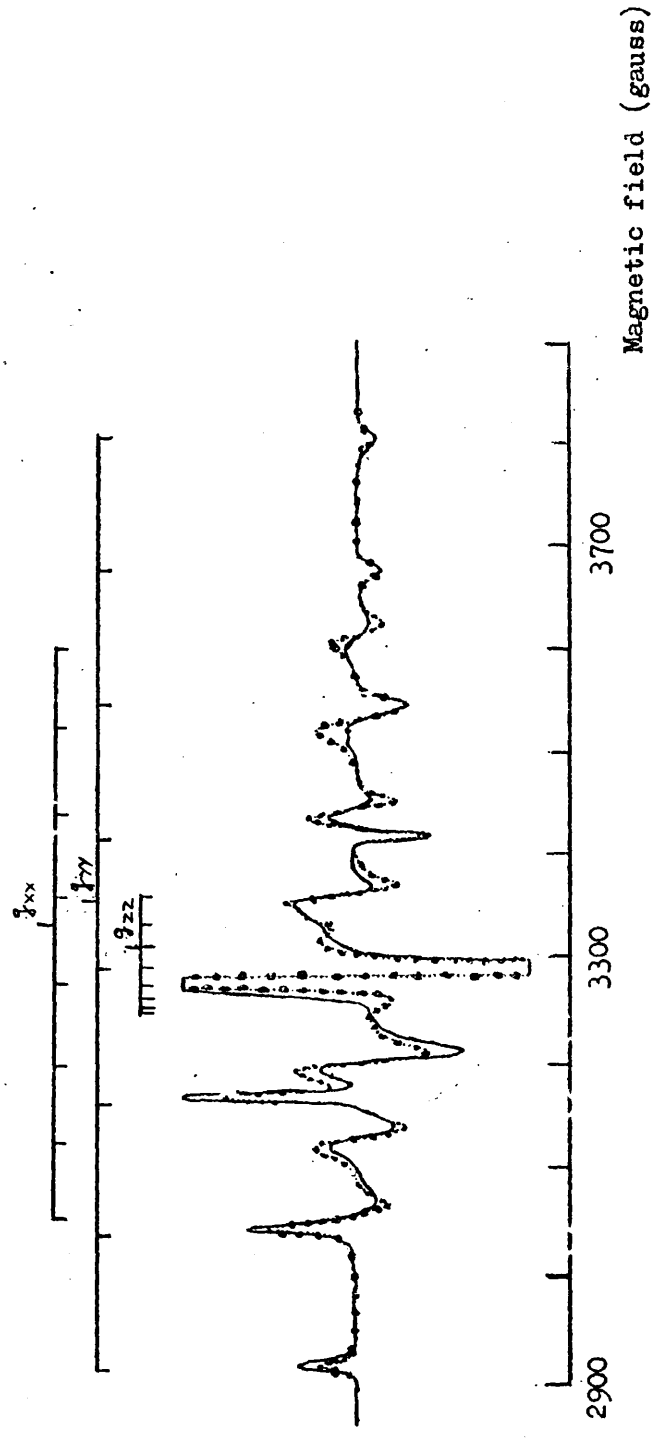

Figure 6.1 Observed (——) and calculated (•••••) e.p.r. spectra of a 10^{-3}M solution of (π -C_5H_5)$_2$ VCl_2 in $CHCl_3$: EtOH glass (9:1) at 77K.

containing 10% ethanol has been reported and analysed in detail by Stewart and Porte [6]. The spectrum is illustrated in Figure 6.1, and as indicated in the figure it is possible to distinguish peaks in the spectrum corresponding to the cases where the applied magnetic field lies along each of the x,y and z principal axes of the complex. Since the complex has effective C_{2v} symmetry the principal axes may be taken to be those shown in Figure 6.2 below. The glassy spectrum has therefore been

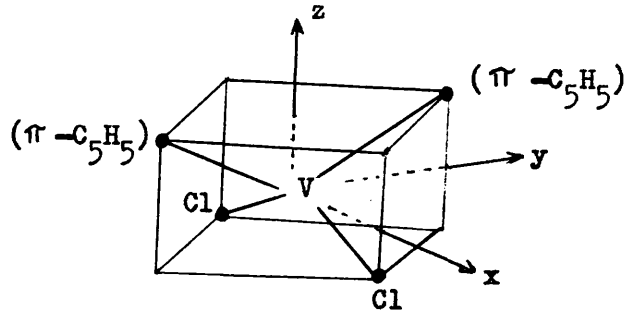

Figure 6.2

interpreted by these authors in terms of the totally anisotropic spin Hamiltonian [10]

$$\mathcal{H} = \beta_e \underline{H}.g.\underline{S} + \underline{S}.A.\underline{I} \qquad 6.1$$

where g and A are the anisotropic g and hyperfine tensors, and it is assumed that the two tensors can be simultaneously diagonalised.

The glassy spectrum can be analysed by computer simulation methods using Kneubühl functions of the type given in equation 5.34, and the best fitting values of the resonant fields H_x,H_y and H_z so found can then be used with equation 5.29 in order to calculate values of the anisotropic spin Hamiltonian parameters. The values obtained in this way, together with the best fitting

value of the Gaussian line broadening parameter β , are listed in Table 6.1. Since it is not possible to say which of the observed g - tensor values corresponds to g_{xx} and which to g_{yy}, referred to the axis system of Figure 6.2, from the e.p.r. data alone, the choice of g_{xx} as the larger of the two values is dictated by the results of the molecular orbital calculations carried out by these authors. [6]

The fact that the g_{zz} value is approximately equal to the spin-only value shows immediately that the unpaired electron occupies a molecular orbital which is primarily metal ion d_{z^2} in character, since for any other orbital all the g-tensor values would deviate from the spin-only value. The marked deviation from axial symmetry in both the g and A tensors however shows that the metal ion $d_{x^2-y^2}$ orbital, which belongs to the same irreducible representation as the d_{z^2} orbital in this complex, also contributes to the ground state.

The major difficulties in an analysis of this kind are first that the assumption must initially be made that the g and A tensors are coaxial, which is reasonable in the present case in which the unpaired electron is largely localised on the central metal atom. The second problem is that in order to analyse the glassy spectrum unambiguously all the peaks in the spectrum must be well resolved.

Bakalik and Hayes [7] have carried out an e.p.r. study of a magnetically dilute sample of $(\pi\text{-}C_5H_5)_2VCl_2$ doped into $(\pi\text{-}C_5H_5)_2$ Ti Cl_2. This work was carried out before the crystal structure of the host molecule had been determined [11,12] so that the orientation of the principal axes of the g and A tensors

Table 6.1

Spin Hamiltonian parameters for the complex $(\pi\text{-}C_5H_5)_2\ VCl_2$ at 77K, obtained from a magnetically dilute glass in chloroform containing 10% ethanol.[6] All hyperfine tensor components are in units of cm^{-1}. The Gaussian broadening factor, β, is in units of gauss.

g_{xx}	g_{yy}	g_{zz}	A_{xx}	A_{yy}	A_{zz}	$\langle g \rangle$	$\langle A \rangle$	β
1.986	1.971	2.000	-0.00740	-0.01170	-0.00152	1.986	-0.00687	3.5

Table 6.2

Spin Hamiltonian parameters[7] for the complex $(\pi\text{-}C_5H_5)_2\ VCl_2$ at room temperature obtained from a magnetically dilute single crystal of $(\pi\text{-}C_5H_5)_2\ VCl_2$ doped into $(\pi\text{-}C_5H_5)_2 Ti\ Cl_2$. All hyperfine tensor components are in units of cm^{-1}.

g_3	g_1	g_2	A_3	A_1	A_2	$\langle g \rangle$	$\langle A \rangle$
1.965	1.946	1.967	-0.00749	-0.01189	-0.00267	1.959	-0.00735

could not be found relative to the molecular axes, and the molecular geometry assumed in the molecular orbital calculations was based on the earlier electron diffraction [13] study of $(\pi - C_5H_5)_2 TiCl_2$. The spin Hamiltonian parameters deduced from the single crystal study are summarised in Table 6.2, and the data can be seen to differ significantly from the results of the polycrystalline analysis in Table 6.1. The trends in the two sets of data are similar, but although two of the hyperfine values agree fairly well, the A_{zz} value and all three principal g values differ markedly from the results quoted from Stewart and Porte's polycrystalline analysis. Both groups of workers assign the unpaired electron to an orbital which is primarily a linear combination of the metal ion $d_{x^2-y^2}$ and d_{z^2} orbitals; as already mentioned the g-factors found by Stewart and Porte show that this orbital is primarily d_{z^2} in character, while the results of Bakalik and Hayes suggest that the $d_{x^2-y^2}$ orbital is the more important.

In order to further investigate the discrepancies between these two studies a number of steps have been taken. It is of course possible that the paramagnetic $(\pi -C_5H_5)_2 VCl_2$ is forced to adopt a slightly different geometry in the single crystal environment from that in the glass; this has been investigated by preparing a polycrystalline sample of $(\pi -C_5H_5)_2 VCl_2$ doped into $(\pi -C_5H_5)_2 Ti Cl_2$. The spectrum of this sample is found to be identical to the glassy spectrum shown in Figure 6.1, showing that the differences in results obtained by the two groups of workers is not due to stereochemical changes in the different environments.

The spin Hamiltonian parameters from reference 7 have therefore been used to calculate the resonant fields H_x, H_y and H_z from equation 5.29, and these field values, in conjunction with Kneubühl functions of the type given in equation 5.34, provide the computer simulated polycrystalline spectrum shown in Figure 6.3. Qualitatively this simulated spectrum is similar to the observed polycrystalline spectrum of $(\pi\text{-}C_5H_5)_2\ VCl_2$ doped into the titanium analogue, which is also shown in the figure, but the differences in field values between the two spectra are very much larger than the likely experimental error.

The simplest way to establish whether the results of the single crystal analysis are in error, as Figure 6.3. appears to imply, would be to carry out an identical study on a single crystal of $(\pi\text{-}C_5H_5)_2\ Ti\ Cl_2$ doped with $(\pi\text{-}C_5H_5)_2\ VCl_2$. However the successful preparation of such a crystal is very difficult, since $(\pi\text{-}C_5H_5)_2\ Ti\ Cl_2$ almost invariably twins.[12] Bakalik and Hayes do not mention this twinning in their paper, and it is possible that the inconsistencies in their results might originate in not having taken this into account. Several attempts by the author of this thesis to prepare a doped single crystal large enough for e.p.r. analysis, from a variety of solvents including chloroform and benzene, have been unsuccessful, and so attention has been focussed on closely related derivatives which are expected to crystallise more readily.

6.3 Preparation of (1,1′ - trimethylenedicyclopentadienyl)vanadium dichloride

The preparation [14] and crystal structure [15] of the complex (1,1′ - trimethylenedicyclopentadienyl) titanium dichloride (I)

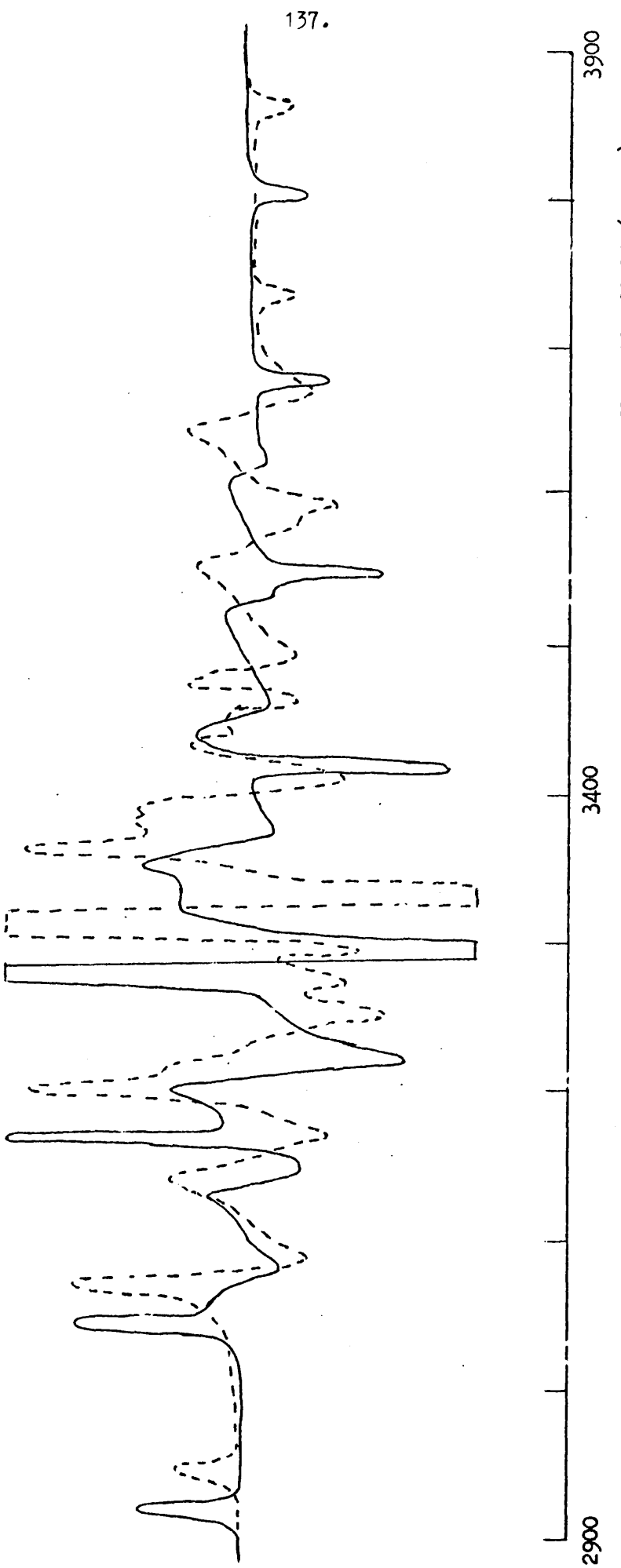

Figure 6.3. Observed e.p.r. spectrum (———) of a polycrystalline sample of (π - $C_5H_5)_2$ VCl_2 doped into (π -$C_5H_5)_2$ Ti Cl_2 together with the spectrum calculated (- - - -) from the spin Hamiltonian parameters given in reference 7.

have been reported, this complex being structurally very similar

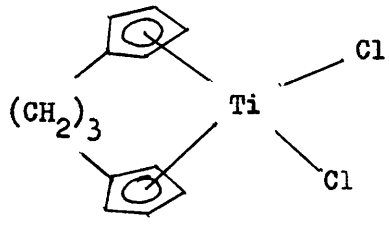

(I)

to (π -$C_5H_5)_2$ $TiCl_2$. Since the "bite" of the "chelating" trimethylene group is of virtually the same size as the ring-ring separation in (π -$C_5H_5)_2$ $TiCl_2$ the addition of the methylene chain makes little difference to the geometry of the complex. The bridged derivative $(CH_2)_3(C_5H_4)_2$ $TiCl_2$ can be crystallised much more readily than can (π -$C_5H_5)_2$ Ti Cl_2; this ease of crystal growth may be related to the marked reduction in vibration of the ring fragments which occurs when the bridging trimethylene group is introduced.

The structural similarity of the two titanium complexes is exemplified by the data in Table 6.3 in which bond lengths and angles around the central metal ion are quoted. It follows that the vanadium complexes (π -$C_5H_5)_2VCl_2$ and $(CH_2)_3(C_5H_4)_2$ VCl_2 should also have closely similar structural parameters, and that their e.p.r. spectra should also be very similar. It was therefore decided to attempt to prepare the vanadium complex $(CH_2)_3(C_5H_4)_2$ VCl_2 in order to carry out a full electron paramagnetic resonance study of this species doped into the corresponding titanium complex.

The preparative technique adopted is based on that for the

Table 6.3

Comparison of molecular parameters for $(CH_2)_3(C_5H_4)_2\ TiCl_2$ and $(\pi\text{-}C_5H_5)_2\ TiCl_2$ based on data in references 12 and 15.

Compound	Ti–Cl bond length (Å)	Cl–Ti–Cl (degrees)	Ti–ring distance (Å)	Ring–Ti–ring (Degrees)	Ring–Ti–Cl (degrees)
$(CH_2)_3(C_5H_4)_2\ Ti\ Cl_2$	2.368	93.69	2.061	132.64	105.95
$(\pi\text{-}C_5H_5)_2\ Ti\ Cl_2$	2.364	94.53	2.059	130.97	106.40

titanium species [14] which is in turn derived from an earlier method, [16] and proceeds as follows, all reactions being carried out in a nitrogen atmosphere. Freshly prepared cyclopentadiene monomer (0.5 moles) is added slowly to a stirred suspension of finely divided sodium in 250 ml of tetrahydrofuran at 0°C, to form sodium cyclopentadienide. 1,3 - Dibromopropane (0.25 moles) is then added slowly and the mixture is stirred for about three hours until the reaction has ceased. The pink solution is now filtered to remove any unreacted sodium, and the filtrate is slowly added to a stirred mixture of sodium hydride (0.5 moles) in 50 ml of tetrahydrofuran at 45-50°C. This reaction takes place very slowly, and is best allowed to proceed overnight. The resulting solution of the di-anion (II) is now added

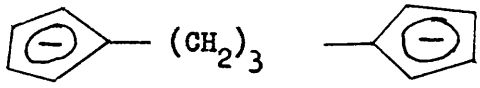

(II)

slowly to a suspension of vanadium tetrachloride (0.25 moles) in 200 ml of tetrahydrofuran, prepared by slowly adding the VCl_4 to tetrahydrofuran at 0°C with vigorous stirring, and the mixture is again stirred overnight. The solvent is now removed by evaporation under reduced pressure, and the resulting black solid repeatedly extracted with chloroform; the combined extracts are concentrated and added dropwise to a large volume of hexane, with stirring. The resulting green solid is re-extracted in the same way, and finally recrystallised from benzene. Attempts to purify the solid by sublimation are not successful since extensive decomposition occurs, although small amounts of material do sublime at 260°C

and 10^{-4}mm.

A black oil is also found in the reaction mixture, which can be removed from the product by the extraction procedure above. This oil is probably produced by a polymerisation of dianion (II) or its immediate precursor $(CH_2)_3(C_5H_5)_2$. The latter compound is very unstable, and decomposes spontaneously in the absence of solvent.

The paramagnetic green solid isolated from this reaction is $(CH_2)_3(C_5H_4)_2\ VCl_2$, as shown by microanalysis (calculated C 53.43%, H 4.83% ; observed C 53.32%, H 5.20%). The infra-red spectrum is similar to that of $(\pi\text{-}C_5H_5)_2\ VCl_2$ with extra peaks corresponding to the vibrations of the methylene groups; the spectrum exhibits the pattern of bands expected for a π-bonded cyclopentadienyl grouping.[17] The electron paramagnetic resonance spectrum of a chloroform : ethanol (9:1) glass of $(CH_2)_3(C_5H_4)_2\ VCl_2$ at 77K is shown in Figure 6.4. Both solution and glassy spectra of this compound are extremely similar to those found for $(\pi\text{-}C_5H_5)_2\ VCl_2$, and the spin Hamiltonian parameters extracted from the glassy spectrum are summarised in Table 6.4.

Table 6.4

Spin Hamiltonian parameters for the complex $(CH_2)_3(C_5H_4)_2VCl_2$ at 77K, extracted from a magnetically dilute glass in chloroform containing 10% ethanol. All hyperfine tensor components are in units of cm^{-1}, and the β value is in gauss.

g_{xx}	g_{yy}	g_{zz}	A_{xx}	A_{yy}	A_{zz}	β	$\langle g \rangle$	$\langle A \rangle$
1.988	1.972	2.000	-0.00740	-0.01185	-0.00154	5	1.987	-0.00693

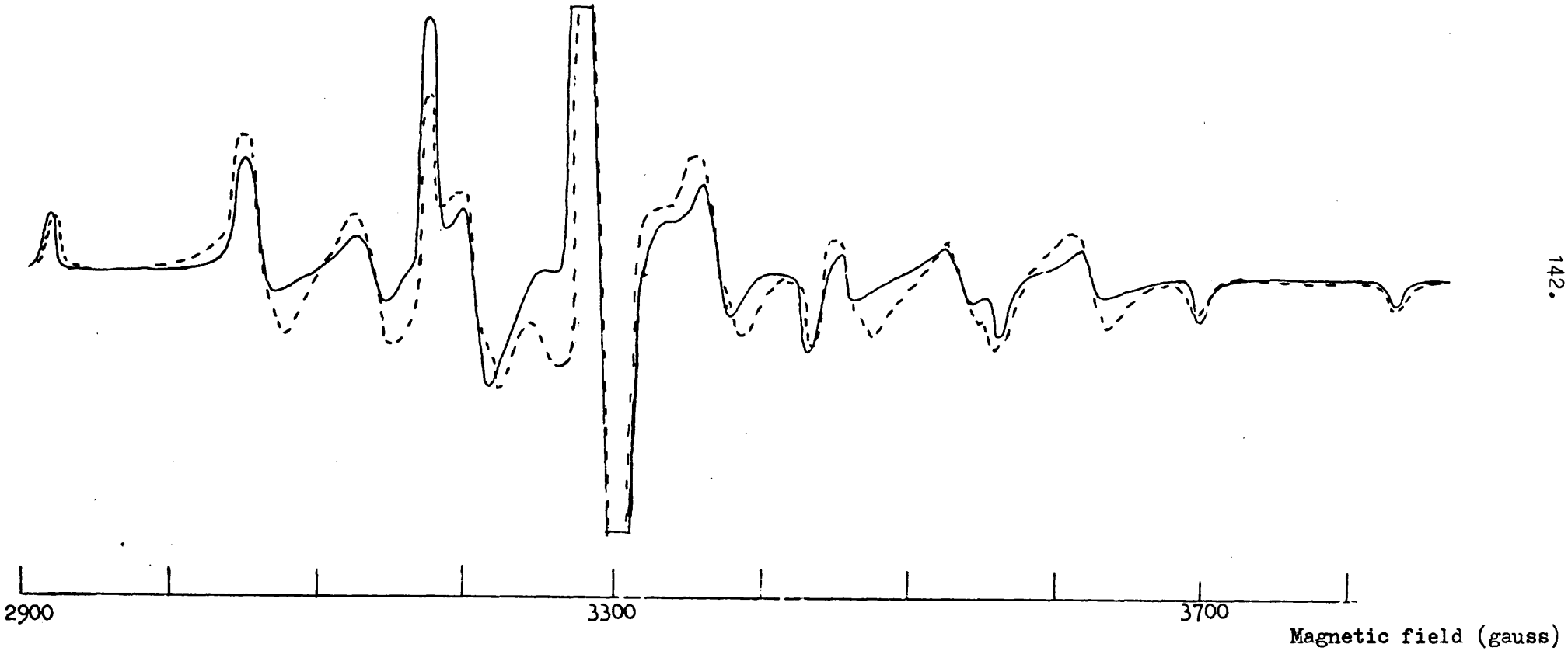

Figure 6.4 Observed (_____) and calculated (- - -) e.p.r. spectra of a 10^{-3} M solution of $(CH_2)_3 (C_5H_4)_2 VCl_2$ in chloroform : ethanol (9:1) glass at 77K.

Another paramagnetic species has been detected in the reaction mixture, and this turns out to be the tetrahydrofuran adduct of VCl_4, which has been previously reported [18] although its e.p.r. spectrum has not been given. The spin Hamiltonian parameters found from analysis of solution and frozen solution spectra of this compound are summarised in Table 6.5 together with data for vanadyl acetylacetonate in tetrahydrofuran [19] in which the vanadium is in a similar distorted octahedral environment.

Table 6.5

Spin Hamiltonian parameters for the complexes $VCl_4.2THF$ and $VO(acac)_2$ in THF. All hyperfine tensor components are in units of cm^{-1}

Compound	$g_{\parallel}$	$g_{\perp}$	$\langle g \rangle$	$A_{\parallel}$	$A_{\perp}$	$\langle A \rangle$
$VCl_4.2THF$	1.941	1.983	1.969	0.01507	0.00551	0.01004
$VO(acac)_2$	1.945	1.981	1.969	0.01535	0.00572	0.00896

The observed polycrystalline spectrum of the tetrahydrofuran adduct is shown in Figure 6.5. The fact that this species can be detected in the final reaction mixture indicates the instability of the dianion (II), and the consequent difficulty of obtaining a completely stoichiometric reaction mixture.

On one occasion a third paramagnetic compound was detected during attempts to purify $(CH_2)_3(C_5H_4)_2VCl_2$ by sublimation, when the $(CH_2)_3(C_5H_4)_2VCl_2$ which did sublime was found to be mixed with an approximately equal amount of this new species. This compound has an isotropic g factor of 1.994 and hyperfine

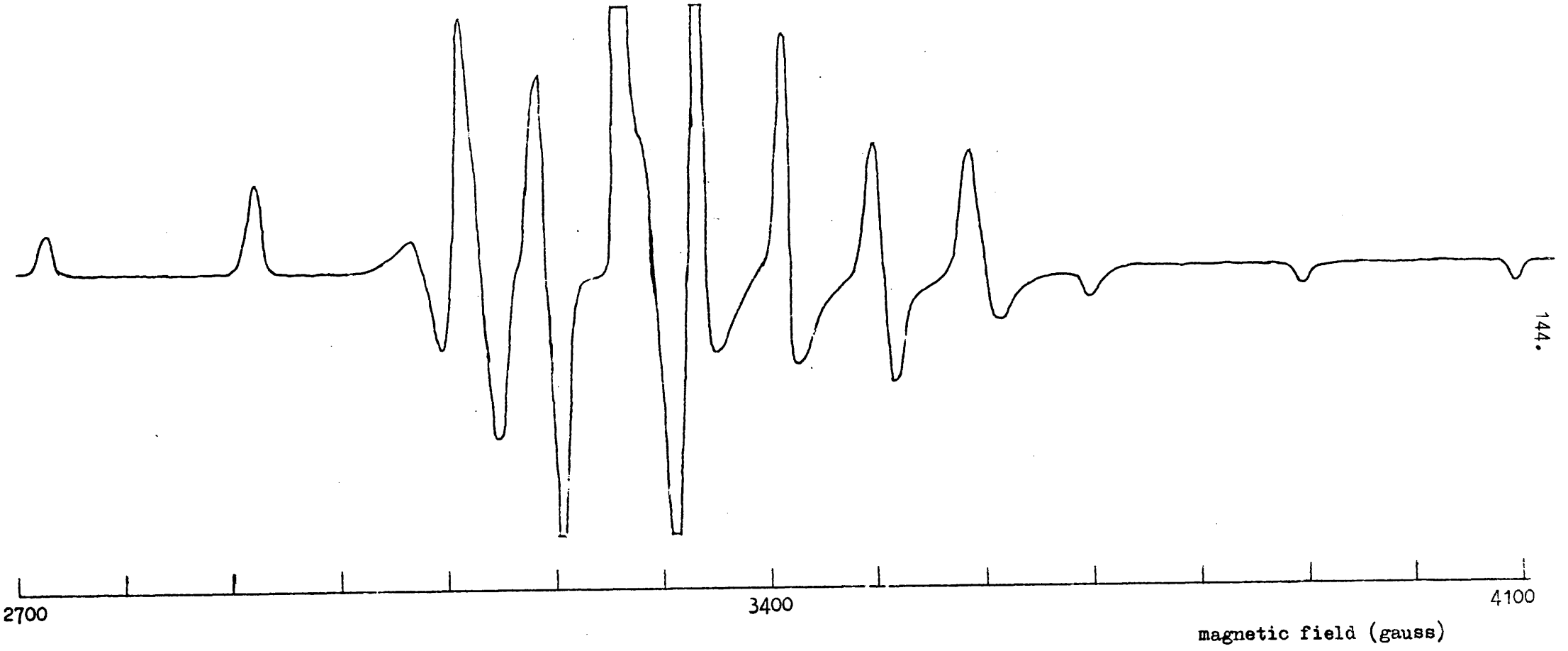

Figure 6.5 Observed e.p.r. spectrum of a 10^{-3} M solution of the tetrahydrofuran adduct of VCl_4 in a tetrahydrofuran glass at 77K.

coupling constant, A, of 0.0065 cm^{-1} in chloroform solution at room temperature. Although the nature of this species has not been further investigated in this work, its formation during the sublimation experiment implies that it may be produced as a result of a rearrangement reaction of either $(CH_2)_3(C_5H_4)_2VCl_2$ or the tetrahydrofuran adduct of VCl_4, and this is worthy of further study.

Despite the success in the synthesis of $(CH_2)_3(C_5H_4)_2$ VCl_2, it has not proved possible to grow crystals of this material doped into $(CH_2)_3(C_5H_4)_2$ Ti Cl_2, presumably because of the instability of the vanadium complex, as any decomposition would tend to markedly inhibit the growth of good quality crystals.

6.4 Experimental aspects of the electron paramagnetic resonance studies

The electron paramagnetic resonance spectra reported in this work were recorded on a Decca X - 3 spectrometer, operating in the X-band region of the microwave spectrum at 9270 M.Hz., in conjunction with a Newport 11-inch magnet system. The detection system employed 100 K.Hz. audiomodulation together with a phase sensitive detector, and the e.p.r. spectrum was recorded as a first derivative. The e.p.r. spectrum was calibrated using proton magnetic resonance methods, and the calibration system itself was checked using a finely powdered sample of diphenylpicrylhydrazyl, whose g-factor is known accurately to be 2.0036.

Samples studied at room temperature were contained in spectrosil quartz tubes. Spectra recorded at 77K were obtained by placing some of the sample in a long-tailed dewar, the spectrosil quartz tail of which was inserted into the sample cavity, and pouring liquid nitrogen on top of it.

A P P E N D I X A

THE USE OF A COMPUTER OF AVERAGE TRANSIENTS IN CONJUNCTION WITH THE DECCA RADAR N.Q.R. SPECTROMETER

The Zeeman - n.q.r. experiments described in Chapter III require a small constant magnetic field to be applied to a polycrystalline sample of $(Cl_3PNCH_3)_2$. This broadens the resonance signals so severely that the detection of the polycrystalline lineshape predicted by Morino and Toyama from a single pass through the spectrum is only possible at relatively low magnetic fields. In order to carry out Zeeman - n.q.r. experiments in magnetic fields of up to 30 gauss it is necessary to couple the spectrometer output to a computer of average transients. The experimental arrangement adopted is described in detail in this section.

The computer of average transients available for use in this work was a Technical Measurement Corporation C-1024 Time Averaging Computer. This has only one Y input so that it is not possible to record the signal and markers simultaneously. In Zeeman - n.q.r. experiments this is not a serious limitation since an absolute frequency measurement is not necessary; the measurements which are necessary in this work are those of frequency difference between different parts of each spectrum, and this is facilitated by recording adjacent sideband signals which then supply an internal estimate of the frequency range scanned.

The mode of operation of the time averaging computer (CAT) with the n.q.r. spectrometer is illustrated in Figure A1.

The C A T supplies a ramp voltage of up to 25 volts to the n.q.r. spectrometer MW312 unit, and this voltage is used to pull the frequency of the spectrometer, so sweeping through the resonance. The phase sensitive detector output from the spectrometer is connected to the C A T input plug. After accumulating the signal it is fed from the "analogue output" socket of the C A T to the chart recorder via a D.C. output balancing circuit. The latter is fully described in the C A T manual, its function being to add or subtract a constant voltage to the C A T output in order to allow the recorder to display a normal signal with a centre zero presentation. The magnetic field necessary for the Zeeman experiments is generated by passing a suitable current through the Helmholtz coil arrangement shown in the figure. No attempt was made to cancel the earth's magnetic field at the sample.

All other connections are made as for normal spectrometer operation. As an example of the use of the time averaging computer, the operating conditions employed in recording the Zeeman – n.q.r. spectrum illustrated earlier in Figure 3.4 are summarised in Table A1. Once the spectrometer and computer averager have been set up as in Table A1 the process of accumulating the spectrum proceeds as follows. First the frequency of the n.q.r. spectrometer is accurately adjusted to the value required. The function selector switch on the C A T is set to "internal trigger" and the process of recording the spectrum is started by switching the "Trigger source" control to "recur". Accumulation of data continues automatically until the required number of scans have been completed. The final spectrum can be recorded by plotting on the chart recorder, or alternatively by displaying it on the C A T

oscilloscope and photographing it. With the same spectrometer conditions as above a good signal to noise ratio can be obtained with only 25 scans in zero magnetic field.

When recording polycrystalline spectra in magnetic fields in this way it is possible to obtain an estimate of the magnetic field applied from the spectrum, since the separation of the two "derivative" features in the spectrum is equal to twice the chlorine - 35 Larmor precession frequency in this magnetic field. The spectra recorded for the ν_1 and ν_2 resonances in $(Cl_3PNCH_3)_2$ have been analysed to give the magnetic field in each case, and a plot of magnetic field against the current in the Helmholtz coils is given in Figure A2. This figure shows that the Helmholtz coils used in this work have a magnet constant of 134 gauss. amp^{-1}.

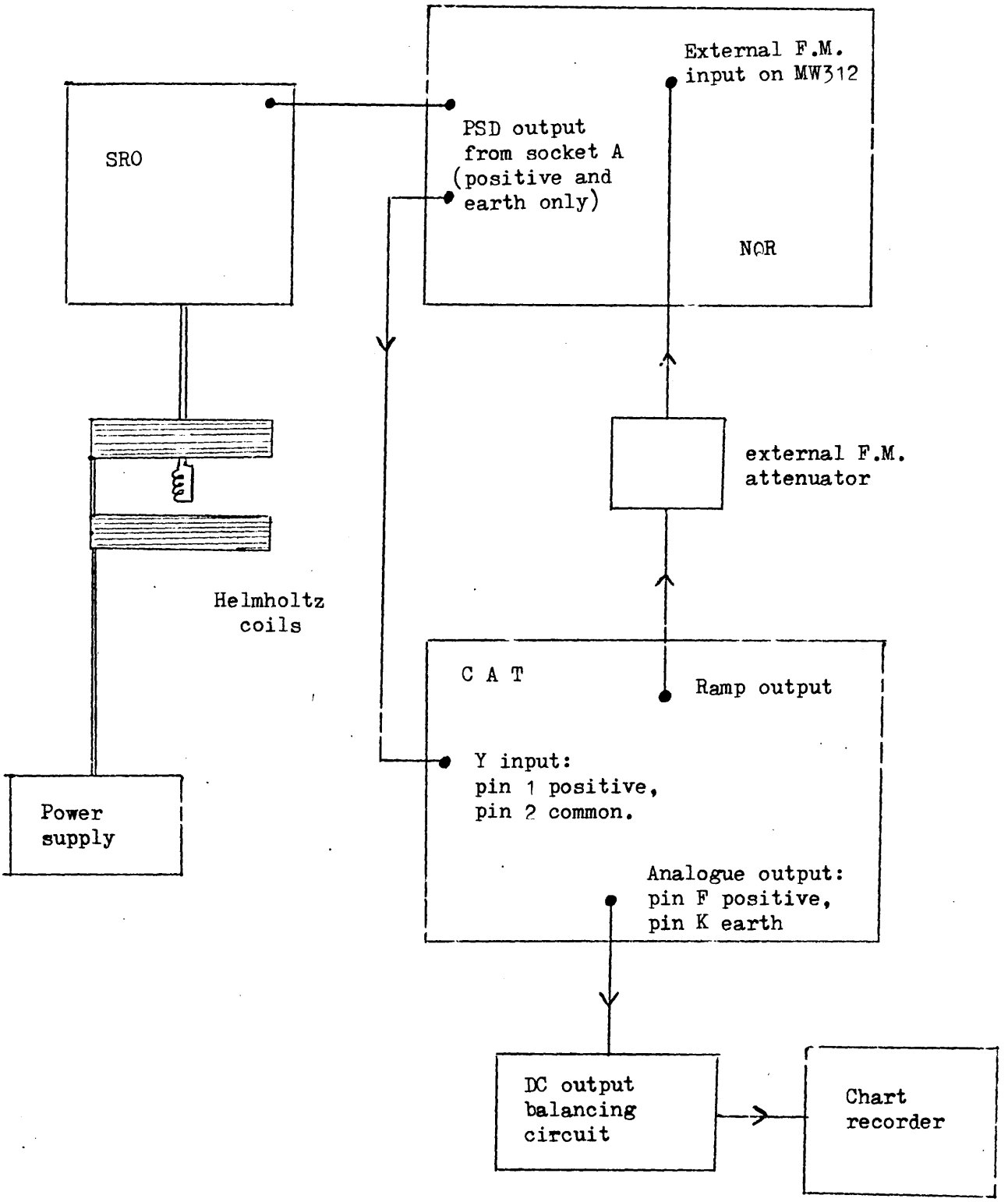

Figure A1 Block diagram of the experimental arrangement when using the Time Averaging Computer together with the Decca Radar n.q.r. spectrometer to record Zeeman - n.q.r. spectra. All other connections are assumed to be as for normal spectrometer operation.

Table A1

Operating conditions employed in recording the Zeeman -n.q.r. spectrum of the ν_2 resonance in $(Cl_3PNCH_3)_2$ in a magnetic field of 21.5 gauss; this spectrum is illustrated in Figure 3.4.

NQR Spectrometer Settings		C A T Settings	
r.f. level	7	stand by switch	add
quench p.r.f.	50 K.Hz.	flyback time	0
FM1 amplitude	3 x 0.1	search rate	min
amplifier	10	sweep width	10 x 25
PSD phase	1 0'clock	sweep time	25 sec
time constant	0.3 sec	memory location	1-1024
AGC	3	preset counter	1225
coherence	4.8		
sideband suppression	off		
external FM attenuator	2 x 1		

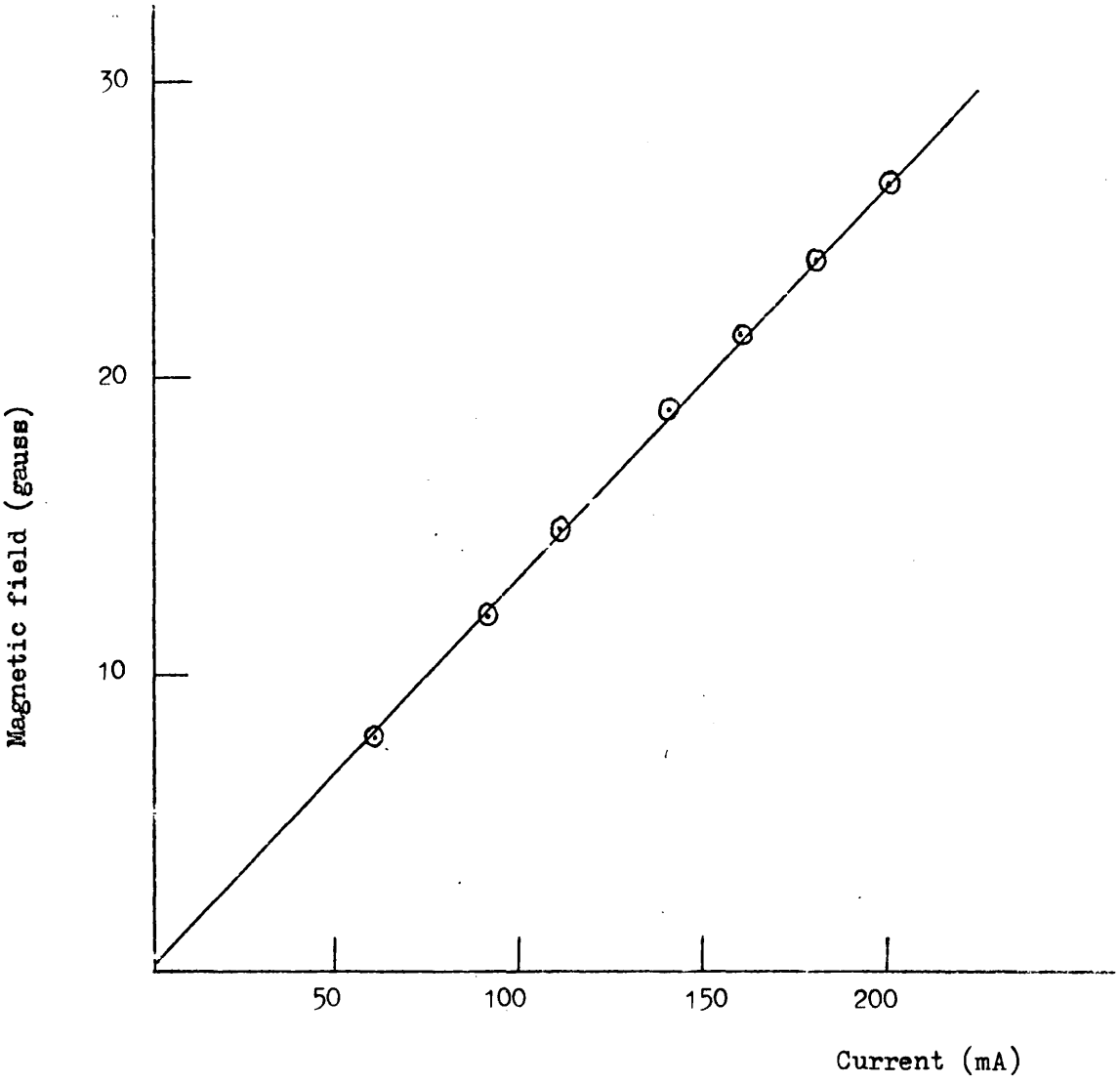

Figure A2

Plot of current passing through the Helmholtz coils against magnetic field produced; magnetic fields were measured from Zeeman - n.q.r. spectra of $(Cl_3PNCH_3)_2$ recorded using the time averaging computer.

APPENDIX B

QUADRUPOLE RESONANCE AT HIGH PRESSURES

Although there have been several investigations of magnetic resonance phenomena at high pressures, and brief descriptions of some of the pressure vessels employed have been published, [1,2] the design criteria which should be applied do not seem to have been outlined in a form suitable for the newcomer to the field. For this reason the design and operation of the pressure vessels constructed for the present work are discussed in detail below.

The nuclear quadrupole resonance studies undertaken here at elevated pressures are designed to provide information concerning the vibrational motions of the compounds studied, in the solid state. It is therefore possible to limit the extent of the pressure range to be investigated to that which is readily accessible using conventional equipment and a liquid pressure transmitting medium. The apparatus described here is therefore designed for routine use over the pressure range $1 \leqslant P \leqslant 2800$ Kg.cm^{-2}.

Figure B1 is a block diagram of the system employed. The pressure is generated by a simple hydraulic handpump, an "Enerpac" laboratory pump, which can produce pressures of up to 2,800 Kg.cm^{-2}. The pressure transmitting fluid is a normal hydraulic oil, and connection to the pressure vessel is made by stainless steel tubing. This "Novaswiss" pressure tubing has 3/8" outside diameter, 1/8" internal diameter, and a pressure rating of 4,000 Kg.cm^{-2} so that a large safety factor is built into the system. All connections to the pressure tubing are made by conventional cone to cone sealing systems, and the valves, elbows and tee-pieces are of similar specification to the tubing. The pressure generated in the system is measured by a conventional Budenberg pressure gauge which is accurate to

$\pm$ 2 $Kg.cm^{-2}$ over the pressure range up to 2,800 $Kg.cm^{-2}$. The calibration of the gauge was checked by recording the n.q.r. spectrum of Cu_2O as a function of pressure and comparing the results with the literature data for this compound.

The construction of the pressure vessel itself is a more difficult undertaking. Previous studies of magnetic resonance phenomena under high pressure have been carried out using pressure vessels constructed of both beryllium - copper alloy [3,4] and of stainless steel.[3] The former, although expensive, has the advantage of being non-magnetic, and so can be used in experiments in which a magnetic field is applied to the sample. Since the present work is concerned with pure quadrupole resonance, magnetic fields are unnecessary so long as frequency modulation is employed, so that stainless steel is the preferred material.

Figure B2 shows the pressure vessel used in the experiments described in Chapters III and IV. The component parts of the system are individually illustrated, with a note of their dimensions, in Figure B3, B4 and B5. This system is constructed from an EN58B stainless steel, and is intended for use throughout the pressure range $1 \leqslant P \leqslant 1000$ $Kg.cm^{-2}$. The body of the pressure vessel, A, is a steel cylinder into which fits the electrical plug B, which is held in place by tightening down the collar, C.

The design used here, incorporating a separate plug and collar, was adopted after initial consideration of the type of system used by some other workers [3,4] in which the electrical plug is itself threaded to mate with a thread on the inside of the pressure vessel, the collar in this case being unnecessary. Since the thread area needed to withstand a given internal pressure is the same for either

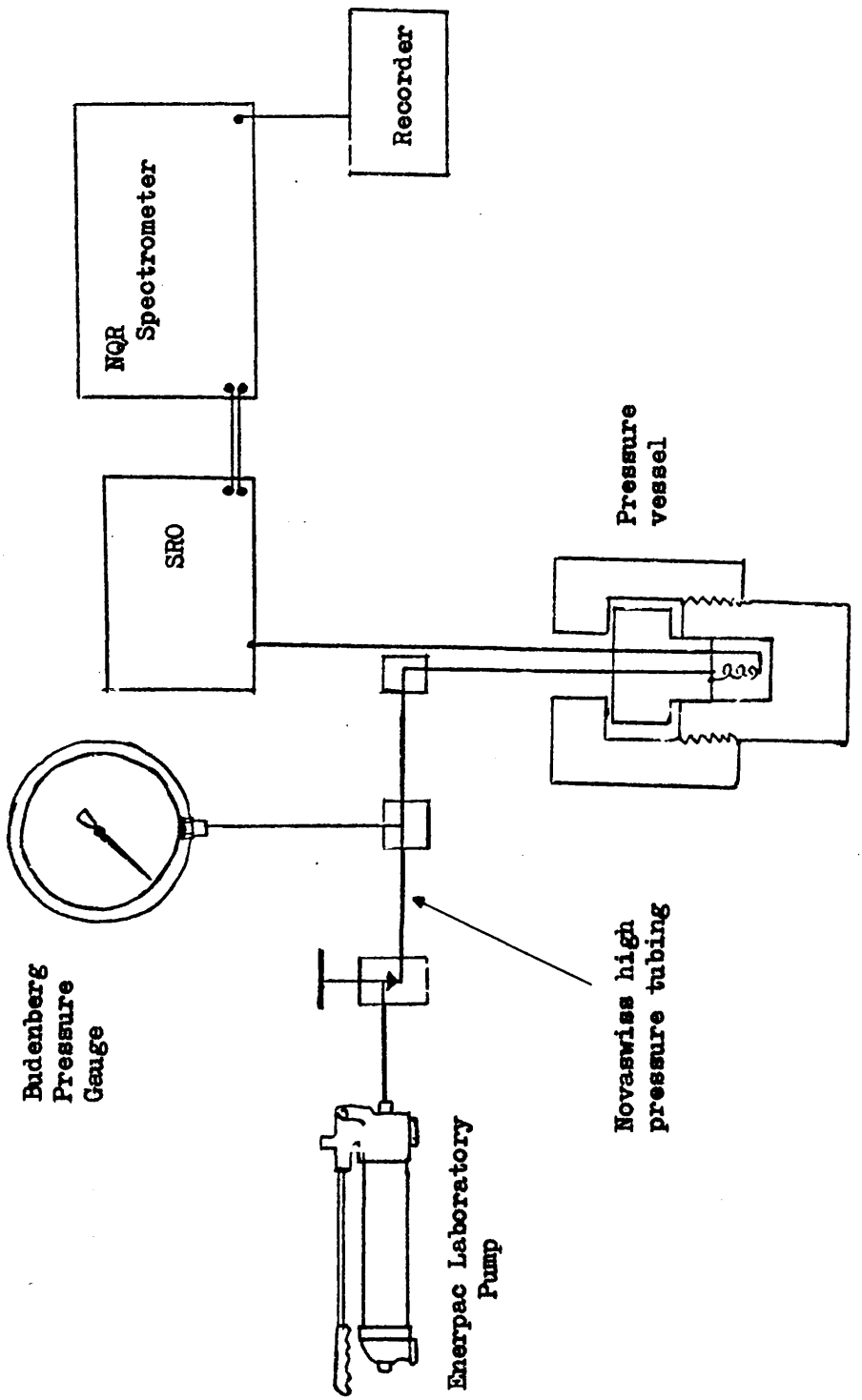

Figure B1 Block diagram of the pressure system.

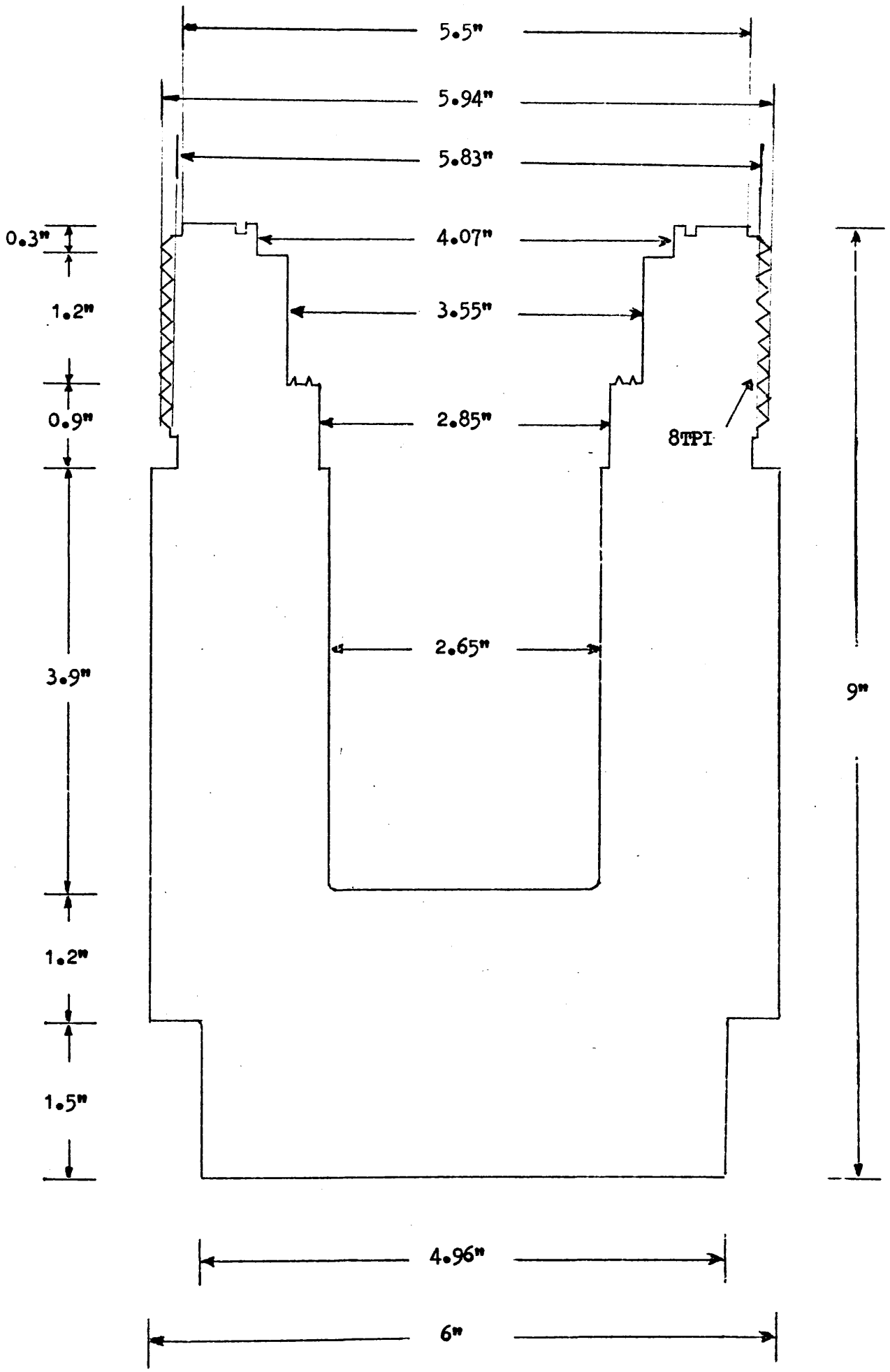

Figure B.3

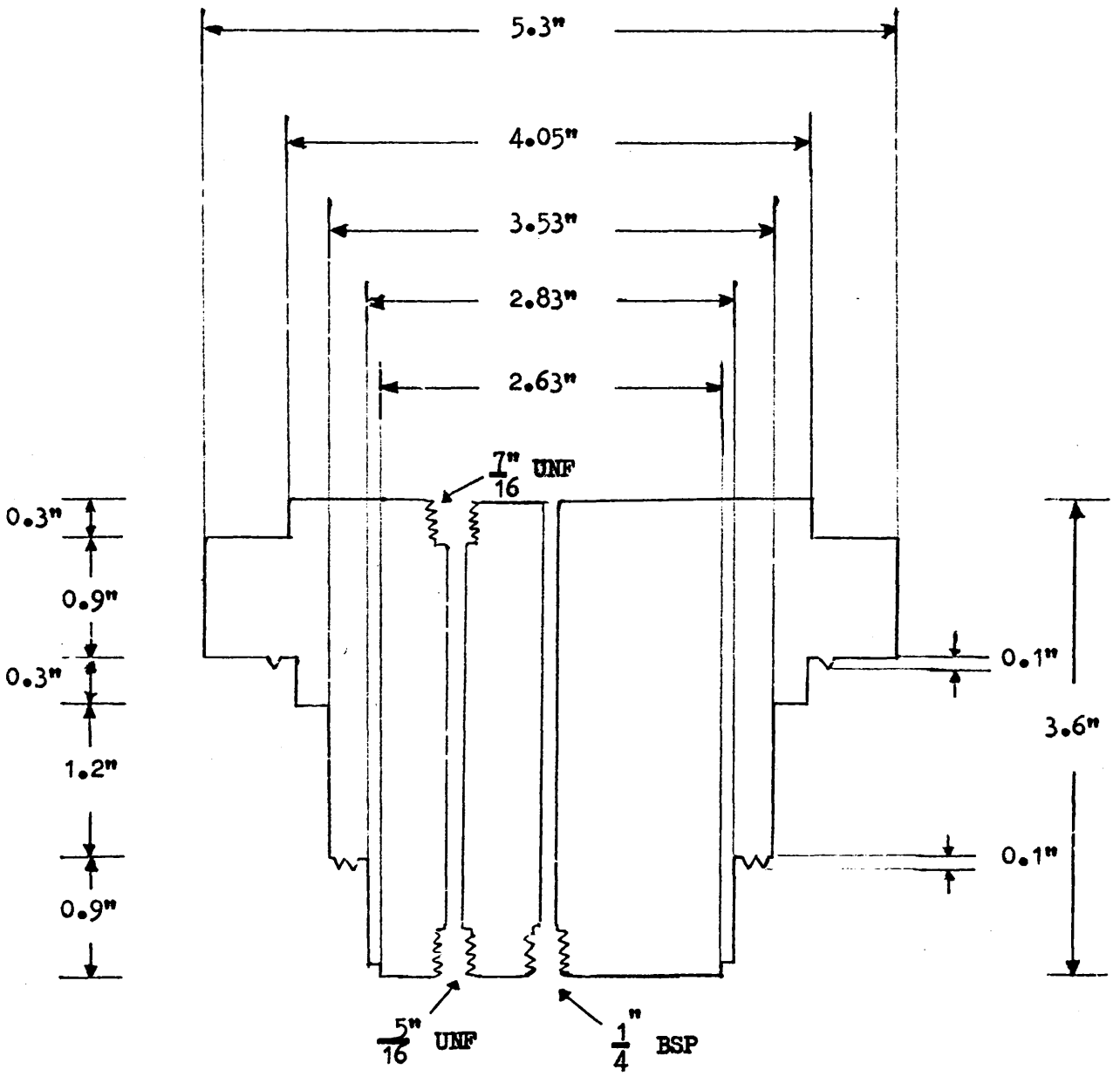

Figure B4.

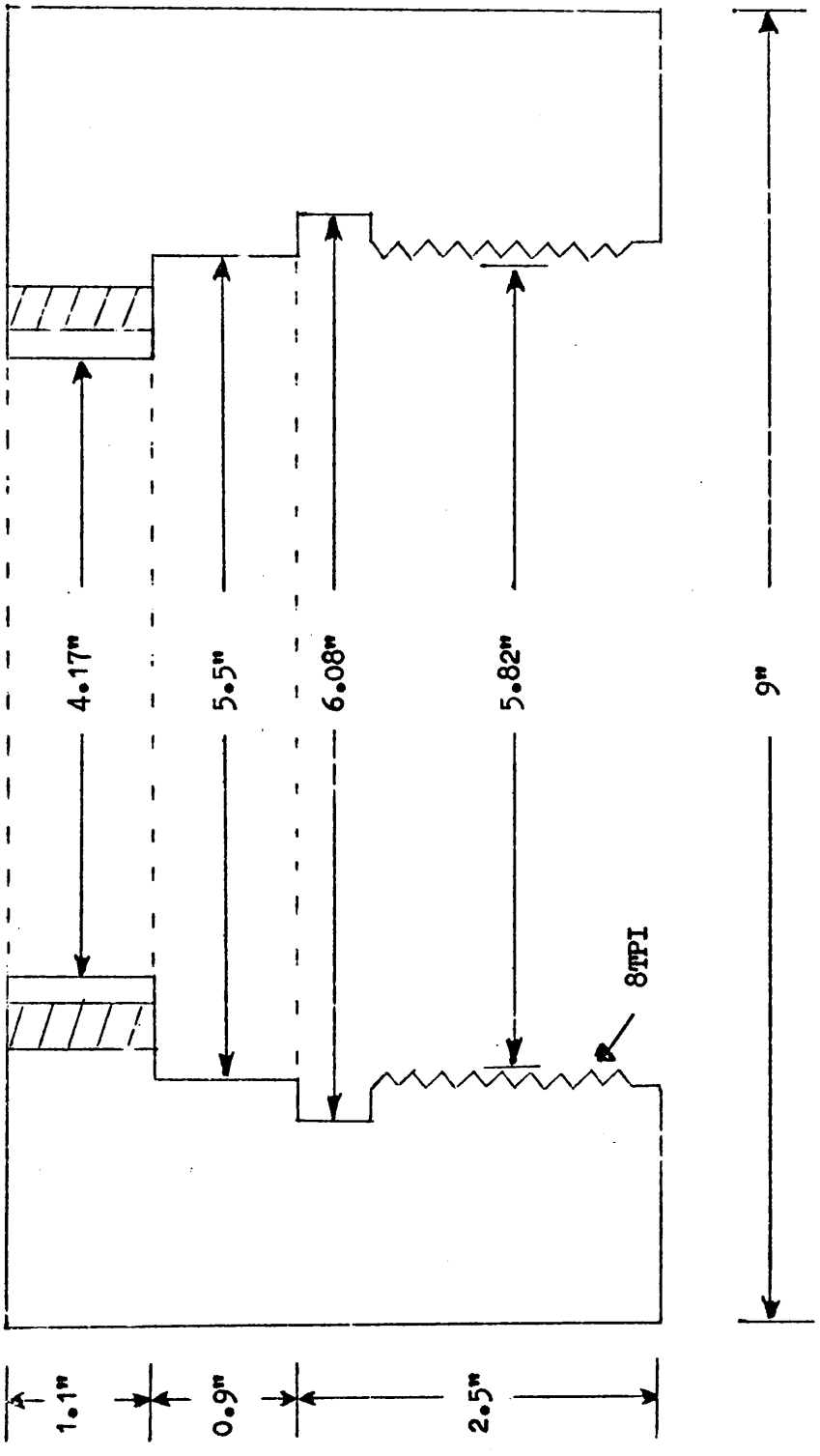

Figure B5

of these designs, assuming the internal diameter to be the same, it follows that the internally threaded system must necessarily be longer than an equivalent externally threaded system of the type used here. The internally threaded system is therefore better suited to experiments in magnetic fields in which the pressure vessel must fit inside the gap between the magnet pole faces, although there is little to choose between the two designs for experiments in zero field.

Returning to Figure B2, it is seen that both the electrical lead from the spectrometer, D, and the pressure tubing, E, enter the system through the plug B. The system is assembled by tightening down the collar, and the plug is further tightened against the washers, F, by means of the high tensile steel bolts, G, which thread through the collar and press against the electrical plug. A torque wrench is normally used in tightening the bolts so that the same force can be reproducibly used. It has been found that when the system is used at high pressures the bolts tend to cause some slight deformation of the electrical plug at the points of contact, implying that the local stress in these regions is too great.

The use of the bolts in the design makes it possible to release the pressure in the washer system by removing these bolts before attempting to remove the collar. This means that the threads on the collar and pressure vessel do not have to be rotated relative to each other while under pressure, so reducing the possibility of seizing which is always present in stainless steel threads. As a further safeguard against "firing", all threads are coated before use by a commercial thread lubricant such as "Rocol A.S.P." or "Never-Seez".

When the collar and bolts are tightened down, the knife-edges shown in Figure B2 bite quite deeply into the washers ensuring a good seal. Washers have been made of lead, copper and Teflon, and experience has shown that Teflon is the most suitable material for this application. The tendency of Teflon to deform and flow very slowly under pressure helps to compensate for any inaccuracies in the machining of the vessel and to maintain an efficient seal, while the deformation takes place so slowly that each washer can be used continuously for several weeks before needing replacement.

The pressure tubing E is threaded into the electrical plug and sealed by means of a small washer. The electrical lead into the pressure vessel, C, is sealed into the system by means of a cone of epoxy adhesive behind which sits a highly compressed Teflon plug. Standard cone, sleeve and nut fittings are used to connect the epoxy cone into the electrical plug; any tendency to leakage in these fittings can be overcome by coating the joints lightly with further epoxy adhesive. The use of epoxy seals for electrical connections to high pressure apparatus has been mentioned by several authors, [5] and is extremely convenient because of the ease of construction and renewal of the seal. The seals used here have been constructed from both undegassed "Araldite" and "Uniguard", and have been found to be satisfactory over the pressure range $1 \leq P \leq 1500$ Kg.cm^{-2}.

During its passage through the body of the electrical plug the electrical lead is insulated by a heat-shrink sleeving; outside the plug the lead passes through a rigid copper tube to the oscillator head of the spectrometer, to which it is connected in the usual way. Throughout its length there is an air-gap between the radio frequency lead and the walls of the electrical plug, so as to keep the capacitance

of the oscillator circuit as low as possible. This is to ensure that the system can be used with the Decca Radar n.q.r. spectrometer without making any changes to the normal spectrometer specification. Naturally the electrical lead from the pressure vessel to the spectrometer is much longer than the normal lead from the spectrometer to the oscillator tank coil, so that a marked increase does occur in the capacitance of the lead, with the result that a smaller frequency range than normal is accessible when using the high pressure apparatus. In fact the system described here can only be used with the Decca spectrometer at frequencies below 35 M.Hz. whereas the normal operating range of the spectrometer extends to 55 M.Hz. In order to use this system at frequencies above 35 M.Hz. some modifications to the oscillator circuitry would be necessary.

The capacitative changes noted above also lead to a significantly lower signal to noise ratio when the pressure system is used compared to the normal spectrometer system. Again this is not an insuperable problem since compounds, such as those studied in this work, which give reasonably strong signals, can be easily recorded when using the pressure system, while compounds with weaker resonance signals could be studied by coupling the use of the pressure vessel with the time-averaging computer apparatus described in Appendix A.

In the pressure vessel the sample is contained in a small plastic holder which sits in the radio frequency coil. There are several small holes in the lid of this container which allow the pressure transmitting fluid to mix with the sample to ensure that pressure is transmitted to the sample hydrostatically. All compounds studied under pressure were therefore suspended in the hydraulic fluid before carrying out experiments under pressure, to check that no reaction or

decomposition occurred; in fact all compounds investigated were unaffected by this treatment.

The one vitally important topic which has not yet been discussed is the calculation of the maximum safe working pressure of a vessel of the type described here. There are essentially two steps in evaluating this safe working pressure for any proposed design. The first of these is the calculation of the stresses, and strains if required, which are induced in the walls of the vessel when the system is used at a given internal pressure. The second step is the determination of some criterion of failure for the pressure vessel, expressed in terms of some limiting combination of the stress system in the walls. In this procedure it is necessary to allow suitable safety factors to take account of any unknown variables.

The calculations involved in these analyses are outlined below, together with a brief discussion of the nature of the stresses and strains introduced when the vessel is pressurised.

Stress calculations for pressure vessels.

The behaviour of a cylindrical steel vessel under the influence of unbalanced internal and external pressures can readily be illustrated. If the steel is isotropic and initially free from strain then the distribution of stress and strain does not vary along the length of the vessel, except in the region close to its ends. Under the influence of an internal pressure the principal stresses acting on a small element of the cylinder wall at a given radius are illustrated in Figure B6. These are a radial compressive stress, σ_r, a tangential tensile stress, σ_t, and an axial tensile stress, σ_z.

The response of the pressure vessel to these applied stresses is complex. Figure B7 represents a typical pressure–expansion diagram for a thick-walled pressure vessel constructed of a ductile material such

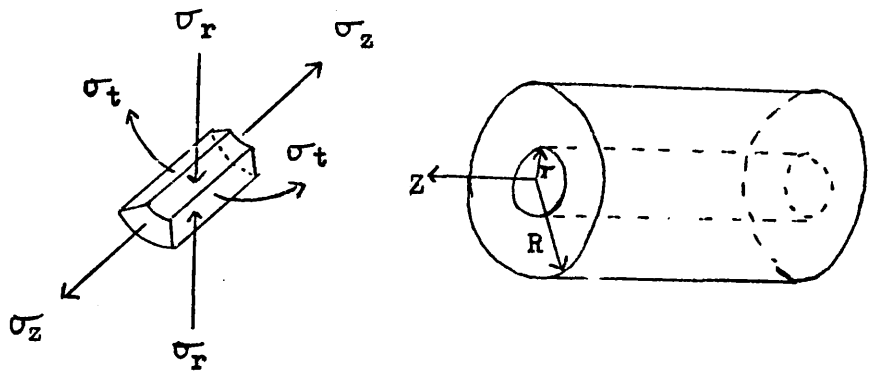

Figure B6 The directions of the principal stresses in a thick-walled cylinder with closed ends under internal pressure.

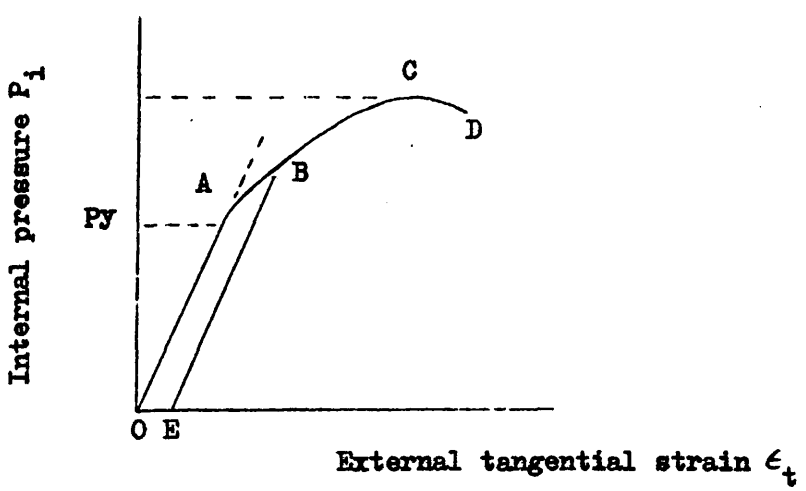

Figure B7 Pressure - expansion curve for a typical thick-walled cylinder made of ductile material. The curve has the same form as the corresponding stress-strain diagram.

as steel, in which the tangential strain at the outside surface of the vessel is plotted against the internal pressure.

In the region from O to A in the figure the cylinder behaves elastically, so that when the pressure is released the vessel returns to its original dimensions. At A the material at the bore reaches its elastic limit and, if the pressure is further increased, plastic deformation progresses through the wall until the vessel becomes completely plastic at some point between A and C. At C a condition of instability is reached and localized bulging occurs, the material having reached its ultimate stress. The vessel finally ruptures at some slightly lower pressure, denoted by the point D. If the pressure is reduced to zero from some intermediate value, such as the point B, then OE is a measure of the permanent deformation of the vessel.

When designing a pressure vessel it is important to ensure that no excessive permanent deformation occurs under working conditions. Thus the pressure P_y, which causes the material at the bore of the vessel to yield, should be known. Often however such information may be difficult to obtain, so that it may be necessary to base design calculations on a knowledge of the ultimate stress which the material can support, corresponding to the stress applied at point C in Figure B7; in this case care must be taken in choosing a suitable safety factor.

As noted above the three principal stresses acting on the cylinder wall are σ_r, σ_t and σ_z. Of these only the axial tensile stress σ_z, is constant across the walls of the vessel; both σ_r and σ_t have their maximum values at the bore, and decrease towards the outer portions of the wall. The maximum value of the radial compressive stress, σ_r, is numerically equal to the internal pressure, P, so that [6]

$$(\sigma_r)_{max} = -P \qquad \text{B1}$$

where we have introduced the normal sign convention that tensile stresses are positive, and compressive stresses negative. The maximum value of the tangential tensile stress or hoop stress is now given by

$$(\sigma_t)_{max} = P\left(\frac{R^2 + r^2}{R^2 - r^2}\right) \qquad \text{B2}$$

where r is the internal radius of the pressure vessel, and R its external radius, and again this maximum occurs at the bore. The axial tensile stress can similarly be shown to be

$$\sigma_z = \frac{P\,r^2}{R^2 - r^2} \qquad \text{B3}$$

All these equations assume that the vessel can be regarded as a thick cylinder, sealed under closed end conditions, and it follows that at the bore

$$\left|(\sigma_t)_{max}\right| > \left|\sigma_z\right| > \left|(\sigma_r)_{max}\right| \qquad \text{B4}$$

The corresponding equations for a thin-walled cylinder under pressure are

$$\begin{aligned} \sigma_r &= 0 \\ \sigma_t &= \frac{P\,r}{t} \\ \sigma_z &= \frac{P\,r}{2t} \end{aligned} \qquad \text{B5}$$

where t is the wall thickness. In this case σ_t is assumed to be evenly distributed across the wall thickness.

Equations can also be derived for the stresses imposed on the electrical plug and collar. The applied pressure acting on the electrical plug exerts on it a compressive stress equal in magnitude

to the hydrostatic pressure. Further the force exerted on the electrical plug by the hydrostatic pressure must ultimately be passed to the collar. The situation is illustrated in Figure B8 and it can be seen that under the action of the applied pressure the plug presses against the collar so that contact stresses, known as bearing stresses, are developed against the collar. Figure B8(b) also shows that there is a tendency to shear the plug along the sections ab and cd.

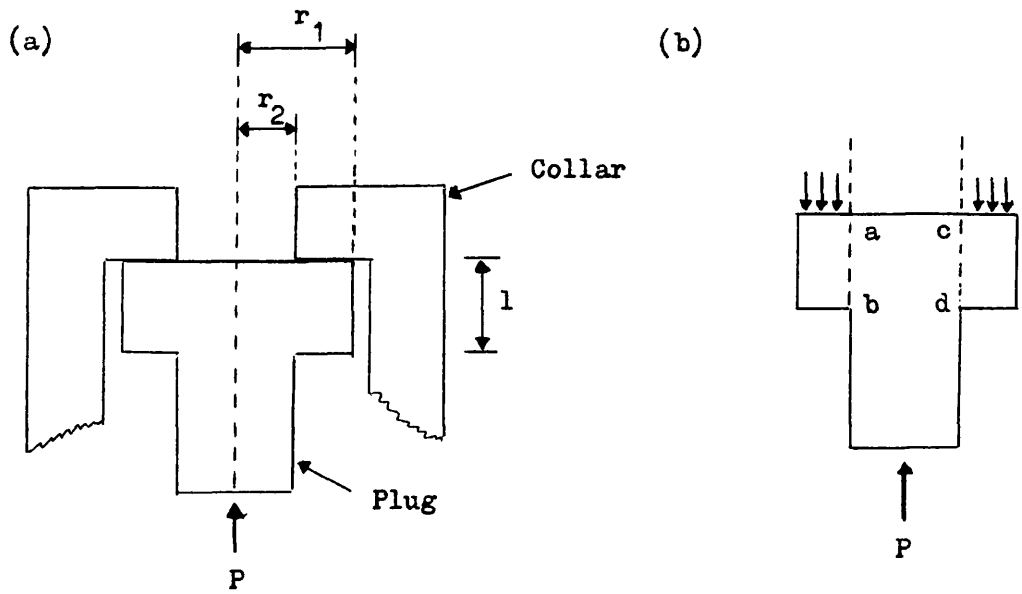

Figure B8 (a) Arrangement of plug and collar; (b) bearing stresses developed on the electrical plug. The shearing forces act along the lines ab and cd.

The bearing stress can be calculated from the expression

$$\beta = \frac{P.A}{\pi(r_1^2 - r_2^2)} \qquad \text{B.6}$$

where A is the area of the electrical plug on which the internal pressure acts, and $\pi(r_1^2 - r_2^2)$ is the area of contact of the flanges on the electrical plug and the collar. The shear stress, τ,

can be found from

$$\tau = \frac{P.A}{2\pi r_2 l} \qquad B.7$$

where l is the thickness of the flange as shown in Figure B8.

Since the load applied to the collar, given here by P.A, must be held by the thread joining the collar and the pressure vessel itself, it is possible also to calculate the shear stress applied to the thread. This is found from

$$\tau = \frac{3\ P.A}{2\pi r l} \qquad B.8$$

Here r is the minimum radius of the thread, l is the length of the threads which overlap, and P and A are as above.

The equations given above now make it possible to evaluate the important stresses in the system when the internal pressure has the value P, and a similar analysis can of course be carried out for the electrical lead into the system. In order to use these expressions to decide how thick the walls of the vessel must be to withstand a given internal pressure, some criterion of failure for the vessel must be defined. One rather simplistic way of doing this is to set maximum allowable stresses based on the known characteristics of the constructional material. Thus the EN58B steel used in the construction of the pressure vessel already described, has an ultimate stress of 35 tons force in $^{-2}$, so that the maximum allowable stresses during normal usage of the pressure system can be set as follows.

Maximum allowable tensile stresses = 10 ton.f.in^{-2} = 1575 Kg.cm^{-2}

Maximum allowable bearing stresses = 20 ton.f.in^{-2} = 3150 Kg.cm^{-2}

Maximum allowable shear stresses = 6 ton.f.in^{-2} = 945 Kg.cm^{-2}

These values imply that the safe maximum working pressure for this vessel is of the order of 1000 Kg. cm^{-2}, and this has been taken as its upper limit in normal usage, although it has been tested up to 1500 Kg.cm^{-2} in the experiments on $(Cl_3PNCH_3)_2$.

The stress analysis discussed here, while not rigorous, is adequate for the type of system described. In order to extend the analysis further it is necessary to use a better criterion of failure for the pressure vessel, but unfortunately there are several possible theories and there does not appear to be a single universally accepted criterion.[6] For our purposes perhaps the best criterion of pressure vessel failure is the so-called "maximum shear stress criterion" which implies that the internal pressure which just causes yielding at the bore, P_y, is given by

$$P_y = \frac{\sigma_y}{2}\left(\frac{R^2 - r^2}{R^2}\right) \qquad \text{B.9}$$

where R and r are the external and internal radii of the vessel, and σ_y is the yield stress in tension, and at the elastic limit,

$$\tau = \frac{\sigma_y}{2} \qquad \text{B.10}$$

When using this maximum shear stress criterion it is customary[6] to design thick-walled pressure vessels so that the (maximum) working pressure is two-thirds of the yield pressure. Thus the vessel is on the point of yielding at the bore when it is tested to one-and-a-half times its working pressure.

In addition to the high pressure vessel already described the engineering calculations discussed above have been used in the design of a second vessel, for use at higher pressures than the

first. This second vessel is shown in Figure B9, and its individual components are illustrated in Figures B10, B11 and B12.

A number of important changes have been made from the previous system in order to allow the new vessel to operate conveniently throughout the pressure range $1 \leqslant P \leqslant 2800$ Kg.cm^{-2}. The first change is that this new system is constructed from a tougher steel, specifically KE805 steel which is supplied hardened and tempered to 55/65 tons tensile, yield point 45/55 tons, and which can be readily machined in this condition. The internal diameter of the vessel has been significantly reduced, and the flanges on the electrical plug and collar strengthened in order to reduce the shear stresses induced in the flanges and the threads. The other major change is the use of only one washer. This change is introduced because the end force generated in the original pressure vessel is much larger when sealing against the second washer than when sealing the system by the small washer, so that the large washer is really unable to fulfil its intended function of providing a back-up to the internal gasket, if the pressure vessel is to be used well within its design limits.

Although this new pressure vessel has been constructed, it has not yet been tested under pressure. However the stresses generated in the vessel are low at all pressures accessible with the hydraulic pump available so that the system should operate successfully at pressures of up to 2800 Kg.cm^{-2}.

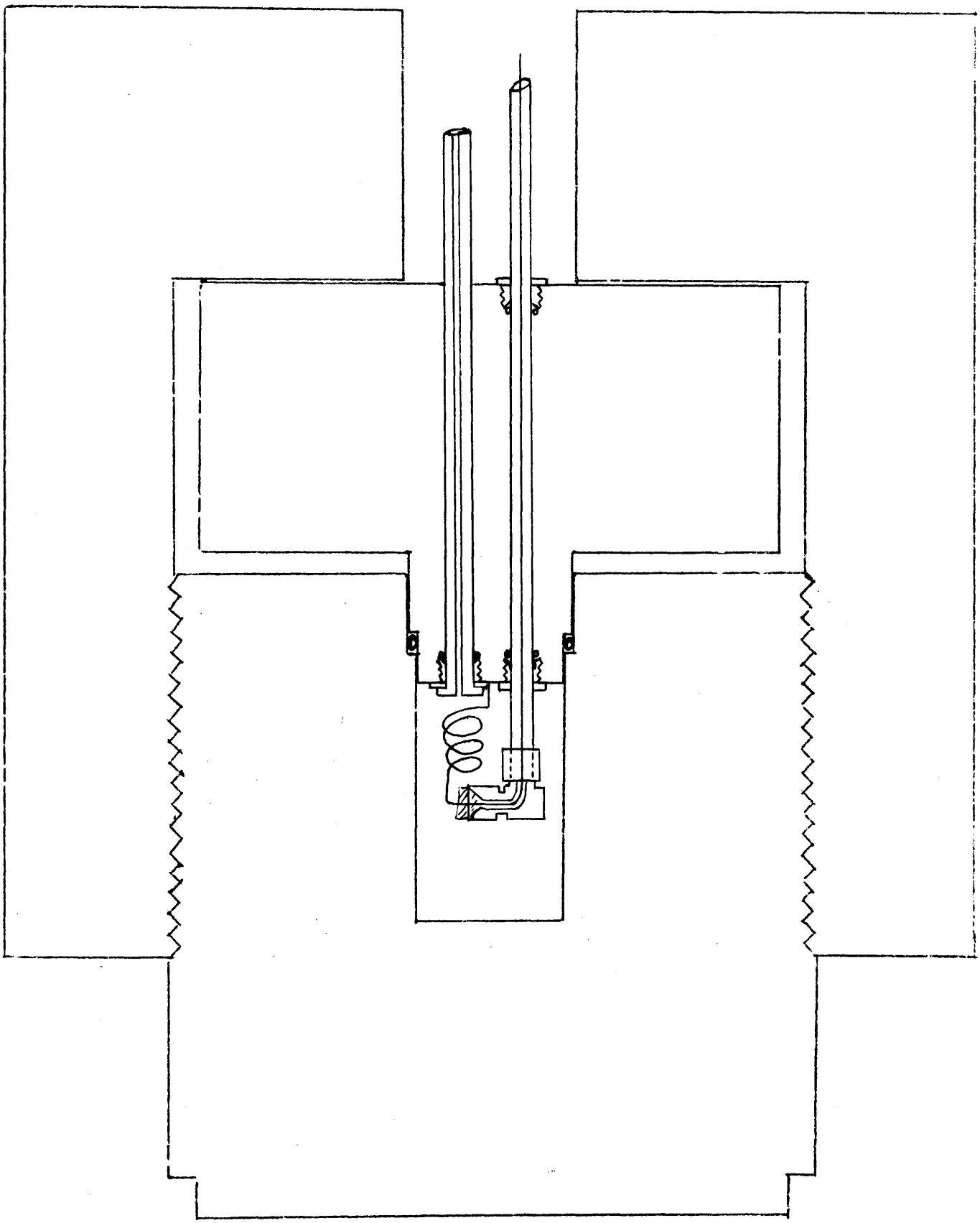

Figure B9 Pressure vessel for use at pressures of up to 2,800 Kg. cm^{-2}.

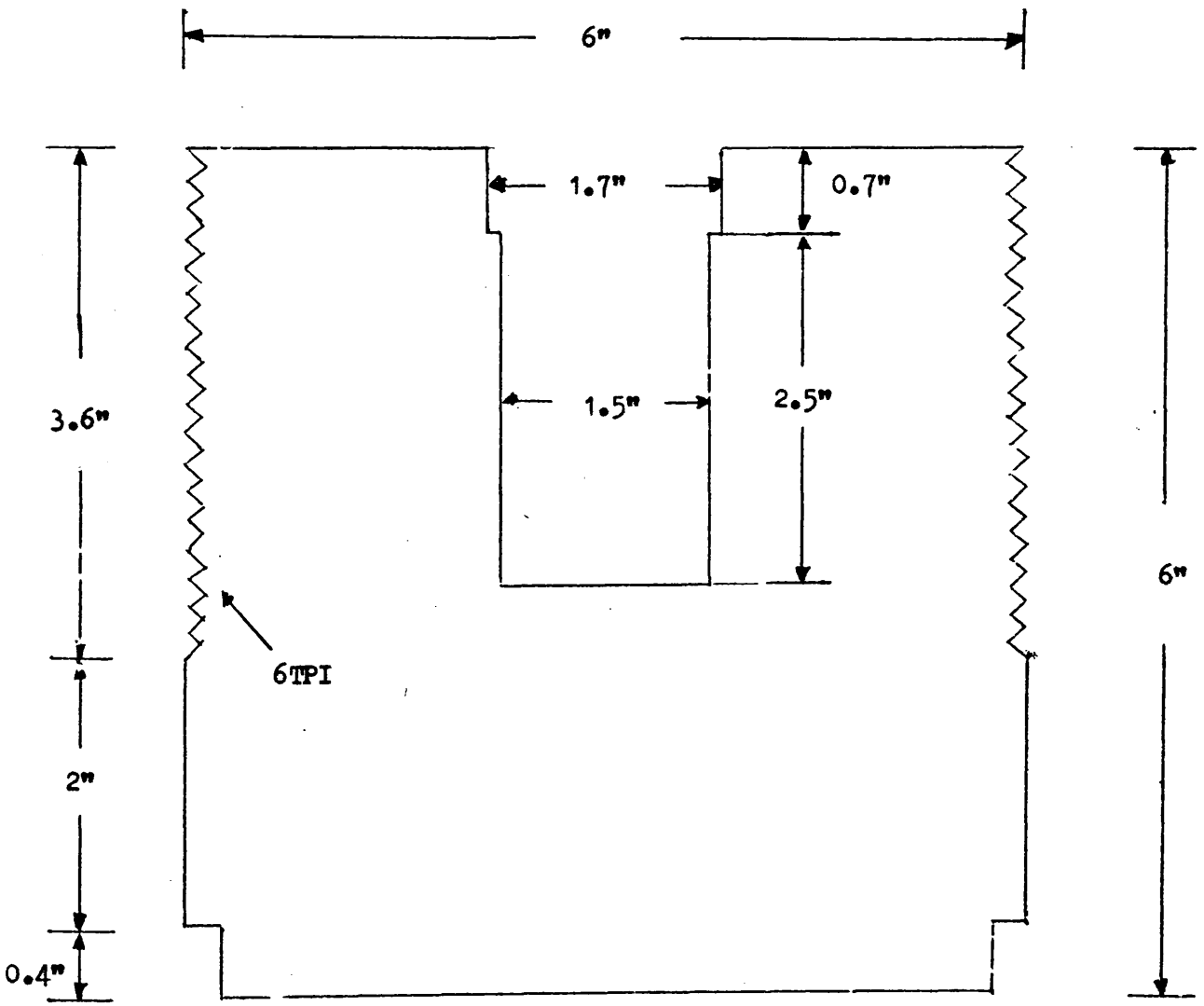

Figure B10

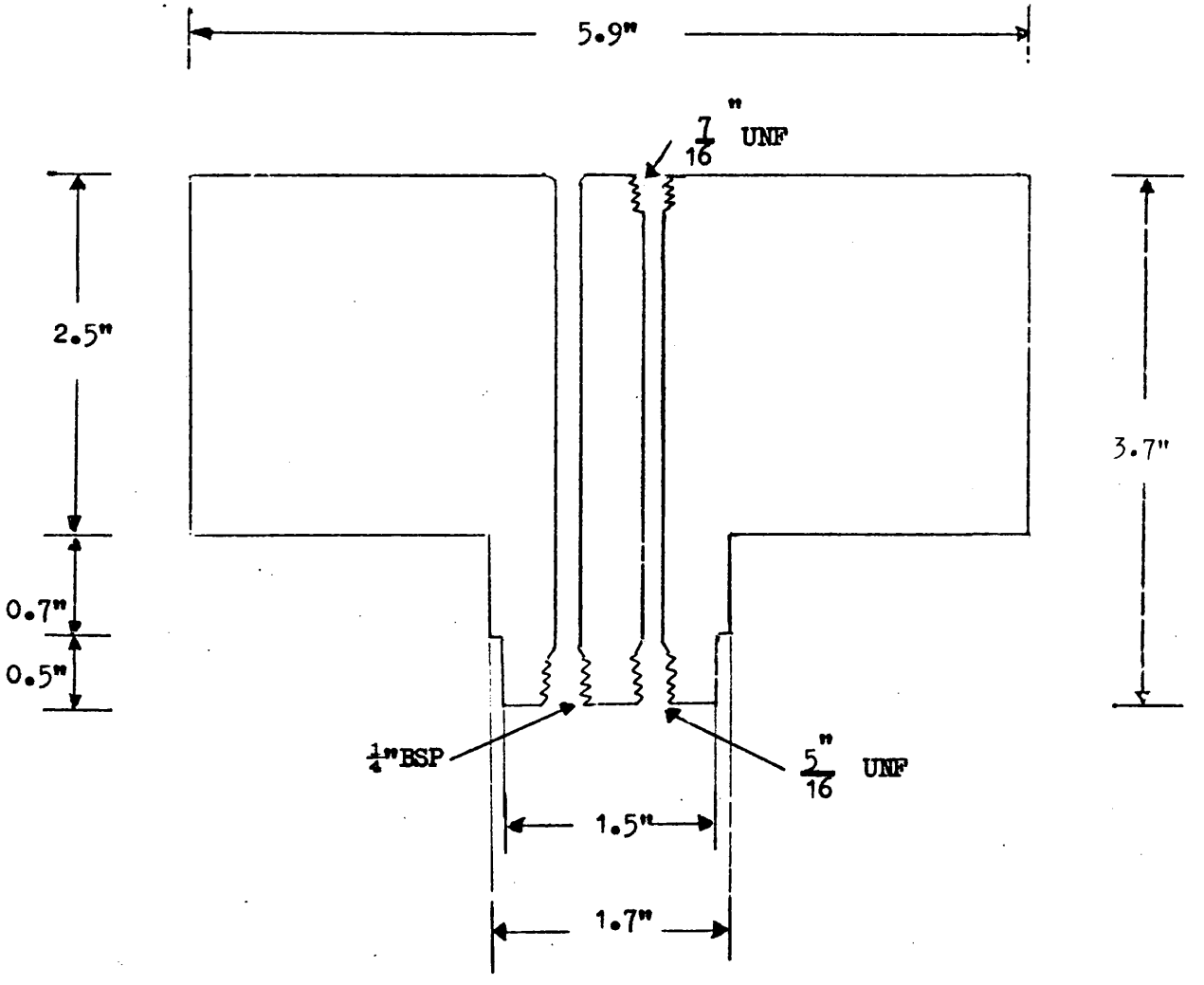

Figure B11

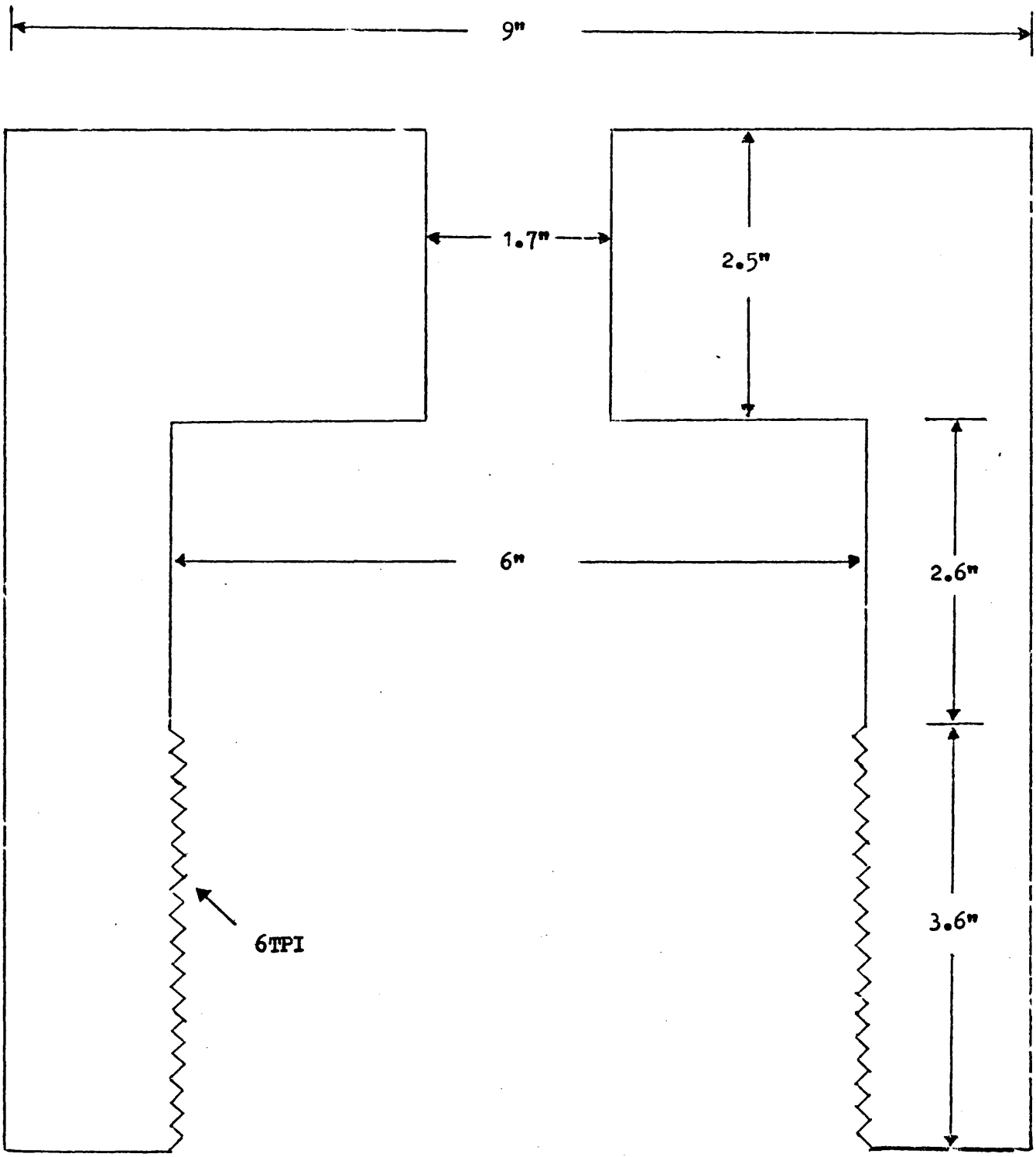

Figure B12

APPENDIX C

A NITROGEN GAS-FLOW SYSTEM FOR TEMPERATURE CONTROL IN QUADRUPOLE RESONANCE STUDIES

In the nuclear quadrupole resonance studies reported in this work, spectra have been recorded over the temperature range $77 \leq T \leq 350K$. The recording of spectra at room temperature and at 77K is straightforward; in order to achieve the latter temperature the entire tank coil of the radio frequency oscillator can simply be immersed in a Dewar flask of liquid nitrogen. At temperatures intermediate between 77K and ambient it is more difficult to maintain a steady temperature across the entire sample for the fairly long period of time needed to record an n.q.r. spectrum. In order to overcome this problem and to enable any temperature in the range $100 \leq T \leq 350K$ to be easily obtained, the Decca Radar n.q.r. spectrometer system normally used has been modified for variable temperature work as shown in Figure C1.

As shown in the figure the radiofrequency coil is placed inside a special Dewar flask which is fitted with an inlet at its base, and a steady stream of nitrogen gas is passed through the system. The gas is pre-chilled by passing it through a copper coil immersed in liquid nitrogen, and then brought to any desired temperature by means of a small heating coil.

All temperatures above 77K were obtained using this gas-flow system. Temperatures close to room temperature can be reached with quite low flow rates, usually of the order of 2 - 5 litres per minute, but in order to cool the system to 100K the nitrogen

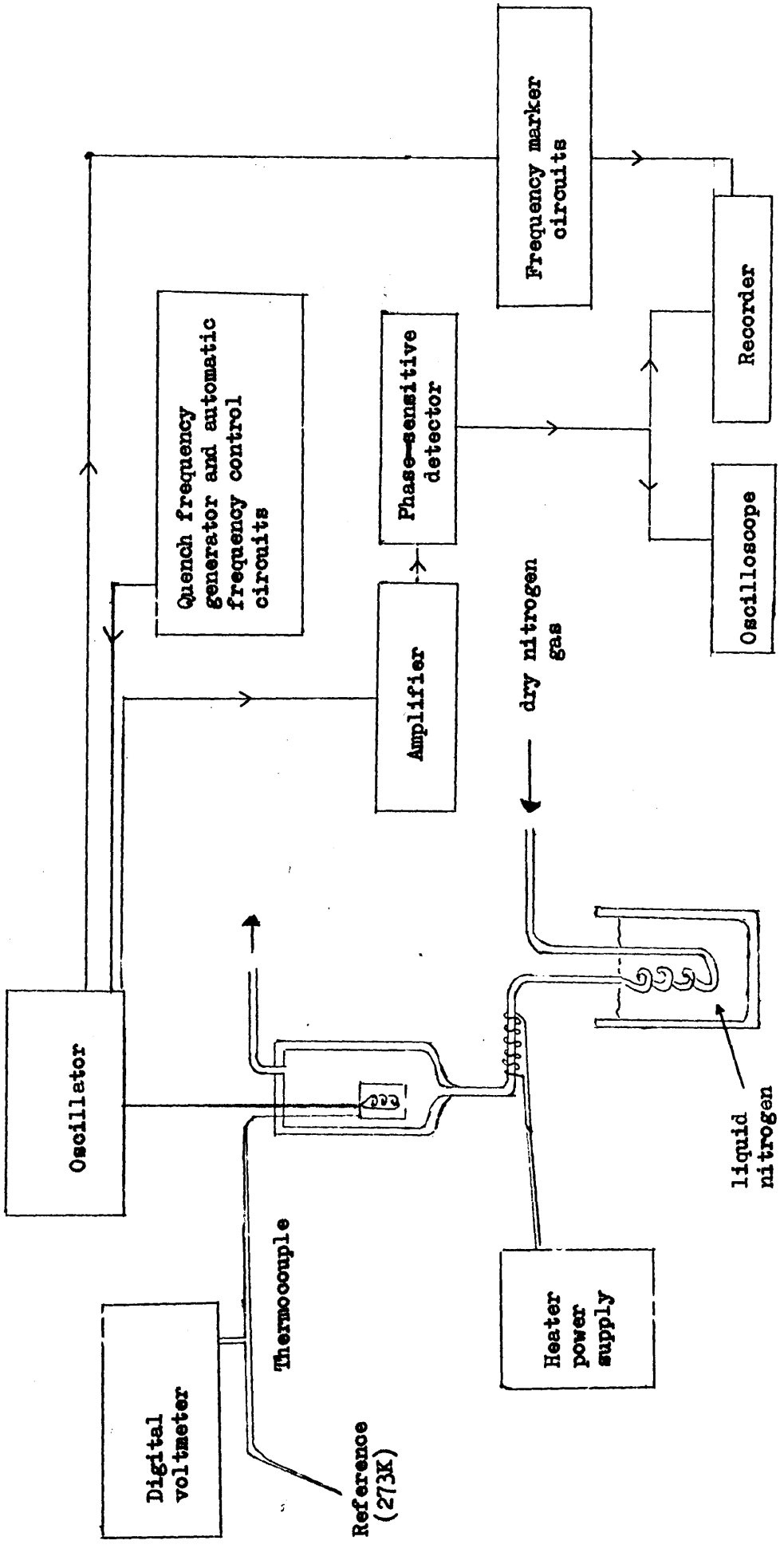
Frequency marker circuits
Recorder
Quench frequency generator and automatic frequency control circuits
Phase-sensitive detector
Oscilloscope
Amplifier
dry nitrogen gas
Oscillator
liquid nitrogen
Thermocouple
Heater power supply
Digital voltmeter
Reference (273K)

Figure C1

gas must be passed through the system at up to 12 litres per minute. The gas-flow system, used without the bath of liquid nitrogen, can be employed to reach temperatures above room temperature by suitable adjustment of the heater.

Temperatures are measured by means of a copper-constantan thermocouple whose reference junction is maintained at 273K by immersion in an ice-water bath. No spectra were recorded until the system had remained at a constant temperature for at least thirty minutes, to remove as far as possible the effect of temperature inhomogeneities across the sample. The temperature measurements made by the thermocouple are accurate to $\pm$ 1K.

REFERENCES

Chapter I

The discussion presented in Chapter I was based on the following sources.

1. E.A.C. Lucken, "Nuclear Quadrupole Coupling Constants", Academic Press Inc., New York, N.Y., 1969.

2. T.P. Das and E.L. Hahn, "Nuclear Quadrupole Resonance Spectroscopy", Academic Press Inc., New York, N.Y., 1958.

3. J.A.S. Smith, J. Chem. Ed., 1971, 48, 39, A77, A147 and A243.

4. E. Schempp and P.J. Bray, "Physical Chemistry", H. Eyring, D. Henderson and W. Jost eds., Academic Press Inc., New York, N.Y., 1970, IV, Chapter 11.

5. C.P. Slichter, "Principles of Magnetic Resonance", Harper and Row, New York, N.Y., 1963, Chapter 6.

Chapter II

1. For references before 1968 see E.A.C. Lucken, "Nuclear Quadrupole Coupling Constants", Academic Press Inc., New York, N.Y., 1969.

2. R.M. Hart and M.A. Whitehead, J. Chem. Soc. (A), 1971, 1738.

3. R.M. Hart and M.A. Whitehead, Mol. Phys., 1970, 19, 383.

4. M. Hashimoto, T. Morie and Y. Kato, Bull. Chem. Soc. Japan, 1971, 44, 1455.

5. M. Kaplansky and M.A. Whitehead, Canad. J Chem., 1967, 45, 1669.

6. R. Clipsham, R.M. Hart and M.A. Whitehead, Inorg. Chem., 1969, 8, 2431.

7. M Dixon, H.D.B. Jenkins, J.A.S. Smith and D.A. Tong, Trans. Faraday Soc., 1967, 63, 2852.

8. M.A. Whitehead, Canad. J. Chem., 1964, 42, 1212.

9. R. Keat, A.L. Porte, R.A. Shaw and D.A. Tong, J. Chem. Soc. Dalton, 1972, 1648.

10. E. Hobbs, D.E.C. Corbridge and B. Raistrick, Acta. Cryst., 1953, 6, 621.

11. D.W.J. Cruickshank, Acta. Cryst., 1964, 17, 671.

12. H.R. Allcock, R.L. Kugel, G.F. Konopski and E.G. Stroh, Chem. Commun., 1970, 985.

13. N.L. Paddock, Quart. Rev., 1964, 18, 168.

14. M.J.S. Dewar, E.A.C. Lucken and M.A. Whitehead, J. Chem. Soc., 1960, 2423.

15. K.A.R. Mitchell, Chem. Rev., 1969, 69, 157.

16. E.A.C. Lucken, "Structure and Bonding", P. Hemmerick et. al., eds., Springer - Verlag, Berlin and New York, 1969, page 1.

17. K.A.R. Mitchell, J. Chem. Soc. (A), 1968, 2676 and 2683.

18. D.P. Craig and K.A.R. Mitchell, J. Chem. Soc., 1965, 4682.

19. E.A.C. Lucken, "Magnetic and Electric Resonance and Relaxation" (Proceedings of the XIth Colloque Ampère, Eindhoven, 1962), J. Smidt ed., North Holland Publishing Company, Amsterdam, 1963.

20. F.R. Ahmed and D.R. Pollard, Acta. Cryst., 1972, B28, 513.

21. F.R. Ahmed and D.R. Pollard, Acta. Cryst., 1972, B28, 3530.

22. R. Keat and R.A. Shaw, J. Chem. Soc., 1966, 908.

23. G.J. Bullen and P.A. Tucker, Chem. Commun., 1970, 1185.

24. G.J. Bullen and P.A. Tucker, J. Chem. Soc. Dalton, 1972, 2437.

25. D.J. Osokin, I.A. Safin and I.A. Nuretdinov, Org. Mag. Res., 1972, 4, 831.

26. W.S. Sheldrick, J. Chem. Soc. Dalton, 1975, 943.

27. Y.S. Li, M.M. Chen and J.R. Durig, J. Mol. Struct., 1972, 14, 261.

28. T. Moritani, K. Kuchitsu and Y. Morino, Inorg. Chem., 1971, 10, 344.

29. I.R. Cameron, A.F. Cameron and R. Keat, unpublished results.

30. R. Livingston, J. Phys. Chem., 1953, 57, 496.

31. R.R. Holmes, R.P. Carter and G.E. Peterson, Inorg. Chem., 1964, 3, 1748.

32. E.A.C. Lucken and M.A. Whitehead, J. Chem. Soc., 1961, 2459.

33. G.K. Semin and T.A. Babushkina, Teor. Eksp. Khim., 1968, 4, 835.

34. J.K.W. Bishop, W.R. Cullen and M.C.L. Gerry, Canad. J. Chem., 1971, 49, 3910.

35. R. Keat and R.A. Shaw, J Chem. Soc., 1965, 2215.

36. B. Grushkin, M. Gali Sanchez and R.G. Rice, Inorg. Chem., 1964, 3 , 623.

37. M. Biddlestone and R.A. Shaw, J. Chem. Soc. Dalton, 1973, 2740.

38. H. Rose, unpublished results.

39. L. Maier, Helv. Chim. Acta, 1965, 48, 133.

40. G. Bulloch and R. Keat, J. Chem. Soc. Dalton, 1974, 2010.

41. R. Appel, U.S. Patent 3358021; Chemical Abstracts, 1968, 69, 10212 j.

42. R. Keat, J. Chem. Soc. (A), 1970, 2732.

Chapter III

1. R.R. Holmes, R.P. Carter and G.E. Peterson, Inorg. Chem., 1964, 3, 1748.

2. H. Chihara, N. Nakamura and S. Seki, Bull. Chem. Soc. Japan, 1967, 40, 50.

3. V.I. Svergun, V.G. Rozinov, E.F. Grechkin, V.G. Timokhin, Yu. K. Maksyutin and G.K. Semin, Izv. Akad. Nauk. SSSR, Ser. Khim., 1970, 8, 1918.

4. R. Keat, A.L. Porte, R.A. Shaw and D.A. Tong, J. Chem. Soc. Dalton, 1972, 1648.

5. A.D. Gordeev, E.S. Kozlov and G.B. Soifer, Zhur. Strukt. Khim., 1973, 14, 934.

6. I. Haiduc, "The Chemistry of Inorganic Ring Systems", Wiley-Interscience, Chichester, 1970.

7. A.C. Chapman, W.S. Holmes, N.L. Paddock and H.T. Searle, J. Chem. Soc., 1961, 1825.

8. G.C. Demitras, R.A. Kent and A.G. MacDiarmid, Chem. Ind., 1964, 1712.

9. I.N. Zhmurova and A.V. Kirsanov, Zhur. Obshch. Khim., 1960, 30, 3044.

10. D. Hess and H. Forst, Z. Anorg. Chem., 1966, 342, 240.

11. L.G. Hoard and R.A. Jacobson, J. Chem. Soc. (A), 1966, 1203.

12. H. Fleig and M. Becke-Goehring, Z. Anorg. Allgem. Chem., 1970, 376, 215.

13. M.P. Yagupski, Inorg. Chem., 1967, 6, 1770.

14. C. Dean, Phys. Rev., 1952, 86, 607.

15. V. Rehn, J. Chem. Phys., 1963, 38, 749.

16. M. Toyama, J. Phys. Soc. Japan, 1959, 14, 1727.

17. Y. Morino and M. Toyama, J. Chem. Phys., 1961, 35, 1289

18. R.B. Creel, S.L. Segel and L.A. Anderson, J. Chem. Phys., 1969, 50, 4908.

19. J. Darville, A. Gerard and M.T. Calende, J. Mag. Res., 1974, 16, 205.

20. J. Darville and A. Gerard, Computer Physics Communications, 1975, 9, 173.

21. H.R. Brooker and R.B. Creel, J. Chem. Phys., 1974, 61, 3658.

22. J.D. Graybeal and P.J. Green, J. Phys. Chem., 1969, 73, 2948.

23. C.H. Townes and B.P. Dailey, J. Chem. Phys., 1949, 17, 782.

24. E.A.C. Lucken, "Nuclear Quadrupole Coupling Constants", Academic Press Inc., New York, N.Y., 1969.

25. J.A.S. Smith, J. Chem. Ed., 1971, 48, 39.

26. V. Jaccarino and J.G. King, Phys. Rev., 1951, 63, 471.

27. Lj. Manojlović - Muir and K.W. Muir, J. Chem. Soc. Dalton, 1974, 2395.

28. H. Bayer, Z. Physik, 1951, 130, 227.

29. T. Kushida, J. Sci. Hiroshima Univ., 1955, A19, 327.

30. T. Kushida, G.B. Benedek and N. Bloembergen, Phys. Rev., 1956, 104, 1364.

31. C.T. O'Konski, "Determination of Organic Structures by Physical Methods", F.C. Nachod and W.D. Phillips eds., Academic Press, New York and London, 1962, 2, Chapter 11.

32. I. Ichishima, J. Chem. Soc. Japan, Pure Chem. Sect., 1950, 71, 607.

33. Landolt – Börnstein, K. Schäfer and G. Beggerow eds., Springer-Verlag, Berlin, 1971, Band II, Teil I.

34. P.W. Bridgman, Proc. Amer. Acad. Arts Sci., 1929, 64, 51.

35. P.W. Bridgman, Proc. Amer. Acad. Arts Sci., 1948, 76, 71.

36. P.W. Bridgman, Proc. Amer. Acad. Arts Sci., 1949, 77, 187.

37. W. Biltz, A. Sapper and E. Wünnenberg, Z. Anorg. Chem., 1932, 302, 277.

38. T.P. Das and E.L. Hahn, "Nuclear Quadrupole Resonance Spectroscopy," Solid State Physics, Supplement 1, Academic Press Inc., New York, N.Y., 1958.

39. M.M. McEnnan and E. Schempp, J. Mag. Res., 1973, 11, 28.

40. M.M. McEnnan and E. Schempp, "Advances in Nuclear Quadrupole Resonance", J.A.S. Smith ed., Heyden, London, 1974, 1, 263.

41. I.N. Zhmurova and B.S. Drach, Zhur., obshchei Khim., 1964, 34, 1441.

42. M. Becke – Goehring, L. Leichner and B. Scharf, Z. Anorg. Chem., 1966, 343, 154

43. M. Green, R.N. Haszeldine and G.S.A. Hopkins, J. Chem. Soc. (A), 1966, 1766.

Chapter IV

1. M. Kaplansky and M.A. Whitehead, Canad. J. Chem., 1967, 45, 1669.

2. R. Clipsham, R.M. Hart and M.A. Whitehead, Inorg. Chem., 1969, 8, 2431.

3. G.J. Bullen, J. Chem. Soc. (A), 1971, 1450.

4. E.A.C. Lucken, "Magnetic and Electric Resonance and Relaxation", (Proceedings of the XIth Colloque Ampère), J. Smidt ed., North Holland Publishing Company, Amsterdam, 1963, 678.

5. D.M. Adams and W.S. Fernando, J. Chem. Soc. Dalton, 1972, 2503.

6. S.K. Das, R. Keat, R.A. Shaw and B.C. Smith, J. Chem. Soc. (A), 1966, 1677.

Chapter V

The treatment of the theory in Chapter V of this thesis was based on the following sources.

1. A. Carrington and A.D. McLachlan, "Introduction to Magnetic Resonance", Harper and Row, New York, N.Y., 1967.

2. C.P. Slichter, "Principles of Magnetic Resonance", Harper and Row, New York, N.Y., 1963.

3. B.R. McGarvey, "Transition Metal Chemistry", R.L. Carlin ed., Edward Arnold, London, 1966, 3, 90.

4. A. Abragam and B. Bleaney, "Electron Paramagnetic Resonance of Transition Ions", Clarendon Press, Oxford, 1970.

5. N.M. Atherton, "Electron Spin Resonance", Ellis Horwood, London, 1973.

Chapter VI

1. D.W. Pratt, Nuclear Science Abstracts, 1967, 21, 34254.

2. G.F. Kokoszka, H.C. Allen jun., and G. Gordon, Inorg. Chem., 1966, 5, 91.

3. D.C. Bradley, R.H. Moss and K.D. Sales, Chem. Commun., 1969, 1255.

4. E.C. Alyea and D.C. Bradley, J. Chem. Soc. (A), 1969, 2330.

5. C.E. Holloway, F.E. Mabbs and W.R. Smail, J. Chem. Soc. (A), 1968, 2980.

6. C.P. Stewart and A.L. Porte, J. Chem. Soc. Dalton, 1973, 722.

7. D.P. Bakalik and R.G. Hayes, Inorg. Chem., 1972, 11, 1734.

8. J.L. Petersen and L.F. Dahl, J. Amer. Chem. Soc., 1974, 96, 2248.

9. C.P. Stewart, Ph.D. Thesis, Glasgow University, 1973.

10. A. Abragam and M.H.L. Pryce, Proc. Roy. Soc. (A), 1951, 205, 135.

11. V.V. Tkachev and L.O. Atovmyan, Zhur. Strukt. Khim., 1972, 13, 287.

12. A. Clearfield, D.K. Warner, C.H. Saldarriaga-Molina, R. Ropal and I. Bernal, Canad. J. Chem., 1975, 53, 1622.

13. N.V. Alekseev and I.A. Ronova, Zhur. Strukt. Khim., 1966, 7, 103.

14. M. Hillman and A.J. Weiss, J. Organometallic Chem., 1972, 42, 123.

15. B.R. Davis and I. Bernal, J. Organometallic Chem., 1971, 30, 75.

16. A. Lüttringhaus and W. Kullick, Makromol. Chem., 1960 44-6, 669.

17. H.P. Fritz, Adv. in Organometallic Chem., 1964, 1, 239.

18. D. Nicholls, Coord. Chem. Rev., 1966, 1, 379.

19. D. Kivelson and S.K. Lee, J. Chem. Phys., 1964, 41, 1896.

Appendix B

1. G.B. Benedek, "Magnetic Resonance at High Pressure", Interscience, New York, N.Y., 1963.

2. W. Paul and D.M. Warschauer eds., "Solids Under Pressure", McGraw-Hill Inc., New York, N.Y., 1963.

3. W. Paul, G.B. Benedek and D.M. Warschauer, Rev. Sci. Instr., 1959, 30, 874.

4. G.B. Benedek and E.M. Purcell, J. Chem. Phys., 1954, 22, 2003.

5. W.S. Goree, B. McDowell and T.A. Scott, Rev. Sci. Instr., 1965, 36, 99, and references therein.

6. K.E. Bett and D.M. Newitt, "Chemical Engineering Practice", H.W. Cremer and T. Davies eds., Butterworths, London, 1958, 5, 196.